UNIVERSITY OF CALIFORNIA, SAN DIEGO

Bioactive and Bioresponsive Nanoparticle Surface Modifications for Vaccine and Systemic Drug Delivery

A dissertation submitted in partial satisfaction of the requirements for the degree Doctor of Philosophy

in

Bioengineering

by

Corbin Zean Clawson

Committee in charge:

Professor Michael J. Heller, Chair
Professor Sadik C. Esener, Co-Chair
Professor Liangfang Zhang, Co-Chair
Professor David A. Gough
Professor William C. Trogler

2011

The Dissertation of Corbin Zean Clawson is approved, and it is acceptable in quality and form for publication on microfilm and electronically:

_____

_____

_____
Co-Chair

_____
Co-Chair

_____
Chair

University of California, San Diego

2011

DEDICATION

For my beloved wife and best friend, Alice, who deserves this degree more than I. For her love, support, and encouragement through it all. Without her light, I would be but a pale shadow of the man I am today. For my one year old son, Daxton, who had better love learning as much as I do or else he's grounded. For my Mom, who instilled a love of learning in me…on threat of grounding. For my Dad, whose frequent admonition 'think before you do things' served me well in graduate school. For my brothers, Zac and Chas, who taught me how to think out of the box, and not just by literally locking me in a box. And for my sisters, Cassie and Taralyn, who taught me how to love life and care deeply. And for all my friends who are too numerous to name, and too valuable to ever forget.

EPIGRAPH

There is no medicine like hope, no incentive so great, and no tonic so powerful as expectation of something better tomorrow.

Orison Swett Marden

TABLE OF CONTENTS

LIST OF FIGURES

LIST OF TABLES

ACKNOWLEDGEMENTS

I would like to thank Professor Sadik Esener for his continued mentorship and guidance throughout my graduate career. He has been an inspirational example of a truly interdisciplinary scientist and engineer. His confidence in me has made all the difference.

Professor Liangfang Zhang has likewise been an incredible mentor and advisor. His encouragement, support, and counsel through these last few years have helped me achieve great things. His door was always open and he was ever ready with a listening ear and an insightful observation.

I thank Professor Michael Heller for chairing my committee and being always available for questions and advice.

My colleagues in Professor Zhang's group have been an invaluable asset to my intellectual and scientific development as well as great friends. Much credit goes to Dr. Li Zhang for her help with the apolipoprotein project and the *in vivo* mouse work. Dr. Santosh Aryal has been like an older brother and an invaluable resource whenever I got stuck on a particularly challenging problem, especially chemical synthesis problems. I appreciate Jack Hu's incredible philosophical insights as much as his scientific ones. The contagious smiles and uplifting personalities of Dissaya Nu Pornpattananangkul and Soracha

Kun Thamphiwatana are ever appreciated. Thanks to Ronnie Fang for putting up with my good-natured ribbing and to Kathy Stavropoulos for her unique perspective on life and her positive outlook. I acknowledge Marta Sartor who paved the way. I recognize the invaluable contributions of Linh Ton and all her hard work on the PEG shedding and apolipoprotein projects. And thanks to the other undergraduate students, Kristin Chan, Connie Cheung, Victoria Fu, and Cody Carpenter for their optimism and examples of hard work. I thank them all for their contributions to my research and for their friendship.

I owe a lot to Dr. Davorka Messmer and her whole research group for their incredible work on the vaccine project. Jasmine Huang, Diahnn Futalan, and Dan Seible spent many late hours with me making and washing nanoparticles. Becca Saenz was always available for advice on research problems or challenges. Ila Bharati was always available with a protocol or supplies to loan.

I want to thank all my colleagues in Professor Esener's group. Inanç Ortaç and Ahmet Erten for their friendship and examples of true innovators and engineers. Mike Benchimol deserves a lot of credit for waking up for early morning surf sessions that helped me relieve the tension of grad school. Thanks to Jason Steiner for his insights into life and grad school as well as his example of passion and dedication.

Stuart Ibsen is an inspiring adventurer and good friend. Carolyn Schutt deserves recognition for her calming demeanor and caring personality.

Many thanks to all others who have helped me with my research, made me laugh or smile, or taught me through their example or words: Jennifer Marciniak, Sergio Sandoval, Alex Liberman, Jessie Fecteau, Gen Yang, and many others.

And finally thanks to UCSD, the Bioengineering Department, and all my professors for providing the foundation and infrastructure that made my incredible education possible.

Chapter 2, in part, is a reprint of the material as it appears in Nanomedicine, 2010, Corbin Clawson, Chien-Tze Huang, Diahnn Futalan, Daniel Martin Seible, Rebecca Saenz, Marie Larsson, Wenxue Ma, Boris Minev, Fiona Zhang, Mihri Ozkan, Cengiz Ozkan, Sadik Esener, and Davorka Messmer. The dissertation author was the primary investigator and co-author of this paper.

Chapter 3, in part, has been submitted for publication as it may appear in Small, 2011, Corbin Clawson, Linh Ton, Santosh Aryal, Sadik Esener, Liangfang Zhang. The dissertation author was the primary investigator and author of this paper.

Chapter 4, in part, is currently being prepared for submission for publication of the material. Corbin Clawson, Li Zhang, Linh Ton, Sadik Esener, Liangfang Zhang.

VITA

2006 Bachelor of Science, Virginia Polytechnic and State University

2011 Master of Science, University of California, San Diego

2011 Doctor of Philosophy, University of California, San Diego

PUBLICATIONS

1. Mora L, Chumbimuni-Torres KY, Clawson C, Hernandez L, Zhang LF, Wang J. Real-time electrochemical monitoring of drug release from therapeutic nanoparticles. Journal of Controlled Release. 2009;140(1):69-73.

2. Chumbimuni-Torres KY, Wu J, Clawson C, Galik M, Walter A, Flechsig GU, et al. Amplified potentiometric transduction of DNA hybridization using ion-loaded liposomes. Analyst. 2010;135(7):1618-23.

3. Clawson C, Huang CT, Futalan D, Seible DM, Saenz R, Larsson M, et al. Delivery of a peptide via poly(D,L-lactic-co-glycolic) acid nanoparticles enhances its dendritic cell-stimulatory capacity. Nanomedicine-Nanotechnology Biology and Medicine. 2010;6(5):651-61.

4. Kagan D, Laocharoensuk R, Zimmerman M, Clawson C, Balasubramanian S, Kong D, et al. Rapid Delivery of Drug Carriers Propelled and Navigated by Catalytic Nanoshuttles. Small. 2010;6(23):2741-7.

5. Clawson, C.; Esener, S.; Zhang, L. "Lipid-Polymer Nanomaterials" in Organic Nanomaterials for Life Sciences (Kumar, C., Ed), Wiley-VCH Press, 2011, 259-284.

6. Clawson, C.; Ton, L.; Aryal, S.; Esener, S.; Zhang, L.; "Synthesis and Characterization of Lipid-Polymer Hybrid Nanoparticles with pH-Triggered PEG Shedding " 2011, submitted to *Small*.

7. Clawson, C.; Zhang, L. Ton, L.; Esener, S.; Zhang, L.; "Self-assembly of biomimetic lipoprotein-polymer hybrid nanoparticles for use as long-circulating drug delivery vehicles" 2011, prepared for submission to *Biomaterials.*

FIELDS OF STUDY

Major Field: Drug delivery and Nanoengineering

Studies in Cancer therapeutics
Professor Sadik Esener

Studies in Drug delivery and Nanoengineering
Professor Liangfang Zhang

ABSTRACT OF THE DISSERTATION

Bioactive and Bioresponsive Nanoparticle Surface Modifications for Vaccine and Systemic Drug Delivery

by

Corbin Zean Clawson

Doctor of Philosophy

University of California, San Diego, 2011

Professor Michael J. Heller, Chair
Professor Sadik C. Esener , Co-Chair
Professor Liangfang Zhang, Co-Chair

Nanomedicine is a research field that has recently made significant progress in the areas of drug delivery. A drug delivery vehicle must be able to carry a therapeutic cargo and be able to reach the target tissue and the intended intracellular target or

compartment. This dissertation will focus on two major applications of drug delivery vehicles and novel improvements in these areas.

The first area is vaccine delivery, where sensitive biological cargo must be delivered to and activate immune cells. A new peptide adjuvant called Hp91 was chosen to be co-delivered to dendritic cells along with an antigen to ensure activation. The vaccine drug delivery vehicle designed to deliver these biomolecules consists of a poly(lactic-co-glycolic acid) (PLGA) core with the antigen encapsulated inside and the peptide adjuvant either co-encapsulated or conjugated to the outside. The PLGA successfully protected the protein and peptide from degradation, maintaining its activity. The vaccine delivery vehicles showed a marked improvement over free Hp91 in both human and mouse dendritic cell activation, with a maximum of 44 fold increase in IL-6 stimulation when the peptide was conjugated to the surface.

The second area of research presented here is systemic drug delivery. For systemic delivery, long circulation is a desirable characteristic and poly(ethylene glycol) (PEG) is the current state of the art. However, PEG presents two challenges: 1. PEG can hinder the nanoparticle from entering the cytosol across the endosomal or cellular

membrane, and 2. PEG can sometimes induce immunogenicity resulting in accelerated blood clearance after repeated dosing.

A novel PEG shedding nanoparticle is presented as a solution to the first challenge. The ability to shed the PEG layer in response to a reduction in pH allows a fusogenic lipid layer to be exposed, which promotes membrane disruption. For patients who respond immunogenically to PEG, a biomimetic apolipoprotein coating to replace PEG altogether is presented. Apolipoprotein A1 is shown here to stabilize PLGA nanoparticles and increase their circulation half-life beyond that of the traditional PEG coating.

These drug delivery vehicles were engineered from the foundation of a biodegradable, biocompatible PLGA polymer core with characteristic surface properties designed to overcome these specific challenges to drug delivery.

1. INTRODUCTION

1.1 Drug Delivery: Rationale

In our everyday lives, the word 'deliver' has many meanings. Arguably, it is most commonly used in the sense 'to send to an intended target or destination'.(1) Especially regarding the delivery of commercial goods, we understand the need for vehicles – trucks, cars, ships, and planes – in order to transport and deliver to us the objects we buy and use everyday. Without careful organization and planning, one 'John Smith' of Ohio might receive a package intended for another 'John Smith' of Iowa. Or perhaps the correct recipient receives the package, but the handling of the package resulted in a

mangled box and contents that are broken and unusable. Modern businesses and organizations expend a lot of effort to reduce or eliminate such occurrences in order to save costs associated with inefficient delivery as well as increase customer satisfaction.

These same concerns of providing efficient and effective delivery are also being applied to the delivery of drugs within the human body. Drug delivery 'vehicles' include minute nanoparticles that encapsulate drugs inside and macromolecules such as natural and synthetic polymers. These drug delivery vehicles are being used to carry drug molecules to their intended destination while preventing damage to the drug molecules or removal from the body before they reach their target. The need for such drug delivery vehicles becomes obvious when the multitude of prevalent diseases is considered along with the human body's innate ability to neutralize, counteract, eliminate, or degrade foreign substances through an incredible variety of biological responses.

The goals of drug delivery can be divided into three categories: 1. Improving drug efficacy, 2. Improving drug safety, and 3. Improving patient convenience and compliance.

1.1.1 Improving drug efficacy through delivery

Improving drug efficacy is especially important in the fight against hard to treat diseases such as cancer, antibiotic resistant bacterial infections, and chronic viral infections such as HIV and Hepatitis C. While new drug discovery efforts are invaluable, improving the efficacy of existing therapies can help turn the tide against these deadly diseases, resulting in millions of lives saved.

Cancer is an especially intractable disease due to high variability between incidents. For example, according to the National Breast Cancer Foundation, the fight against breast cancer is not a fight against a single disease, but a fight against no less than seven major subclasses of breast cancer (Ductal Carcinoma In-Situ, Infiltrating Ductal Carcinoma, Medullary Carcinoma, Infiltrating Lobular Carcinoma, Tubular Carcinoma, Mucinous Carcinoma, and Inflammatory Breast Cancer). Each of these types of breast cancer are classified based on what type of tissue the cancer first develops in as well as physical characteristics of the tumors or cancer cells themselves.(2, 3)

In reality, each of these subclasses may be divided even further based on the actual genetic or epigenetic mutation that caused the cancer.(4) The number of potential mutations in the approximately

20,000 genes in the human genome that might result in cancerous tumor formation is unknown at this time, but it is undoubtedly high. Each mutation represents a different disease, possibly requiring completely different therapeutic strategies, although the histology and presentation may be similar or even identical.(3, 4) It becomes difficult to treat each genetic variation of cancer with a drug uniquely formulated specifically for that mutation. Additionally, mutations may lead to drug resistance in the tumor cells, making the effective use of existing drugs even more challenging.(5-7) By combining existing drugs with nanomedicine and drug delivery technologies, the number of possible tools available to the clinician treating cancer is multiplied and the chances of finding an effective formulation are greatly increased.(8, 9) In addition, using proper drug delivery vehicles, multiple drugs can be delivered simultaneously, further increasing the available treatments for overcoming drug resistance in cancer tumors(6).

Similarly, in the fight against antibiotic resistant microbes, the number of effective antibiotic drugs available is limited. Recently, infections from bacteria strains resistant to our last line of antibiotic defense, the carbapenem class of antibiotic drugs that includes vancomycin, have been increasing in number.(10) There are currently

no new drugs in the pipeline to combat carbapenem resistant bacterial infections.(11) The widespread emergence of such infections is considered a significant threat to the public health.(12) Hospital acquired infections of methicillin-resistant *Staphylococcus aureus* (MRSA) were responsible for the deaths of 19,000 Americans in 2005 (the last year for which the US Centers for Disease Control has records). In order to prolong the lifespan of these critical, life-saving drugs, more efficient and effective delivery using nanomedicine technologies must be explored in earnest.

Vaccination is another strategy that can benefit from the use of drug delivery vehicles.(13, 14) Vaccinations rely on the body's own defenses to combat the infection by providing the immune system with the proper tools to identify the infection. In one immunological pathway, antigens from the infectious pathogen are taken up by dendritic cells (DCs), professional antigen presenting cells, which then present the antigens to other immune cells such as T cells and B cells.(15) In this function, DCs act as messengers between the innate and the adaptive immune system, delivering the necessary information for pathogen identification.(16) Figure 1.1 shows the lifecycle of a dendritic cell. Newly activated B cells produce antibodies that lock onto the pathogenic antigens. The antigen-antibody complex effects

the removal of the pathogen by either the complement cascade or by the liver and spleen.(17) Activated Cytotoxic T cells and lymphocytes actively seek out the pathogens in order to neutralize them.(15)

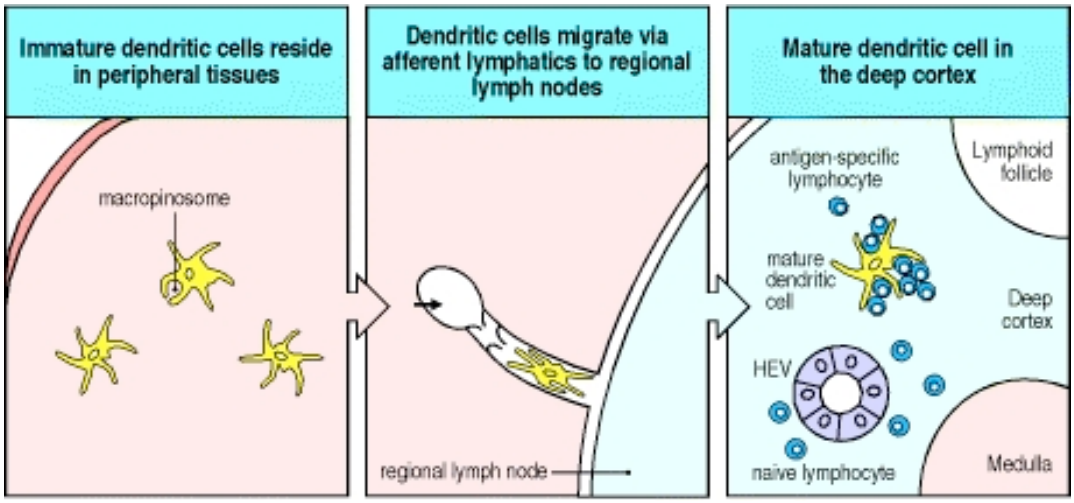

Figure 1.1. Lifecycle of a dendritic cell showing uptake of antigen, migration to lymph nodes and interaction with other immune cells.(15)

Vaccines attempt to artificially activate the immune system, conferring preventive immunity by teaching the immune system to recognize a specific pathogen using inactivated pathogens or specific pathogen associated proteins or other molecules.(15) Drug delivery vehicles that are taken up more efficiently by the professional antigen presenting immune cells can improve the efficacy of the vaccine.(14, 18, 19)

Vaccines have traditionally incorporated adjuvants that increase the immunologic activity but have no antigenic activity themselves. The use of adjuvants allows immune system to respond more strongly, increasing immunity in the recipient. Adjuvants do this by acting as synthetic versions of evolutionarily conserved molecules called pathogen-associated molecular patterns, or PAMPs.(15) Without the use of adjuvants, the innate immune system is not activated and immunity is conferred at a much lower level, if at all. This complex series of interactions is a fertile ground for improvements through the use of drug delivery vehicles.

Immune cells preferentially engulf particulates of a certain size.(20, 21) Using a drug delivery vehicle allows selection of particulate size independent of the antigen or adjuvant molecules being delivered.(22) Additionally, co-packaging antigens and adjuvants into the same drug delivery vehicle can ensure that any immune cell that takes up the vehicle will be fully activated.(23-25) This can improve the effectiveness of a vaccine and increase conferred immunity.(26) New strategies are also being explored that combine personalized medicine and vaccination strategies to induce an immune response against cancerous tumors.(27, 28) Drug delivery vehicles will play a key role in this emerging field of personalized

medicine by allowing tumor-associated molecules unique to the patient to be reliably and reproducibly delivered to the immune system. Careful attention needs to be paid to avoid overstimulation of the immune system, which can lead to autoimmunity.

1.1.2 Improving drug safety through delivery

Certain classes of drugs such as potent chemotherapy drugs are effective because of their toxicity. They are used to exploit differences between diseased cells and healthy cells, preferentially killing the diseased cells. Because diseases such as cancer are mutations of healthy cells, these differences are often very slight and systemic toxicity is often a limiting factor in determining the maximum tolerable dose.(29) Doxorubicin is a common chemotherapy drug whose most serious adverse side effect is cardiac toxicity, which can be fatal.(29-34) Adverse side effects such as nausea, hair loss, fatigue, etc. are also commonly associated with the use of chemotherapy drugs. Drug delivery vehicles can be used to preferentially deliver these potent drugs to the tissue of interest through active or passive targeting while shielding the drugs from being taken up by healthy cells.(35-39) This has the potential effect of reducing the overall systemic toxicity while increasing the efficacy.(37, 38, 40-43) The use of drug delivery vehicles

can open up new classes of drugs for use that were previously too cytotoxic to use by delivering the drugs safely to the target site.

1.1.3 Improving patient compliance and convenience through delivery

Finally, patient convenience and compliance can be increased through the use of drug delivery vehicles. Similar to reducing severe adverse side effects, reducing mild to moderate side effects can lead to greater compliance by the patient. Drug delivery technologies can be applied to a wide range of drugs that do not typically cause life-threatening side effects but may cause some slight discomfort or inconvenience in order to lessen the adverse effects of the drugs.(41, 42) Patients who experience fewer side effects are more likely to comply with the recommended course and dosing requirements, leading to an increase in patient satisfaction as well as increased drug efficacy. Drug delivery formulations that make the drug easier to administer are just as likely to have a positive impact on patient compliance as formulations that reduce side effects.(41, 42) Additionally, drug delivery vehicles that release their cargo in a controlled manner can reduce the need for frequent dosing or the need for intravascular infusions.(40, 43) These conveniences for the

patient could have a significant impact on patient satisfaction and compliance.

The rationale behind drug delivery vehicles becomes clear when considering the improvements that can be achieved in drug efficacy, drug safety, and patient convenience and compliance through the use of carefully formulated drug delivery vehicles.

1.2 Drug Delivery Strategies

There is considerable effort to optimize drug delivery vehicles for efficacy, safety, and patient convenience and compliance. Each particular application has its own requirements and constraints that must be accounted for. In this section, several different strategies and key considerations will be discussed that become important when selecting or designing a drug delivery system.

1.2.1 Administration routes

In the rational design of drug delivery vehicles, first the route of administration must be considered. The desirable characteristics of a drug delivery vehicle designed for intravascular injection are

understandably quite different than the desired characteristics of a peroral formulation. As some drugs are not suitable for certain administration methods, the properties of the drug must be considered when choosing which administration route to pursue. In the following I will discuss the most common administration routes along with some of their limitations and benefits, with special attention paid to the application of drug delivery vehicles.

In peroral administration, a patient ingests the drug orally. Patient compliance is highest for peroral formulations because it is convenient and easy to swallow a pill or drink a liquid. While this is therefore the most desirable formulation for any given drug, it is not always possible to administer a drug orally. Some reasons why a drug might not be administered orally include: degradation of the drug molecule within the digestive system, inability of certain molecules to cross the gastrointestinal mucosa into the bloodstream due to size, charge, solubility or other characteristics, and slow pharmacokinetics. Although technically peroral delivery is a form of transmucosal delivery due to the fact that drugs taken orally must cross the gastrointestinal mucosa, I have singled out peroral delivery as its own administration route because of its ubiquitous and common nature.

Topical administration is the application of a drug directly onto the surface of the skin. Small molecules can diffuse through the extracellular space in into the bloodstream while larger molecules are usually confined to the dermis and epidermis layers of the skin. Additionally, the lipid/water partition coefficient and degree of ionization of the permeant are important factors to consider for topical delivery. Topical administration can be performed through the use of a cream, lotion, or solution applied directly to the skin or through the use of a transdermal patch that elutes drugs continuously from a polymer or hydrogel reservoir placed in extended contact with the skin. The nicotine patch is the most common transdermal drug delivery device available to consumers. Depending on the permeant being administered, slow pharmacokinetics can be an issue, as can skin irritability or unpleasant residues left on the surface of the skin. The extended, sustained release capability of the transdermal patch is one of its major advantages.

Transmucosal delivery refers to the absorption of a drug through a mucus membrane. Mucosae consist of an epithelial layer and a lamina propria as contrasted to the epidermis and dermis of the skin. Transmucosal delivery can present similar concerns to topical delivery with the added complications of mucosae generally being more

sensitive to irritation as well as increased immunologic activity from the mucosal immune system. The presence of the frontline mucosal immune system has prompted some studies on transmucosal vaccine delivery. Common transmucosal delivery methods are sublingual, vaginal, rectal, and conjuctival delivery as well as inhalation.

Intravascular injection represents one of the quickest ways to administer a drug systemically. Within one to two minutes the drug is uniformly distributed throughout the entire blood volume. The body immediately begins to clear the drug from the bloodstream, typically via the liver, spleen, and renal system. Rapid clearance from the blood is one of the major hurdles for intravascular injection. In order to maintain drug concentration at the optimum therapeutic level, doctors often hook up an IV drip infusion to maintain the concentration over extended periods of time. This limits the patient's mobility and is less convenient and comfortable than a single injection.

Subcutaneous and intramuscular injection involves injecting the drug not into the circulatory system but into the interstitial space of either the dermis or the muscle tissue. This administration method is not as fast as intravascular injection but is generally faster than peroral, topical, or transdermal routes. Repeated injections in the same site can lead to tissue damage over the long term.

Drug delivery vehicles are designed and chosen to maximize the bioavailability of the drug cargo with regard to the route of administration. Particular drugs necessitate particular routes of administration owing to their inherent physical and chemical characteristics. Likewise, particular diseases may dictate a specific administration route. These factors along with safety and patient convenience and compliance should be carefully considered when choosing an administration route.

1.2.2 Release profile modification

One way in which a drug's efficacy is optimized through the use of drug delivery vehicles is by the modification of the drug release profile from the delivery vehicle. Different drugs have different concentration dependent therapeutic windows. When the drug concentration falls below the minimum therapeutic level, little or no effect is observed. When the drug concentration exceeds the maximum therapeutic window, the probability of experiencing adverse side effects is increased. Depending on the disease and the drug being administered, either of these scenarios can be life threatening. When administering a drug bolus, a sharp peak in drug concentration is seen quickly which then quickly begins to taper off as

the drug is eliminated from the body as shown in the single compartment model simulation presented in Figure 1.2. When administered via intravascular injection, the initial mixing is very rapid and complete within one to two minutes. The concentration drops exponentially as the drug is eliminated through the renal system and metabolized in the liver. This necessitates either frequent low dose administrations of the drug in order to maintain the concentration within the therapeutic window or fewer large doses which result in longer times within the therapeutic window per dose but also peaks and valleys that lie outside the therapeutic window. A model example of two such a dosing schedules is presented in Figure 1.3. Intravenous infusions are often used to combat this very problem by continuously adding drug to the bloodstream at a rate sufficient to maintain the drug concentration at a steady state within the therapeutic window. The use of IV infusion is typically limited to hospital settings and restricts the patient's mobility and comfort.

A drug delivery vehicle that can release its cargo in a controlled manner over a period of time can serve as an internal reservoir or depot, maintaining the active drug concentration in the bloodstream within the therapeutic window for extended periods of time without the need for IV infusions and without causing unwanted side effects.

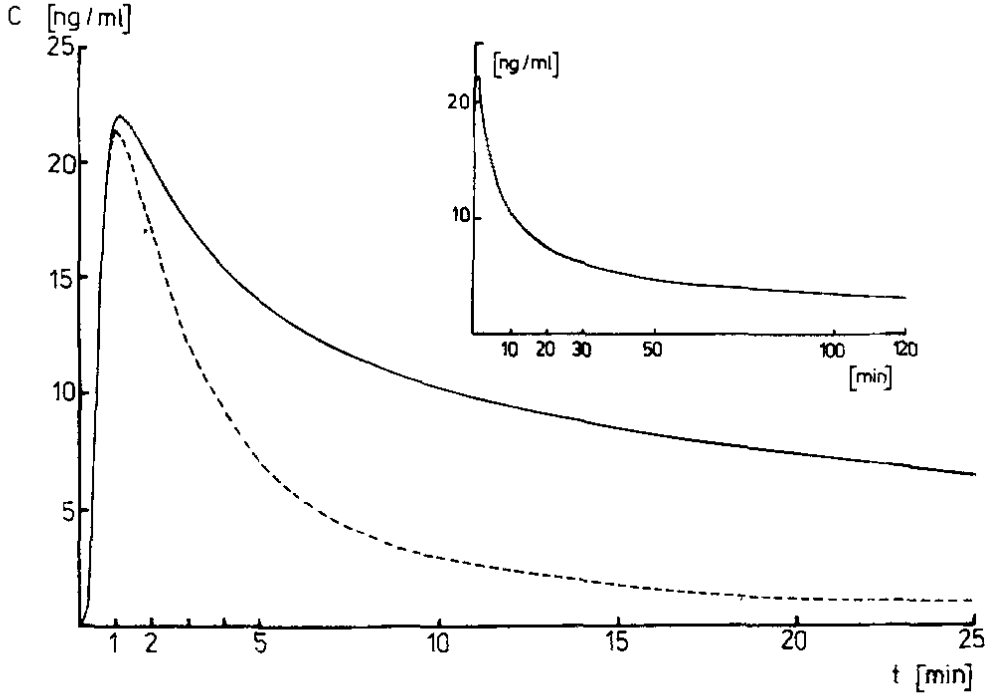

Figure 1.2. Simulated time course of right atrial blood concentration after rapid intravenous injection of drug. Inset shows contracted time scale. Complete mixing occurs after less than two minutes. After the sharp peak, concentration declines exponentially.(44)

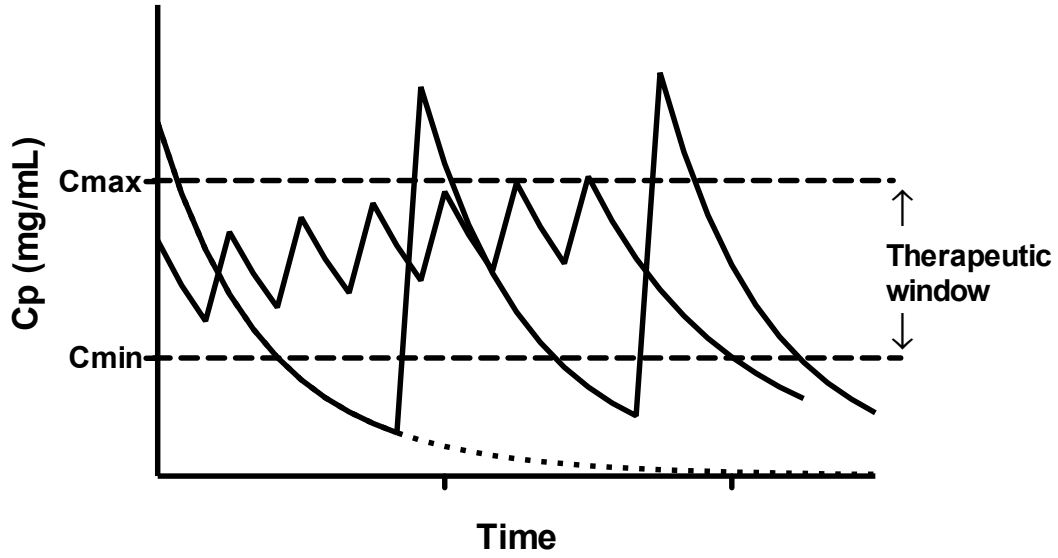

Figure 1.3. Model shows an example pharmacokinetic elimination curve with repeated IV bolus dosing to maintain plasma concentration of drug within the therapeutic window. Curves compare less frequent high doses with more frequent low doses as two different strategies to maintain plasma concentration.

Solid polymer matrices were first shown to be capable of controlled release of proteins and other macromolecules in 1976.(45) The biodegradable polymer became more and more porous as the polymer chains were hydrolyzed, releasing the biomolecules physically encapsulated within the polymer matrix. Since then, many different drug delivery technologies have relied on similar strategies to modify the release pattern of a drug cargo from nanoparticles made from polymers, lipids, biocompatible inorganic solids, and a host of other

materials.(8, 36, 46-51) The ability to synthesize novel structures and polymers, including co-polymers and polymer conjugates, allows for an incredible variability in release kinetics.(52, 53) Couple that with the change in release kinetics that results from modifying the physical structure and size of the drug delivery vehicle and it is not heard to see why advances are still being made in this research field.

Active approaches to controlling the drug release profile are also being explored. External triggers can induce a burst release of cargo from a properly designed delivery vehicle. Ultrasound has been used to release cargo from polymer coated microbubles by varying the ultrasound intensity.(54) Alternating magnetic fields have been used to heat up paramagnetic and superparamagnetic oxide particles in order to speed the degradation of a polymer matrix, thus releasing more cargo. Photo-cleavable pro-drugs can be non-toxic throughout the body, but upon an externally applied stimulus at the target tissue site, the pro-drug is released and converted back into its active state. Drug delivery researchers are investigating strategies that use a variety of external stimuli to control the release rate.

The drug release profile remains one of the key parameters tuned by researchers in order to maximize the benefits of using a drug delivery vehicle.

1.2.3 Improving biodistribution

Controlling biodistribution through the use of drug delivery vehicles is another strategy used to optimize a drugs efficacy and safety. When encapsulated within a drug delivery vehicle, the drug delivery vehicle dominates the biodistribution until the drug is released. In the case of nanoparticle drug delivery vehicles, size is a key factor determining how the particles are cleared from the bloodstream. Tumors are known to have leaky vasculatures due to their irregular angiogenesis.(55) Through the enhanced permeation and retention (EPR) effect, particles between 20-150nm have been shown to be able to exit the leaky vasculature of solid tumors.(56, 57) Particles below 10nm are cleared fairly quickly through the renal system.(57) Particles above 150nm are cleared through the reticuloendothelial system and filtered out by the liver, spleen, and lungs.(58) Thus, by changing the size of a drug delivery vehicle, the biodistribution is radically altered. The use of certain sized delivery vehicles to exploit such phenomenon as the EPR effect is known as passive targeting. Modifying shape and morphology of the delivery vehicle surface has also been shown to have effects on biodistribution, uptake, and blood clearance. Likewise,

mechanical properties such as elasticity and deformability may also play a role in biodistribution.

Modifying other physical and chemical characteristics can also alter biodistribution. Surface zeta potential has been shown to have dramatic effects on the uptake of particles by the liver and spleen. Hydrophobicity has likewise been shown to increase adsorption of proteins onto circulating particles resulting in opsonization and rapid clearance from the bloodstream.

Active targeting can also be used to alter or improve biodistribution. Targeting moieties can be conjugated to or incorporated onto a delivery vehicle's surface to enhance accumulation in certain tissues or promote uptake by certain cells.(59) Common targeting moieties include peptides, proteins, antibodies, and other synthetic and natural molecules shown to have affinity for specific targets expressed by diseased cells(60-65). The search for compatible targets and ligands remains an active area of research to improve biodistribution, although generally other characteristics such as size, surface charge, etc. tend to dominate the biodistribution profile. Active targeting technologies are not yet to the point where the physical and chemical characteristics of the delivery vehicle can be ignored in the design and selection process.

1.2.4 Reducing elimination rates

Another goal of drug delivery vehicles is to reduce the elimination rate so as to increase the residence time within the therapeutic window. As discussed briefly in the preceding section, small molecules and drug delivery vehicles (below ~10nm) are quickly eliminated from the body through the renal system and are expelled through the urine.(58) Larger particles are commonly filtered out and degraded by the liver or become trapped in the exceedingly fine capillary beds in the lungs. Unless the target tissue is the liver or lungs, this fate is essentially equivalent to elimination from the body. The immune system also plays an important role in eliminating foreign material, or in this case administered drug delivery vehicles, from the body. The reticuloendothelial system, or mononuclear phagocyte system, consists of primarily monocytes, macrophages and dendritic cells that filter out foreign material and pathogens through phagocytosis and enzymatic degradation. These phagocytic cells accumulate in the lymph nodes and spleen where they interact with other immune cells. Uptake by these phagocytic cells, along with the Kupffer cells of the liver, must be avoided in order to reduce overall

elimination rates. One notable exception is in vaccine delivery where uptake by the immune cells is the ultimate goal.

Figure 1.4 shows a model of a typical two-compartment pharmacokinetic response to an IV bolus injection. The drug concentration in the plasma is monitored over time and shows a sharp decrease initially followed by a slower exponential decrease which appears as a straight line when plotted on a semi-log scale. The initial fast decay, or α decay, can be thought of as the perfusion and distribution rate as the drug molecules are distributed throughout all of the perfused tissues through the capillary system. The second slower decay, or β decay, represents the true elimination rate from the body. The slope of the α and β portions of the curve when plotted on a semi-log scale can be used to calculate the distribution and elimination half-lives using the following equation

$$Cp = A \cdot e^{-\alpha \cdot t} + B \cdot e^{-\beta \cdot t} \tag{1.1}$$

where *Cp* is the concentration of the drug in the plasma, *A* is a distribution constant and *B* is an elimination constant. The distribution and elimination half-lives can be calculated directly from the slopes with the following:

$$t_{1/2,\alpha} = \frac{\ln 2}{\alpha}, t_{1/2,\beta} = \frac{\ln 2}{\beta} \quad (1.2)$$

Poly (ethylene glycol) or PEG is commonly used to avoid uptake by the mononuclear phagocyte system and to improve circulation half-life of drug delivery vehicles circulating in the bloodstream. PEG is a biocompatible, biodegradable hydrophilic polymer. When attached to the surface of a nanoparticle drug delivery vehicle, the PEG molecules create a hydration layer around the particle preventing the adsorption of serum proteins onto the surface, and thus reducing clearance from the bloodstream by the immune system. Additionally, PEG sterically stabilizes the nanoparticles preventing aggregation during fabrication, storage, and circulation. Other 'stealth' coatings have been developed to function in similar ways to PEG by preventing recognition of the foreign material by the immune system.

1.2.5 Common delivery vehicle formulations

Liposomes are one of the most common drug delivery vehicles approved for clinical use. They consist of a lipid bilayer membrane and an aqueous core. Liposomes are often PEGylated to improve

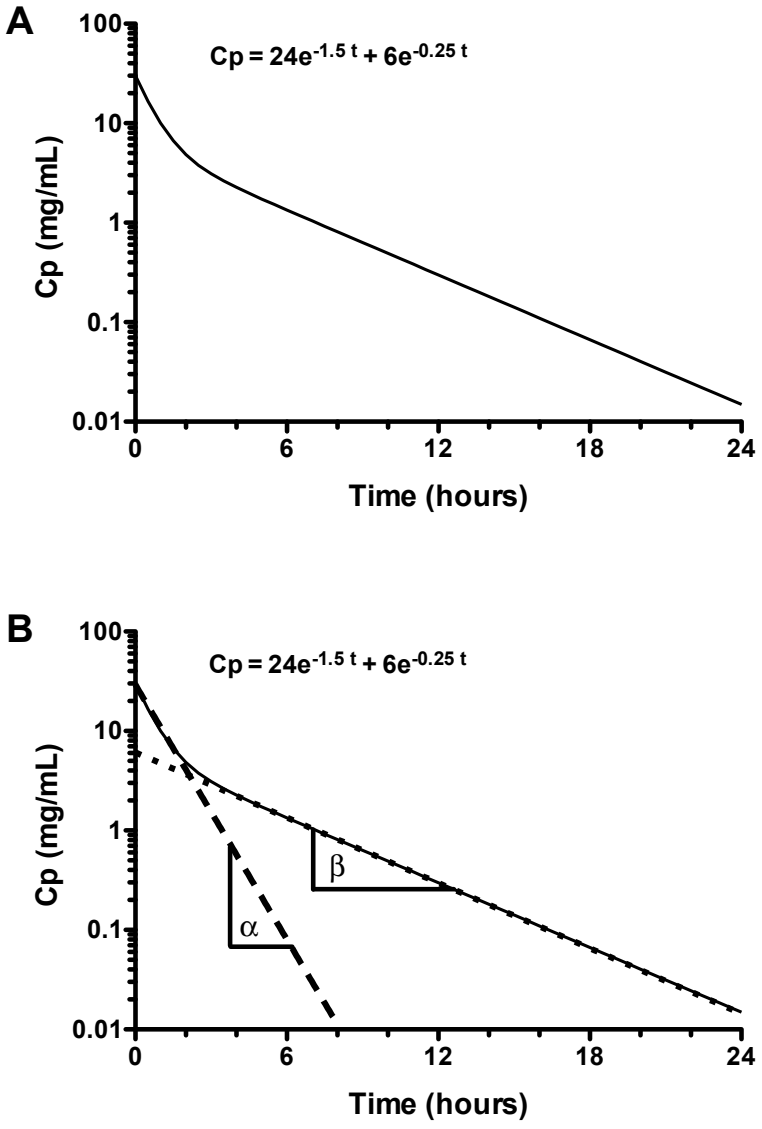

Figure 1.4. Simulation of a two-compartment pharmacokinetic model depicting a single IV bolus dose. A) Typical two-compartment model of plasma concentration of a drug after IV injection. B) Nonlinear regression showing a two-phase decay, a fast (α) and a slow (β) decay, as indicated by the slopes of the two fit lines. For many drugs, the two-compartment model is a very good approximation.

their circulation half-life. Liposomes are typically used to deliver water-soluble drugs encapsulated within their aqueous core, but a limited amount of lipid-soluble drugs can also be incorporated into the lipid bilayer. Methods have been developed to increase the loading capacity of liposomes for certain drugs. The most notable example is Doxil, the first FDA approved liposomal formulation of a drug. An ammonium sulfate gradient (high inside/low outside) is used to preferentially drive doxorubicin, a chemotherapy drug, into the liposome. Once inside the liposome where the concentration is increased, the doxorubicin crystallizes allowing further loading. The drug Myocet is another example of gradient loading, this time relying on a proton gradient to load doxorubicin citrate into liposomes. Since the approval of Doxil in 1995, the FDA has approved many other liposomal formulations of drugs for use in the clinic.(66)

Polymer based drug delivery vehicles are also increasingly common. There currently exist at least 24 approved nanoparticle formulations available on the market, including polymeric and lipidic formulations.(66) Common formulations use synthetic biodegradable and biocompatible polymers such as poly (lactic acid) (PLA), poly (glycolic acid) (PGA), poly (lactic-*co*-glycolic acid) (PLGA), poly-ε-caprolactone (PCL), poly (ethylene glycol) (PEG), and poly

(hydroxybutyrate) (PHB). Other polymers that are biocompatible but not necessarily biodegradable include polycarbonate, polysulfone, polyvinyl chloride, polypropylene, polymethylacrylate, silicones, and polystyrene.

Polymer macrostructures have been implanted to treat tumors through sustained release of drug and drug-eluting stents use polymer coatings containing drugs to reduce thrombosis and formation of clots in blocked arteries. Other implantable devices rely on polymers to deliver drugs over extended periods of time. However, polymeric nanoparticle formulations may prove to be more versatile in delivering drugs without the need for surgery or implantation. Emulsion (single and double), nanoprecipitation, templating, spray drying, electrospinning, and *in situ* polymerization are methods commonly used to produce synthetic polymeric nanoparticles. Hyperbranched polymers and dendrimers are also used for drug delivery purposes. Dendrimers have the advantage of being monodisperse and symmetric. They are also able to have different properties in their core and shell by changing the polymer reactions at different stages of the synthesis. Each addition of a new branch is allowed to go to completion and therefore, size is highly controllable by changing the number of branch generations that are allowed to form. Dendrimers

have been used as drug delivery vehicles but are expensive to produce, limiting their commercial viability.

Natural biopolymers include polypeptides and proteins, polynucleotides, polysaccharides, and cellulose. Due to manufacturing constraints, biopolymers are not yet as widely used in FDA approved drug delivery formulations as synthetic polymers.

In addition to nanoparticle based drug delivery systems, drug-polymer conjugates are also used. In this strategy, one or more small molecule drug molecules are directly conjugated to a polymer or other macromolecule and administered as such. The polymer conjugated to the drug can dominate the bioavailability, biodistribution, and elimination characteristics of the conjugate due to its much higher molecular weight compared to small molecule drugs. The release profile only becomes an issue if the molecule must be cleaved from the polymer in order to regain activity.

1.3 Challenges to drug delivery

Having given a brief overview of the various goals and some of the strategies of drug delivery vehicles, this dissertation will now focus on challenges associated with two specific drug delivery areas: 1. Vaccine delivery, and 2. Systemic delivery.

1.3.1 Vaccine delivery challenges

Vaccines are used as a prophylactic measure against many common diseases. Traditionally, a vaccine consists of material that mimics the disease causing pathogen but does not itself cause disease. When administered, the body's immune system recognizes the foreign material and develops an immune memory against the pathogen. In the future, when the person is infected with the disease causing pathogen, the immune system is already primed and able to deal with the infection much more efficiently due to the previous exposure, thus preventing the infection from developing. Vaccine material is often prepared from attenuated or killed pathogens. Vaccines can also be prepared from inactivated toxoids that cause the disease, as in the case of tetanus and diphtheria.(25, 26, 67)

Additional research is being performed in the area of therapeutic vaccines where the goal is to treat a disease rather than prevent or ameliorate a future occurrence.(14, 24, 27) This research is especially promising in the area of cancer vaccines. Because cancerous cells are derived from self, they still maintain all of the self-recognition molecules such as the MHC class of molecules and are often not recognized by the immune system as pathogenic. Cancer vaccines aim to break that recognition as self in order to enlist the help of the immune system to fight the tumor. This strategy involves delivering to immune cells a molecule that is expressed by the caner cells that can also be recognized as an antigen.

This dissertation will discuss several key challenges that present themselves when pursuing this strategy. The first is the successful delivery of the chosen antigen to the proper immune cells. Phagocytic cells such as macrophages, monocytes, and dendritic cells naturally engulf particulate material and pathogens in their environment. Dendritic cells also routinely sample their environment for antigens and even 'nibble' on small quantities of cellular membrane from the healthy cells around them. Memory T cells can be activated by macrophages, B cells, or dendritic cells; however, dendritic cells are the only cells capable of activating a naïve T cells. Therefore, a

cancer vaccine must be able to deliver the tumor expressing antigens to dendritic cells in such a way that the dendritic cells are matured and capable of activating other immune cells. Drug delivery vehicles can enhance the uptake of the antigens by immune cells due to their larger size, which approximates foreign particulate matter.(67, 68) Using a drug delivery vehicle allows particle size to be controlled independent of the cargo being delivered, ensuring phagocytosis.(68, 69)

Vaccines do not need to be delivered systemically; typical administration routes are subcutaneous injection or transmucosal nasal delivery. Immune cells, particularly dendritic cells, patrol the skin and mucosae that come into frequent contact with the environment. Since they are not delivered intravascularly, drug delivery vehicles intended for vaccine delivery do not need to have a long circulation half-life.

Another challenge associated with vaccine delivery is the protection of unstable biomolecules. Peptides, proteins and polynucleotides, which are prime candidates for use as vaccines, are generally not stable *in vivo*. Such biomolecules acting as antigens must be protected from degradation during the delivery to the immune cells, as their potency as a vaccine or adjuvant decreases

upon degradation. A drug delivery vehicle should be capable of protecting sensitive biomolecules from enzymatic degradation, hydrolysis, oxidation, and other forms of degradation that occurs *in vivo*. Drug delivery vehicles that protect biomolecules sufficiently may even play an important role in developing oral vaccines.

The final challenge that will be discussed in connection with vaccine delivery is the co-delivery of both an antigen and adjuvant. Immune cells must receive a secondary activation signal upon recognizing an antigen. In the case of actual infections, pathogen associated molecules such as lipopolysaccharides, components of bacterial cell walls, and specific forms of nucleic acids (double stranded RNA, single stranded DNA, and unmethylated CpG DNA sequences) all may serve as the secondary activation signal. With a vaccine, these secondary signals are artificially introduced through the use of an adjuvant molecule. Common adjuvants are inorganic aluminum salts such as aluminum phosphate and aluminum hydroxide. These inorganic adjuvants work by inducing inflammation at the vaccine injection site, which causes the release of cytokines, chemokines, and other immunomodulators by inflammatory cells. These inflammatory markers act as the necessary secondary activation signals needed for the antigen presenting cells to mature. New

research is being done to explore the use of biomolecules that may serve as adjuvants in place of the inorganic salts. These biological adjuvants function independent of inflammation and therefore are able to reduce the inflammatory side effects associated with traditional adjuvants. However, an immune cell must encounter and engulf both an antigen molecule and an adjuvant molecule at once or the immune cell may become desensitized to the antigen and recognize it as self, making it difficult or impossible to later activate against that antigen. Drug delivery vehicles can play a key role in overcoming this challenge, as many are able to encapsulate and deliver more than one cargo in a single vehicle.

1.3.2 Systemic delivery challenges

Systemic delivery differs from vaccine delivery in that vaccine delivery has the goal of delivering the cargo directly to the immune system while systemic delivery is required to evade the immune system in order to increase the circulation half-life. As was discussed in previous sections, there are several commonly used strategies employed to evade the immune system and increase circulation half-life with the most common strategy being a PEG coating.(70-73) The PEG coating acts to stabilize and prevent protein adsorption onto the

particle surface.(71) As proficient as PEG may be in increasing the circulation half-life of drug delivery vehicles, it may be detrimental to the efficient delivery of the cargo into the cytosol of the cell once the vehicle arrives at its destination.(74, 75) The PEG layer may prevent the particle from being taken up into the cell or prevent it from escaping the endosome after being endocytosed.(76)

If the drug delivery vehicle cannot deliver its cargo to the interior of the cell where it can be active, the benefits of using a drug delivery vehicle are greatly diminished. Developing a drug delivery vehicle that is simultaneously able to maintain a long circulation half-life while also being able to deliver its cargo to the interior of the cell remains a key challenge in systemic delivery.

Although PEG was previously thought to be non-immunogenic, the human immune system is incredibly complex and adaptive and it has been shown that PEG can cause immunogenicity.(77, 78) According to one study, 25% of Americans were shown already to have anti-PEG antibodies in detectable in their bloodstream.(79) Another study showed accelerated blood clearance after repeated dosing with PEGylated nanoparticles.(80) As we have learned from the over prescription of antibiotics and the resulting 'superbugs', it is unwise to rely on a single technology to solve a problem when dealing

with a highly adaptive system. A replacement system for PEG that maintains the long circulation times for drug delivery vehicles is necessary in order to avoid causing adverse reactions in individuals in which PEG causes and immune reaction.

The remainder of this dissertation will focus on novel drug delivery systems that address these challenges with both vaccine and systemic delivery. The primary design elements of the drug delivery vehicles will be the modification of the surface properties in order to impart bioactive or bioresponsive characteristics.

2. PLGA NPs as a Vaccine Drug Delivery Vehicle

2.1 Introduction

Vaccination remains the most successful prophylaxis for infectious disease and in the past decades it has also been explored as an approach to prevent or cure cancer.(27, 28) Since peptides tend to be unstable *in vivo*, NPs can protect them from degradation and potentially increase the immune response to peptide and possibly protein vaccines. Encapsulation of antigen peptides into biodegradable spheres has been shown to increase MHC-class-I presentation.(23) Delivery of OVA protein as antigen in Poly-g-Glutamic acid nanoparticles (gPGA-NPs) lead to increased immune

responses in comparison to vaccinations using the same amount of free OVA protein.(81) Additionally, enhanced immune responses were observed when the cancer associated antigen MUC-1(82, 83) as well as Tetanus Toxoid (25) was delivered using Poly-lactic-glycolic acid nanoparticles (PLGA-NPs).(26)

Dendritic cells (DCs) are the most potent antigen-presenting cells and central for the initiation of adaptive immune responses.(16) Figure 2.1 shows the intercellular relationships the DCs have with other important immune cells. DCs need to receive a maturation signal in order to present antigen, upregulate co-stimulatory and adhesion molecules, and become potent activators of T cells. Antigen-displaying mature DCs can then activate T cells to act as CTLs. Collaborating researchers previously identified several immunostimulatory peptides (ISPs), derived from the endogenous protein HMGB1, which can activate both mouse and human DCs.(84) It was shown that the 18 aa long ISP named Hp91, when used to activate DCs, can induce potent antigen-specific CTL responses(85). Due to their immuno-activating properties, ISPs are attractive candidates for vaccine adjuvants. In an effort to develop ISPs for vaccine adjuvant usage, we evaluated whether Hp91 could be incorporated into PLGA (poly-DL-lactic-*co*-glycolic acid) nanoparticles

(PLGA-NPs) and still maintain its activity. PLGA was chosen as material for our NPs, since it is a biodegradable and biocompatible polymer (18, 52, 53, 86) which has been employed for numerous *in vivo* applications. (87-89) In addition, polymeric NPs are more stable in the gastrointestinal tract as compared to other carriers like liposomes and can be used for oral vaccine development.(90) Different composition polymers allow for controlled and prolonged release of cargo, allowing for antigen depot formation at the injection site, again another major advantage for vaccine development.(91) We found that delivery of Hp91 inside as well as conjugated to the outside of PLGA-NPs not only preserved their DC stimulatory capacity, but was more potent as compared to free Hp91 peptide. Thus, delivery of ISPs inside or outside of PLGA-NPs is a promising delivery platform for subunit vaccines of infectious disease and cancer.

2.2 Experimental Methods

2.2.1 Peptides

Peptides were purchased with an N-terminal biotin at 97% purity from Genscript Corporation (Piscatway, NJ). The peptides contain the

following sequences: Hp91: DPNAPKRPPSAFFLFCSE and Hp121: SIGDVAKKLGEMWNNTAA. When used as free peptide, the peptides were dissolved at 2 mg/ml in 5% DMSO/RPMI.

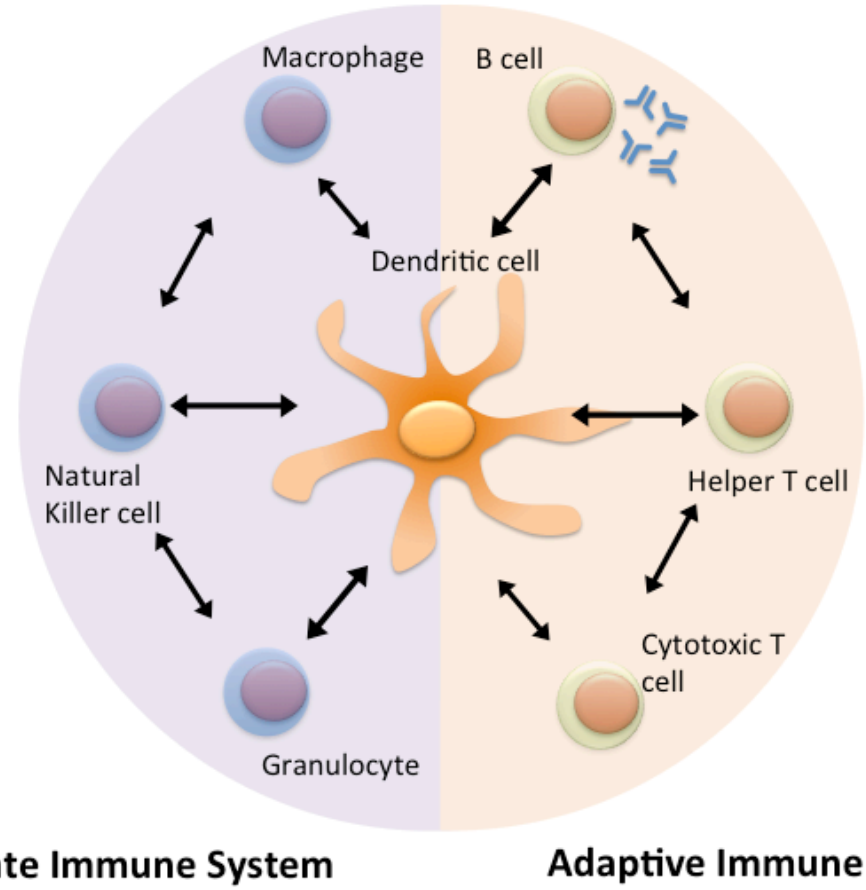

Figure 2.1. Dendritic cells are professional antigen presenting cells and are at the center of the immune system, interacting with other immune cells to mediate an immune response.

2.2.2 Synthesis of PLGA nanoparticles

PLGA (poly-DL-lactic-*co*-glycolic acid) nanoparticles (NPs) that carried the immunostimulatory peptide Hp91 peptide inside or on the outside were synthesized. Whether the nanoparticles had Hp91 inside or outside, bovine serum albumin (BSA) was encapsulated inside to serve as a model antigen. Nanoparticles that contained only the bovine serum albumin, absent the Hp91 adjuvant, were synthesized to serve as "carrier" control.

The particles were made using the water-in-oil-in-water (w-o-w) double emulsion method. The PLGA co-polymer (polymer ratio 50:50) was dissolved at 25 mg/ml in chloroform and vortexed for 1 hour. To make a 30 mg batch of PLGA-NP loaded with Hp91, Hp91 was dissolved in DMSO at 20 mg/ml and 30 μl was added to 270 μl of an aqueous BSA solution (10 mg/ml). As a control, 300 μl BSA solution was used to make empty NPs. The Hp91/BSA solution was added to the PLGA dissolved in chloroform, and then vortexed and sonicated. This created the first emulsion (water in oil). Subsequently this mixture was slowly added to 10x the volume of 2% (w/v) polyvinyl alcohol and the emulsion was vortexed and sonicated to create the double emulsion. The double emulsion was stirred over night at RT to evaporate off the

chloroform, solidifying the particles. The next day the emulsion was stirred under a dessicator in vacuum to remove the remaining chloroform. The particles were washed 3 times with LPS-free water (Thermo Scientific, HyClone Laboratories, Inc., Logan, UT) by ultracentrifugation for 30 min at 30,000 rpm (Beckman Coulter Optima L-90K Ultracentrifuge) and the PLGA-NP were lyophilized for storage at -20°C. PLGA-NPs were dissolved in PBS at 1mg/ml before addition to the cells.

Hp91 was conjugated to the surface of empty NPs using the linker molecule Denacol EX-521 (Figure 2.2). NPs were suspended in borate buffer (pH5) containing Denacol EX-521 (linker) and zinctetrafluroborate hydrate (catalyst). The sample was mixed by vortexing and sonication. For activation of the NPs, the sample was stirred for 30 min at 37°C. To remove un-reacted Denacol, the activated NPs were washed with water by ultracentrifugation and resuspended in borate buffer. To couple the Hp91 peptide, the peptide was dissolved in DMSO and borate buffer and added to the activated NPs. The reaction was carried out for 2h at 37°C under constant stirring. Excess unbound peptide was removed by ultracentrifugation and the samples were lyophilized for storage. The

amount of Hp91 on the surface of NPs was quantified by HPLC. PLGA-NPs were dissolved in PBS at 1mg/ml before addition to the cells.

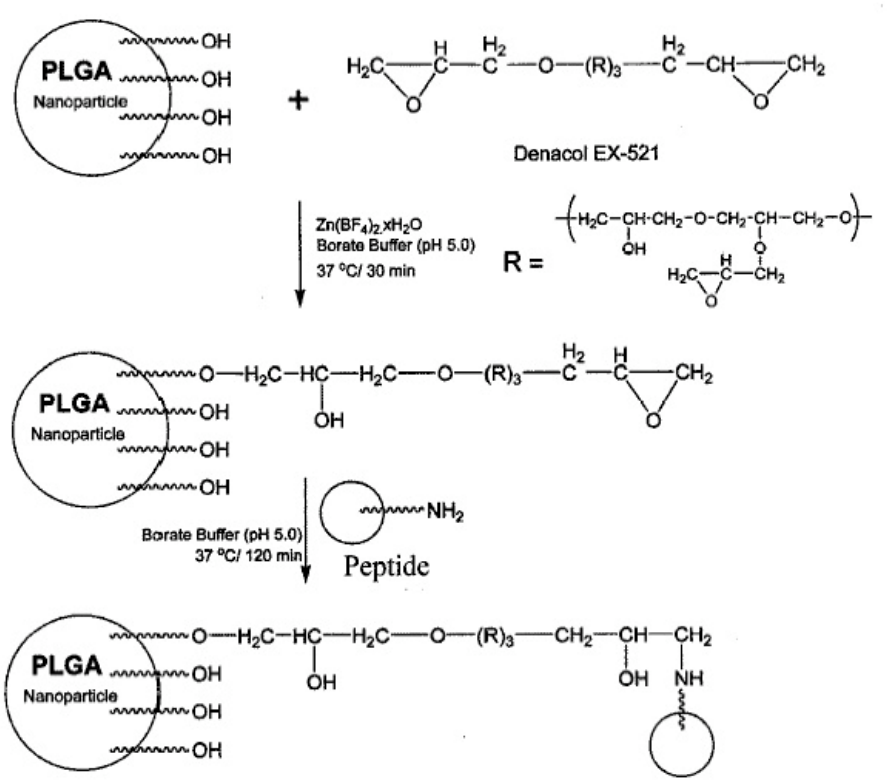

Figure 2.2. Synthesis scheme for conjugation of Hp91 to the surface of PLGA-NPs.

2.2.3 Characterization of PLGA-NPs

The NP formation was analyzed for particle size by dynamic light scattering (DLS) using a Zetasizer Nano ZS (Malvern, Worcestershire, UK). A spectral scan of the Hp91 peptide was performed and the peptide but not the polymer was detected at 211 nm. To quantify the amount of Hp91 present inside or on the surface of the PLGA-NPs, per mg NPs, the NPs were weighed and then dissolved in acetonitrile for 30 min (for NPs loaded with Hp91 inside) or over night (for NPs with Hp91 conjugated to the outside) under constant shaking at room temperature and peptide content was quantified by HPLC (column: WATERS DELTA PAKC18 5 microns, Waters Corporation, Milford, MA) at 211 nm in comparison to a Hp91 standard curve.

To measure stability of the peptide-NPs, 100 ml of particle solution was added to multiple micro dialysis cassettes with a cutoff of 10,000 MW and dialyzed against 1 L of PBS buffer at pH 7.4 or potassium hydrogen phthalate buffer at pH 5. At each time point, two samples were recovered from the micro dialysis cassettes for each buffer condition and the volumes were brought up to 125 ml to keep all volumes constant. To each sample, 125 ml of acetonitrile was added to dissolve the PLGA-NPs and release the remaining Hp91 peptide. The samples were shaken for 1

hour and then the total amount of Hp91 in each sample was quantified using HPLC. The amounts were normalized against the starting concentration of Hp91 before dialysis, which was set at 100% to calculate the percent release.

In order demonstrate that the peptide was covalently linked to the PLGA particles and not only adsorbed to the surface, 100 ml of Hp91 conjugated PLGA-NPs were sonicated for 3 min and the supernatant was removed using a 10k Microcon Amicon spin column (Millipore, Billerica, MA). As control, 10 ml of Hp91 conjugated PLGA particles were filtered using the spin column without the sonication step. Both the filtrate and the retentate were analyzed for peptide content by HPLC.

2.2.4 Atomic force microscopy

AFM experiments were performed with a Multimode V SPM system (Veeco Instruments Inc.). Height, amplitude, and phase images were obtained in tapping mode in ambient environment with Tapping Mode Etched Silicon Probes (TESP, Veeco Instruments Inc.). Only phase images are shown unless specified. The scan rate is 0.5Hz. Here, AFM phase imaging is used to provide nanometer-scale information about surface structure. During the topographic tapping mode scan, the

AFM phase lag of the cantilever oscillation is simultaneously monitored, which is very sensitive to variations in material properties.

2.2.5 Animals

FVB.N*neu*-tg mice were derived from in house breeding stocks at the Moores UCSD Cancer Center animal facility. All animal studies were performed with human care of animals and approved by the Institutional Animal Care and Use Committee of UCSD and were performed in accordance with the institutional guidelines.

2.2.6 Generation of mouse BM- DCs

Bone marrow-derived dendritic cells (BM-DC) were prepared from HER-2/*neu* transgenic mice (H-2^q) as described by Inaba et al. (92) with minor modifications. Briefly, single bone marrow cell suspensions were obtained from femurs and tibias, depleted of lymphocytes, granulocytes, and Ia^+ cells using a mixture of monoclonal antibodies (anti-CD4, anti-CD8, anti-B220/CD45R, and anti-Ia) for 45 min on ice, followed by incubation with low-toxicity rabbit complement for 30 min at 37°C. Cells were resuspended at a concentration of 10^6 cells/ml in medium supplemented with

recombinant murine GM-CSF (10ng/ml). Fresh media (RPMI/5%FCS) containing GM-CSF was added on days 2 and 4 of culture. On day 6 cells were collected for the experiments.

2.2.7 Generation of human monocyte-derived DCs

Peripheral blood mononuclear cells (PBMCs) were isolated from the blood of normal volunteers over a Ficoll-Hypaque (Amersham Biosciences, Uppsala, Sweden) density gradient. Anonymous blood was purchased from the San Diego Blood Bank, thus no IRB approvals are needed. To generate DCs, PBMCs were allowed to adhere to culture plates for 1h. The non-adherent cells were washed off and the adherent cells were cultured in RPMI 1640 medium supplemented with 2 mM L-glutamine (GIBCO-BRL Life Technologies; Grand Island, NY), 50 mM 2-mercaptoethanol (Sigma, St. Louis, MO), 10 mM HEPES (GIBCO-BRL), penicillin (100 U/ml)-streptomycin (100 mg/ml) (GIBCO-BRL), and 5% human AB serum (Human AB serum, Gemini Bio Products West Sacramento, CA), supplemented with 1000 U/ml GM-CSF (Bayer HealthCare Pharmaceuticals (Wayne, NJ) and 200 U/ml IL-4 (R&D Systems, Minneapolis, MN) at days 0, 2, and 4. Immature DCs were harvested on days 5-7.

2.2.8 Stimulation of DCs

10^5 immature DCs were incubated in 100 ml culture media with the indicated amounts of empty or peptide carrying NPs, free Hp91 peptide, free Hp121 peptide, a cocktail of inflammatory cytokines (CyC) consisting of IL-1b at 10 ng/ml, TNF-a at 10 ng/ml (R&D Systems), and PGE2 at 1 mg/ml (Sigma), or 10 ng/ml LPS (Sigma). 48h after activation the cell culture supernatants were collected and analyzed for cytokines by ELISA (eBioscience, Inc. San Diego, CA).

2.2.9 Analysis of DC phenotype

DCs were incubated for 20 min at 4°C in 100 ml of PBS/5% FCS/0.1% sodium azide (staining buffer) with Phycoerythrin-conjugated IgG mAb specific for CD80 and CD40, and APC-conjugated IgG mAb specific for CD11c (eBioscience). Cells were washed four times with staining buffer, fixed in 3.7% formaldehyde in PBS (pH 7.2–7.4), and examined by flow cytometry using the FACSCalibur (Beckon Dickinson). In all experiments, isotype controls were included using irrelevant mAb of the same Ig class conjugated to the same fluorophor. Data was

analyzed using the FlowJo 7.2.2 software. Data are shown as mean fluorescence intensity gated on CD11c+ cells.

2.2.10 Statistical analysis

Data are represented as mean +/- SD if not otherwise indicated. Data were analyzed for statistical significance using Student's t-test. p-values < 0.05 were considered statistically significant.

2.3 Results and Discussion

2.3.1 Characterization of PLGA-NPs

To demonstrate the presence of Hp91 on the surface of the PLGA-NPs, we applied atomic force microscopy comparing empty PLGA-NPs to PLGA-NPs that have been conjugated with Hp91 (NP-Hp91). PLGA-NPs with peptide show a rough surface, note arrows (Figure 2.3 right image) compared to empty PLGA-NPs generated in the absence of peptide (Figure 2.3 left image). Although AFM only indicates the presence of protein on the PLGA-NP surface, since the difference in synthesis was presence or absence of Hp91, we conclude

that the detected protein on the surface is Hp91. The presence of Hp91 on the PLGA-NP surface was confirmed and quantified by HPLC at 211 nm, which detected peptide in the preparation with Hp91 on the PLGA-NP surface, but not on empty NPs. As measured by HPLC 112 mg Hp91 were conjugated per mg PLGA-NP. These data indicate that we successfully conjugated Hp91 to the outside of the PLGA-NPs.

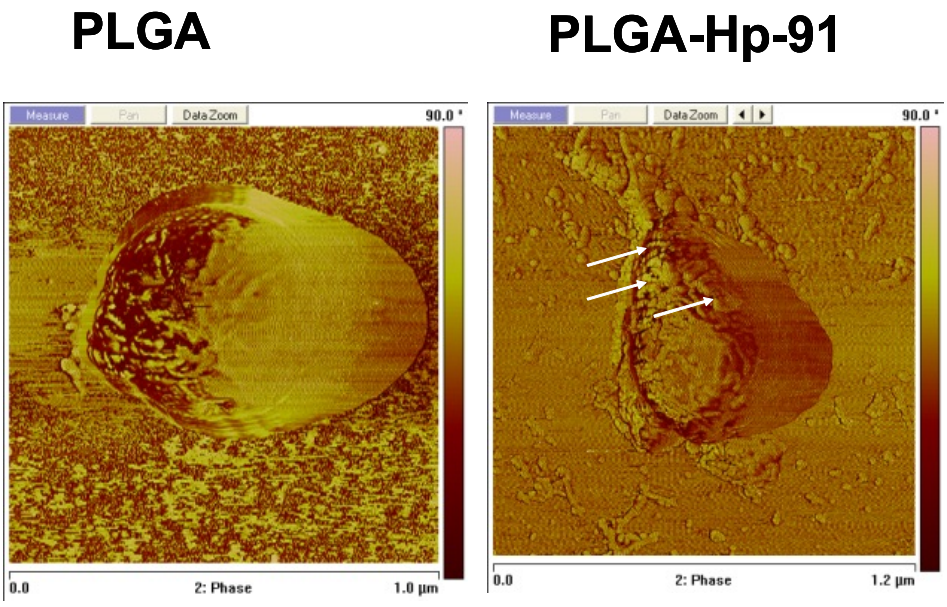

Figure 2.3. Atomic force microscopy phase images of empty NPs and NPs conjugated with Hp91. Arrows point to the areas where peptide was detected on the NP surface.

In order to test whether or not the peptide was covalently linked to the PLGA particles or only adsorbed to the surface, the peptide-conjugated PLGA-NPs were sonicated to release loosely bound peptide, spun down using a using a 10k Microcon Amicon spin column, and the supernatants were analyzed for the presence of peptide by HPLC. After sonication for 3 min, approximately 4.4% of the total Hp91 was measured in the supernatant, while the majority of the peptide, 95.6% was still associated with the particles. Peptide-conjugated PLGA-NPs that were not sonicated, but simply filtered in the same manner, only 0.06% of the Hp91 was measured in the filtrate and 99.9% of the Hp91 remained associated with the particles.

We noted that the PLGA-NPs showed some level of aggregation when observed under the light microscope. In order to improve on the synthesis scheme we investigated at what stage of the synthesis process the aggregation occurred. The size distribution of the PLGA-NPs was measured by dynamic light scattering (see Materials and Methods) after each of the three ultracentrifugation spins which were used to remove un-incorporated peptide from the NPs. Only a slight increase in size was observed. The average size of the PLGA-NPs was 201, 235, and 243 nm after the first to third wash respectively (Table 2.1). Since the NPs were lyophilized for long-term storage, the NP size was

measured before lyophilization and after resuspension of the lyophilized NPs. After resuspension of the lyophilized NPs their average size was 1365 nm (Figure 2.4), which indicates formation of small aggregates/quadruplets

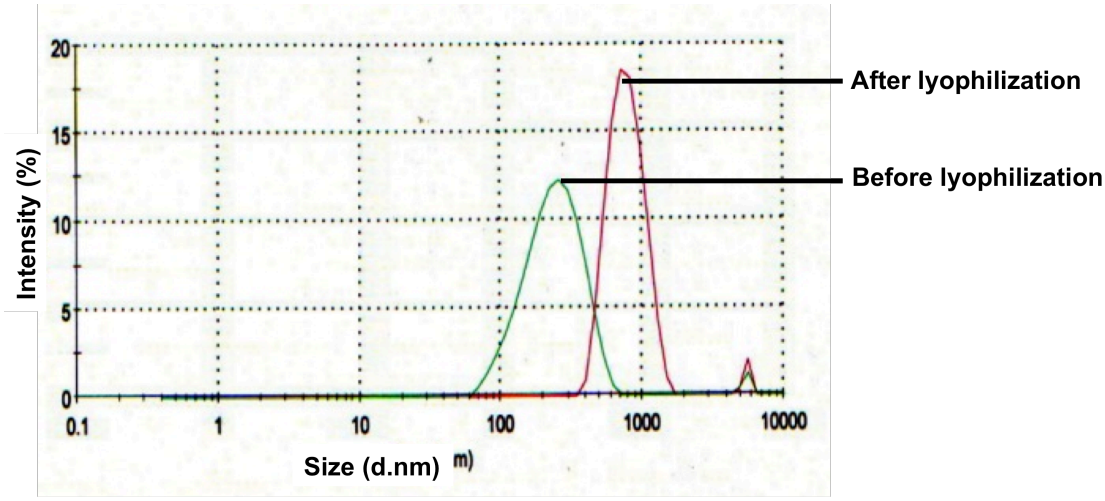

Figure 2.4. The size distribution of PLGA-NPs was analyzed before and after lyophilization by dynamic light scattering. The x-axis represents the size in nm.

Table 2.1. PLGA nanoparticles size distribution during preparation.

Number of washes	Size of PLGA-NPs (nm)*
One	201
Two	235
Three	243

*The size distribution of poly(D,L-lactic-co-glycolic) acid nanoparticles (PLGA-NPs) was measured by Zetasizer Nano ZS (Malvern Instruments) after each of the three washes of ultracentrifugation.

Next, we tested whether sonication for prolonged periods for time would dissolve the aggregates. NPs were measured after different sonication times (1 to 30 min). After 30 min of sonication their size was reduced from 1365+/- 906 to 648+/- 254 nm (Table 2.2). This decrease in size after sonication indicates that although the big aggregates were disrupted, some small aggregates, most likely duplets, were still present. Since the aggregation occurred in the lyophilization step, for all subsequent experiments, the NPs were not lyophilized, but instead stored in a mixture of water/10% sucrose at -20°C to avoid aggregation.

Table 2.2. PLGA nanoparticles size distribution after sonication.

[a] **PLGA-NP sonication time (min)**	[b] **Size of PLGA-NP (nm)**
1 min	1365 +/- 906
15 min	791 +/- 111
30 min	648 +/- 255

[a] PLGA nanoparticles were lyophilized after the final wash and resuspended in PBS. The suspension was then sonicated for 1, 15, or 30 min at 40 kHz in an iced sonicator waterbath (Brandon; Model 2510).

[b] The NP size distribution (+/- SD) was measured by dynamic light scattering using three different batches of NPs after the different sonication times: 1, 15, and 30 min.

We hypothesized that non-aggregated PLGA nanoparticles are more potent than aggregated particles due to the increased surface area. To test this hypothesis lyophilized NPs that were conjugated with Hp91 on the surface were resuspended in PBS and compared to NPs that had never been lyophilized, but were instead frozen in PBS/10%sucrose solution immediately after synthesis. Immature human DCs were generated as we have previously described (84) and exposed to empty PLGA-NPs, previously lyophilized PLGA-NPs containing Hp91, and non-lyophilized PLGA-NPs containing Hp91 (Figure 2.5). As expected the particles that were stored in solution (non-lyophilized) and had very few aggregates if any, caused increased activation of DCs even at the lower amount tested.

We next measured the stability of the Hp91 conjugated to the surface of PLGA-NPs (Figure 2.6). After approximately 3 h, 50% of the conjugated peptide is released from the PLGA-NPs at pH 7.4 and pH5. Although the lower pH results in a slower release of the conjugated peptide than at neutral pH, the difference is not as significant as that for the encapsulated peptide at different pH (Figure 2.6 B). After 3 hours, the release rate begins to flatten out for both pH conditions. After 36 h, PLGA-NPs at pH 7.4 have released approximately 72% of the conjugated peptide, while at pH 5 approximately 50% of the peptide is released.

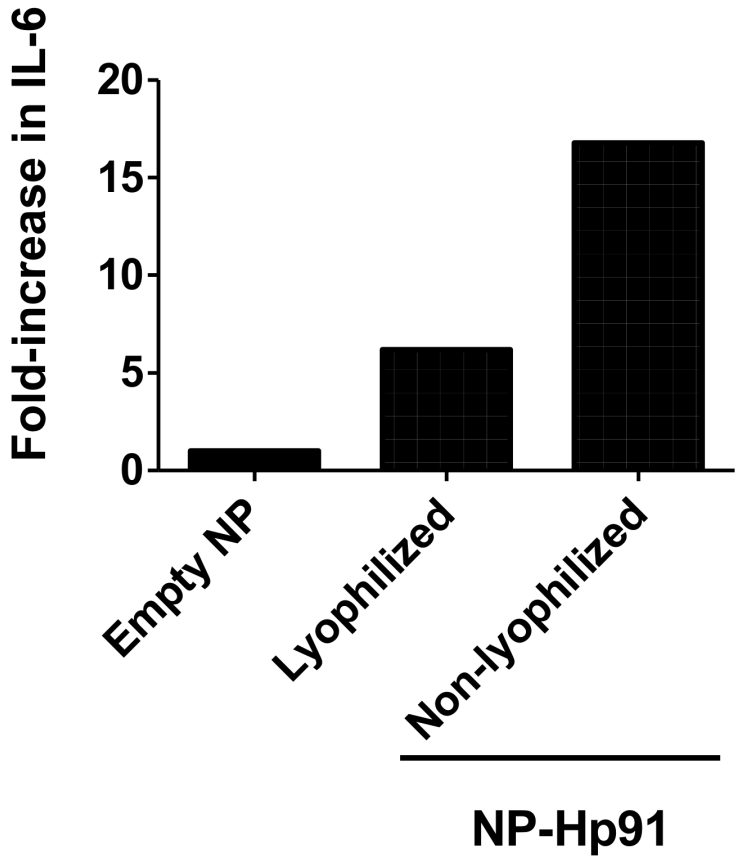

Figure 2.5. Human immature DCs were exposed to media, empty NPs (300 mg/ml), lyophilized PLGA-NPs containing Hp91 (300 mg/ml), and non-lyophilized PLGA-NPs containing Hp91 (240 mg/ml) for 48h. Cell culture supernatants were collected and analyzed for IL-6 by ELISA. Depicted is a representative result showing fold-increase in IL-6 secretion as compared to the empty NP control, which was set as 1.

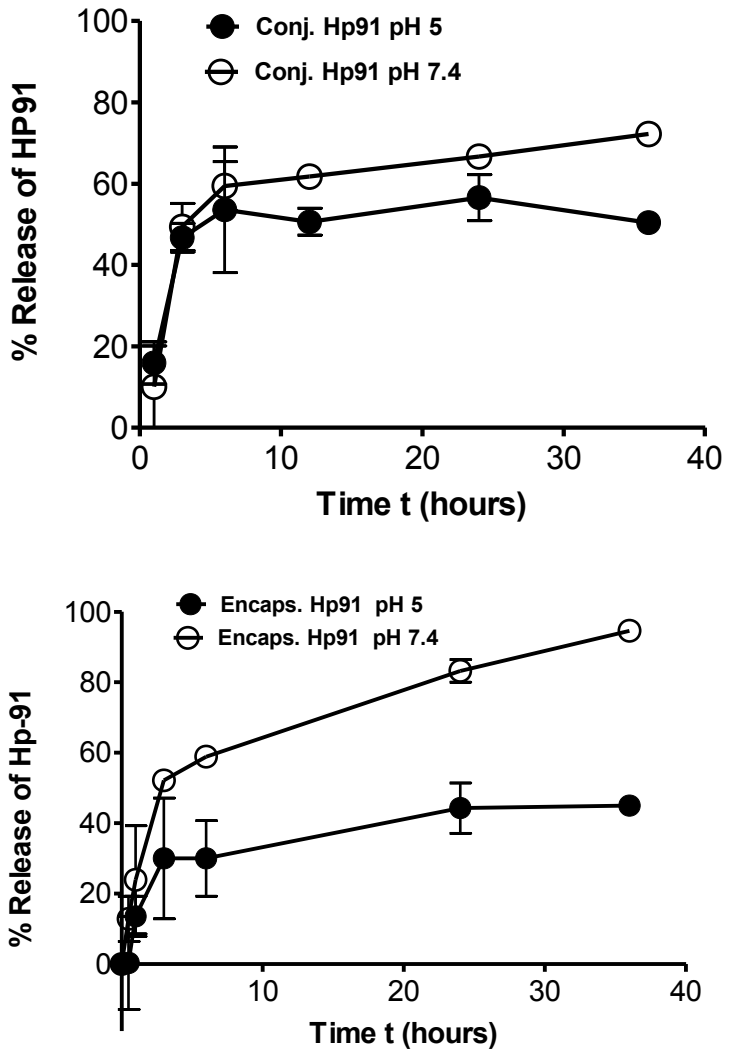

Figure 2.6. A) Hp91 conjugated to the surface of PLGA-NPs. B) PLGA-NPs with Hp91 encapsulated inside the NPs. The graphs show release profiles of Hp91 peptide from PLGA -NPs at pH 7.4 and pH 5 over 36 h. The peptide input at time 0 is set as 100%. Samples were taken at the indicated time points and the amount of peptide in PLGA-NPs was quantified by HPLC. Data shown are mean +/-SEM of triplicate measurements.

A similar trend was observed with Hp91 loaded PLGA-NPs with stronger peptide release at higher pH (Figure 2.6 B). After approximately 3h 50% of the peptide is released from within the PLGA-NPs at pH7.4 and after 36 h, 95% of the peptide is released from the PLGA particles in pH 7.4, while only 45% is released from the PLGA-NPs at pH 5. Both conditions produce an initial burst release with a large proportion of the released peptide being released within the first 3 hours. After 3h, both curves flatten out and the release rate is reduced; however, the PLGA-NPs at pH 7.4 continue to release at a higher rate than at pH 5 throughout the time course (Figure 2.6 B).

2.3.2 Hp91 conjugated to the surface of PLGA-NPs induces cytokine secretion in human DCs

DC activation is characterized by the secretion of inflammatory cytokines such as IL-6.(93) It was previously shown that an 18-amino acid long peptide Hp91, whose sequence corresponds to a part of HMGB1-Bx induced IL-6 secretion in human monocyte-derived DCs.(85) To test whether Hp91 when conjugated to the surface of PLGA-NPs maintains its DC stimulatory capacity, immature human monocyte-derived DCs were exposed to empty PLGA-NPs (NP), PLGA-NPs with Hp91 conjugated to the surface (NP-Hp91), free Hp91 peptide, or a cocktail of inflammatory cytokines (CyC) known to activate DCs. Two

days later the cell culture supernatants were collected and analyzed for the presence of IL-6 by ELISA. A highly significant increase in IL-6 secretion was observed when NP-Hp91 with a final Hp91 concentration of 11.2 mg/ml was added to DCs as compared to the same amount of empty PLGA-NPs ($p<0.0001$) and as compared to 200mg/ml of free Hp91 peptide ($p<0.0001$) (Figure 2.7). At 11.2 mg/ml Hp91 when conjugated to the surface of PLGA-NPs induced 3,923 (+/- 410) pg/ml IL-6, whereas 200 mg/ml free Hp91 induced only 1,485 (+/- 376) pg/ml IL-6. This is a 47-fold increased in IL-6 secretion when normalized for the same amount of Hp91. In addition Hp91 conjugated to the PLGA-NP surface induced higher IL-6 secretion as compared to a cocktail of inflammatory cytokines CyC known to mature DCs.(94) When lower amounts of Hp91 (1.12 mg/ml) conjugated to the PLGA-NP surface were used, although an increase in IL-6 was observed, the differences as compared to the controls were not significant (Figure 2.7).

2.3.3 Hp91 conjugated to the surface of PLGA-NPs causes cytokine secretion in mouse BM-DCs

To determine whether PLGA-NPs carrying Hp91 on the surface also elicit cytokine secretion in mouse DCs, immature mouse bone marrow

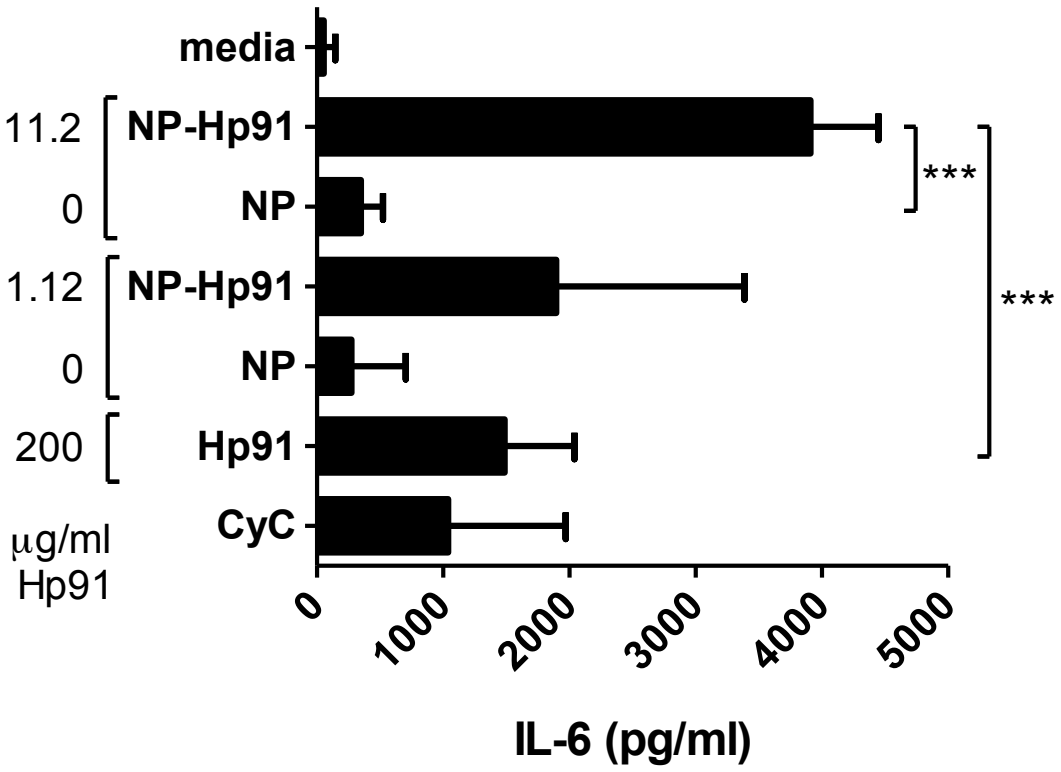

Figure 2.7. *Hp91 conjugated to the outside of PLGA-NPs causes stronger activation of human DCs as compared to free peptide.* 10^5 immature human DCs were exposed to media, PLGA-NPs carrying Hp91 on the surface (Np-Hp91) with 2 concentrations of Hp91: 11.2 and 1.12 mg/ml, empty NPs matching the amount of PLGA-NPs used with peptides (as NP control), 200 mg/ml of free Hp91 peptide, or a cytokine cocktail CyC (see methods for composition). Cell culture supernatants were collected after 48h and analyzed for IL-6 by ELISA. Data shown is mean +/-SD of three independent experiments using DCs from different donors. * indicates a statistically significant increase.

derived DCs (BM-DCs), were generated as previously described (85), and exposed to media only, indicated doses of empty PLGA-NPs (NP) (as particle control; matching the amount of PLGA-NP in peptide carrying PLGA-NP), 3 dilutions of PLGA-NPs that have been conjugated with Hp91 on the surface (NP-Hp91), free Hp91 peptide (200 μg/ml), or LPS (10 ng/ml) as positive control. Two days later the cell culture supernatants were collected and analyzed for the presence of IL-6 by ELISA. As observed with human DC, we found that the peptide Hp91 when conjugated to the surface of the PLGA-NPs induced high levels of IL-6 secretion. NP-Hp91 with a final peptide concentration of 34 μg/ml Hp91 induced an average of 5050 +/- 277 pg/ml IL-6, which was significantly higher than empty NPs at the same dose ($p=0.008$) and than 200 μg/ml free Hp91, which induced an average of 1446 +/- 559 pg/ml IL-6 ($p=0.01$) (Figure 2.8 A). When normalized to the amount of Hp91, Hp91 is ~20-fold more potent when delivered on the surface of PLGA-NPs as compared to free Hp91. NP-Hp91 with a final peptide concentration of 3.4 μg/ml Hp91 elicited significant IL-6 expression as compared to empty NPs at the same dose ($p=0.03$), but it was not significantly different from 200 μg/ml of free Hp91 (Figure 2.8 A).

Figure 2.8. *Hp91 conjugated to the outside of PLGA-NPs causes stronger activation of mouse DCs as compared to free peptide.* 10^5 immature mouse BM-DCs were exposed to media only, PLGA-NPs carrying Hp91 on the surface (Np-Hp91) with 3 concentrations of Hp91: 34, 3.4, and 0.34 μg/ml, empty NPs matching the amount of PLGA-NPs used with peptides (as NP control), 200 μg/ml of free Hp91 peptide, or LPS (10 ng/ml). A) Cell culture supernatants were collected after 48h and analyzed for the presence of IL-6 by ELISA. Data shown is mean +/-SD of two independent experiments using DCs from different donors. B, C) Cells were collected 48h after exposure to the different NP conditions and analyzed for the expression of CD40 and CD80 by surface membrane immunofluorescence techniques using fluorophor conjugated mAbs. DCs were gated on CD11c+ cells and analyzed for expression of the indicated markers. B) depicts percent positive cells and C0 depicts mean fluorescence intensity (MFI). Data shown is mean +/-SD of three independent experiments using DCs from different donors. * indicates a statistically significant increase.

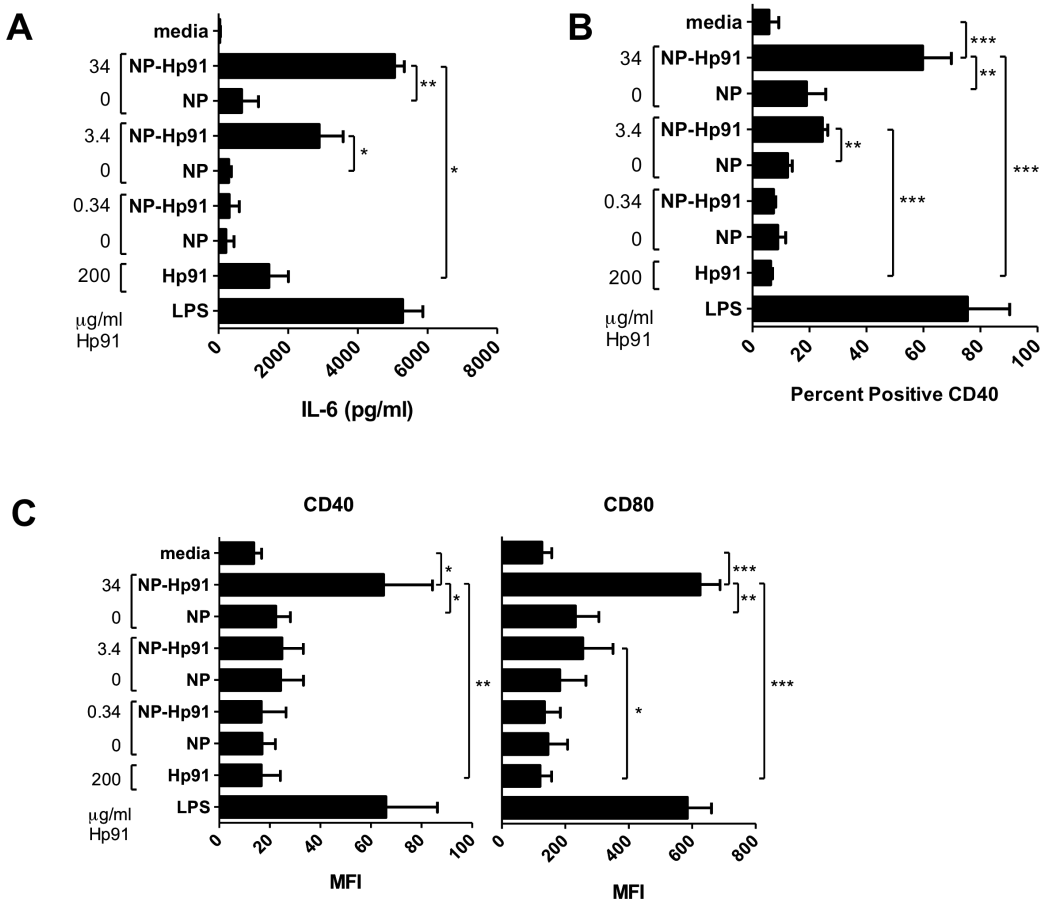
A
media
34
NP-Hp91
0
NP
3.4
NP-Hp91
0
NP
0.34
NP-Hp91
0
NP
200
Hp91
LPS
μg/ml Hp91
0
2000
4000
6000
8000
IL-6 (pg/ml)
B
media
34
NP-Hp91
0
NP
3.4
NP-Hp91
0
NP
0.34
NP-Hp91
0
NP
200
Hp91
LPS
μg/ml Hp91
0
20
40
60
80
100
Percent Positive CD40
C
CD40
CD80
media
34
NP-Hp91
0
NP
3.4
NP-Hp91
0
NP
0.34
NP-Hp91
0
NP
200
Hp91
LPS
μg/ml Hp91
0
20
40
60
80
100
MFI
0
200
400
600
800
MFI

2.3.4 Hp91 conjugated to the surface of PLGA-NPs induces phenotypic maturation of mouse BM-DCs

To determine whether Hp91 when conjugated to the surface of PLGA-NPs can induce phenotypic maturation of mouse BM-DCs, immature BM-DCs were exposed to empty PLGA-NPs (NP), PLGA-NPs with Hp91 conjugated to the surface (NP-Hp91), free Hp91 peptide, or bacterial lipopolysaccharide (LPS), which served as positive control. After 48h cells were harvested and analyzed for surface expression of CD40, CD80, and MHC class II by flow cytometry (Figure. 2.8 B,C). Empty PLGA-NPs did not cause any changes in CD40 and CD80 expression, but they increased MHC II expression in immature DCs by 2-fold as compared to media control. However, no additional changes in MHC II expression were observed with peptide loaded NPs (data not shown). Interestingly, although free HP91 peptide did not increase expression of CD40 or CD80, Hp91 conjugated to the surface of PLGA-NPs caused a significant increase in CD40 and CD80 expression levels comparable to those induced by LPS (Figure. 2.8 B,C). During the process of DC maturation some surface molecules are weakly expressed on immature DCs and are upregulated upon activation. This manifest itself as an increase in mean fluorescence intensity (MFI) when measuring expression levels by flow cytometry. Other surface molecules are not or barely expressed on immature DCs and the

percentage of cells positive for those molecules can increase upon activation.

On immature DCs (=media control) only a small percentage of DCs in the population expressed CD40 (Figure 2.8 B) and on those the expression was very low (Figure 2.8 C). After exposure to NP-Hp91 with a final Hp91 concentration of 34 mg/ml, the number of CD40 positive DCs significantly increased in comparison to media control ($p=0.0009$) and to empty NPs at the same concentration ($p=0.004$) (Figure 2.8 B). Furthermore, NP-Hp91 with 34 μg/ml of Hp91 elicited a highly significant increase in the percentage of CD40 positive cells as compared to 200 μg/ml of free Hp91 ($p=0.0008$). The same was true for the lower concentration of NP-Hp91 with 3.4 mg/ml of Hp91. Even the low dose of peptide (3.4 μg/ml), NP-Hp91 elicited a significant increase in the percentage of CD40 positive DCs as compared to media control ($p=0.04$), the same dose of empty NPs ($p=0.001$), and 200 μg/ml of free Hp91 ($p<0.0001$) (Figure 2.8 B).

In addition to the increase in the number of CD40-positive DCs, NP-Hp91 with 34 μg/ml of Hp91 elicited a significant increase in CD40 cell surface expression levels as compared to media ($p=0.01$), empty NPs at the same concentration ($p=0.02$), and as compared to 200

mg/ml of free Hp91 (p=0.005) (Figure 2.8 C). Although lower amounts NP-Hp91 with a final concentration of 3.4 μg/ml of Hp91 significantly increasing the number of CD40 positive DCs (Figure 2.8 B), no significant increase in CD40 expression were observe additionally (Figure 2.8 C).

In the case of CD80, the majority of the immature DCs (~80%) within the population were already positive for CD80, although the expression levels were very low (Figure 2.8 C), there was no further increase in the number of positive cells (data not shown). However, NP-Hp91 with 34 μg/ml of Hp91 elicited a highly significant increase in CD80 cell surface expression levels as compared to media (p=0.0002), empty PLGA-NPs at the same concentration (p=0.002), and as compared to 200 μg/ml of free Hp91 (p<0.0001) (Figure 2.8 C). Lower amounts NP-Hp91 with a final concentration of 3.4 μg/ml of Hp91 did not significantly increase the CD80 expression levels as compared to empty PLGA-NPs at the same concentration, but did cause a significant increase as compared to 200 μg/ml of free Hp91 (p=0.04) (Figure 2.8 C). Hence Hp91 when delivered on the surface of PLGA-NPs not only maintains its ability to activate DCs, but the peptide is much more potent as a result and gained additional functions like

induction of surface molecule expression on DCs, which is very favorable for vaccine adjuvants.

2.3.5 Delivery of Hp91 inside of PLGA-NPs leads to increased activation of human DCs

We next tested whether Hp91 when packaged inside PLGA-NPs would maintain its ability to activate human DCs. Immature human DCs were exposed to media only, empty-NPs, PLGA-NPs that contained Hp91 inside the nanoparticles NP-(Hp91), and the same amount of free Hp91 peptide as present in the PLGA-NPs. Two days later the cell culture supernatants were collected and analyzed for the presence of IL-6 by ELISA (Figure 2.9 A). Hp91 loaded inside of PLGA-NPs at 9 μg/ml ($p=0.01$) and 18 μg/ml ($p=0.03$) significantly increased secretion of IL-6 by DC as compared to media control. In contrast, free Hp91 peptide at 9 or 18 μg/ml did not induce significant increase in IL-6 as compared to media control, indicating that PLGA-NP delivered Hp91 is more potent. Empty NPs did not induce significant changes in IL-6 expression. At 9 μg/ml Hp91 loaded inside of PLGA-NPs a significant increase (5-fold; ($p=0.02$) in IL-6 secretion was observed as compared to free Hp91 peptide (Figure 2.9 A). Since Hp91 was dissolved in DMSO for the synthesis of the PLGA-NPs and empty PLGA-

NPs carry BSA, we also tested the effect of BSA/DMSO added at the same dose as present in the added PLGA-NPs to DCs. No increase in IL-6 was observed under these control conditions (Figure 2.9 B). To further test whether the observed effects are due to Hp91 or simply caused by the presence of any peptide packaged inside of PLGA-NPs, we incorporated Hp121 as control peptide into PLGA-NPs. Hp121 is derived from the same molecule as Hp91, HMGB1, and we have previously shown has no activity on DCs as free peptide.(84, 85) Here we show that the control peptide Hp121, neither as free peptide, nor packages inside of PLGA-NPs induces secretion of IL-6 by human DCs (Figure 2.9 B).

We also evaluated whether PLGA-NPs exert toxic effects on DCs by comparing empty and Hp91 loaded PLGA-NPs. We did not observe any toxicity with either empty or peptide loaded PLGA-NPs in comparison to media control at doses used in these experiments even after 4 days of culture (data not shown).

Figure 2.9. *Packaging of the immunostimulatory peptide Hp91 inside of PLGA-NPs increases their potency to activate human DCs.* A) Immature human DCs were exposed to media, empty PLGA-NPs, PLGA-NPs containing Hp91 encapsulated (Np-Hp91) at 2 doses of Hp91L 9 and 18 mg/ml, or the same amount of free Hp91 peptide was added to the cells. Cell culture supernatants were collected after 48h and analyzed for IL-6 by ELISA. Data shown is mean +/-SD of three independent experiments using DCs from different donors. * indicates a statistically significant increase. B) Immature mouse BM-DCs were exposed to media only, BSA/DMSO control matching the amount present in the NP preparations, PLGA-NPs that have been filled with Hp91 (NP-Hp91) added at a final concentration of 9 mg/ml of Hp91, PLGA-NPs that have been filled with Hp121 (NP-Hp121) added at a final concentration of 4mg/ml of Hp121, free Hp91 peptide (200 mg/ml), free Hp121 peptide (200 mg/ml), or LPS (10ng/ml). 48h later the cell culture supernatants were collected and analyzed for the presence of IL-6 by ELISA. Data shown is mean +/-SD of three independent experiments using DCs from different donors. * indicates a statistically significant increase.

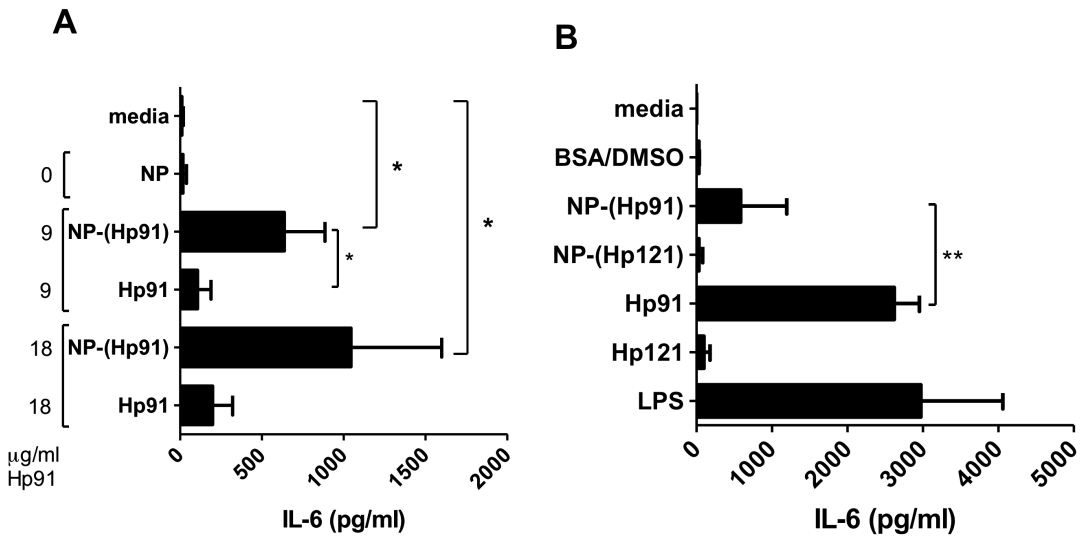
A
media
NP
NP-(Hp91)
Hp91
NP-(Hp91)
Hp91
0
9
9
18
18
μg/ml Hp91
0
500
1000
1500
2000
IL-6 (pg/ml)
*
*
*
B
media
BSA/DMSO
NP-(Hp91)
NP-(Hp121)
Hp91
Hp121
LPS
**
0
1000
2000
3000
4000
5000
IL-6 (pg/ml)

2.3.6 Hp91 packaged inside of PLGA-NPs activate mouse BM-DCs

Since increased biological activity using Hp91 loaded PLGA-NPs as compared to free peptide was observed in human DCs, we next evaluated whether the same was true for mouse BM-DCs . Immature mouse BM-DCs were exposed to media only, empty PLGA-NPs (NP), PLGA-NPs that have been filled with Hp91 (NP-(Hp91)) with the final peptide concentration being (13 μg/ml), or 200 mg/ml free Hp91 peptide. Two days later the cell culture supernatants were collected and analyzed for the presence of IL-6 by ELISA (Figure 2.10). As observed with human DCs, when Hp91 was packaged inside the PLGA-NPs the peptide maintained its ability to induce IL-6 secretion. Hp91 was delivered inside of the PLGA-NPs cause a significant increased in IL-6 expression as compared to media control ($p=0.03$) and as compared to empty NPs ($p=0.04$). At only 13 μg/ml when packaged inside the PLGA-NPs Hp91 induced in average 707 pg/ml IL-6 whereas free Hp91 at 200 μg/ml induced similar levels of 545 pg/ml of IL-6. Thus a 15-fold lower amount of Hp91 was sufficient to elicit a similar level of IL-6.

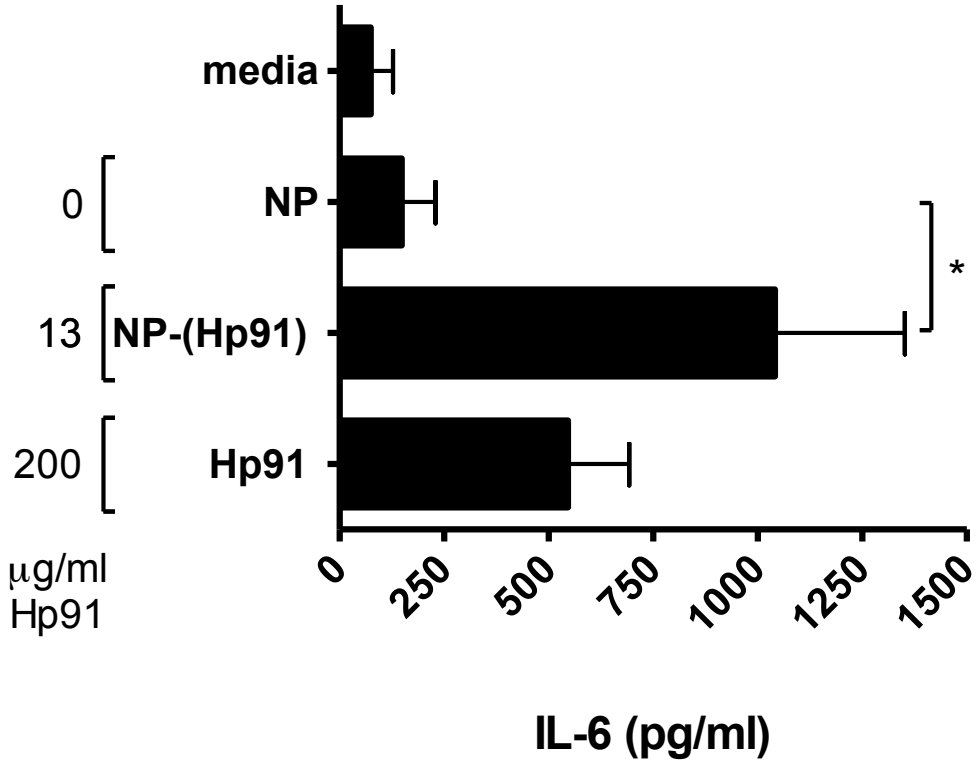

Figure 2.10. *Packaging of the immunostimulatory peptide Hp91 inside of PLGA-NPs increases their potency to activate mouse DCs.* Immature mouse BM-DCs were exposed to media only, empty-NPs, PLGA-NPs that have been filled with 13 μg/ml of Hp91 (Np-Hp91), or, free Hp91 peptide (200 μg/ml). 48h later the cell culture supernatants were collected and analyzed for the presence of IL-6 by ELISA. Data shown is mean +/-SD of three independent experiments using DCs from different donors.

2.4 Conclusion

Nano- and microparticles are being evaluated as vaccine carriers. They are very attractive platforms for vaccine delivery since antigen and adjuvant can be co-delivered to antigen presenting cells such as DCs. It has been shown that the generation of CD4 T cell epitopes requires antigen and TLR agonist (adjuvant) to co-translocate to the endosomes (95) and co-delivery of CpG-ODN together with antigen in PLGA microparticles lead to effective cross-presentation and antigen-specific CD8 T cell responses *in vivo*.(96) Another advantage of using micro- or nanoparticles (NPs) is that the cargo can be protected from degradation by serum or tissue proteases and the co-delivery of antigen and adjuvant ensures that a DC will always encounter both. This is very critical as the uptake of antigen in the absence of adjuvant can lead to generation of tolerance (17), which has to be avoided/minimized to achieve activation of effective immune responses. This is particularly important when trying to break tolerance in the context of a self-antigen for cancer immunotherapy.

Although some materials carry intrinsic adjuvant properties like pluronic-stabilized polypropylene sulfide which activates the immune

system via the complement cascade (97) or poly(g-glutamic acid) (81, 98), addition of adjuvants into NPs should further increase immune responses. In some situations inert materials might be preferable as one can control the type of immune response by selecting appropriate adjuvants for incorporation or attachement. Adjuvants like monophosphoryl lipid A (83), as well TLR agonists: CpG ODN (25, 96, 99), and pI:C (100, 101) have been packaged inside micro- and nanoparticles. Although microparticles show efficacy, depending on the route of application nanoparticles could be of further advantage. Different size NPs are preferably taken up by different cell types. For example 40-50 nm NPs are predominantly taken up by DCs, 20 nm NPs by B cells, and 1 mm NPs by monocytes/ macrophages.(102) Furthermore, it has been shown that 40 nm, but not 750 nm or larger NPs enter epidermal CD1a+ cells after transcutaneous application on human skin.(103)

We have previously shown that the 18 aa long ISP Hp91 is a potent stimulus for mouse and human DCs.(85) In an effort to further develop Hp91 as vaccine adjuvant we tested whether it could be incorporated into or conjugated to the surface of PLGA NPs. PLGA was chosen as material for our NPs, since it is a biodegradable and

biocompatible polymer (18, 52, 53, 86) that has been employed for numerous *in vivo* applications.(87-89)

We synthesized PLGA-NPs that were loaded with Hp91 peptide or that carried it on the surface via conjugation. We measured the amount of peptide loosely attached to the surface in the process of synthesized PLGA-NPs with peptide conjugated to the surface and found that PLGA-NPs approximately 4.4% of the Hp91 peptide dissociated from the PLGA particles after sonication, suggesting that it was not conjugated but loosely attached. Although sonication increased the amount of peptide released from the particles, the overall amount was still very low, indicating that the Hp91 is in fact covalently attached to the PLGA particles and not just loosely adsorbed to the surface. In addition to releasing any peptide loosely associated with the PLGA particles, sonication of the particles is likely to break up some particles, thus releasing a small amount of peptide. Therefore, we cannot firmly conclude that the 4.4% are truly loosely attached. However, the percentage released is small compared to the amount retained.

We found that Hp91, when packaged inside or outside of PLGA-NPs activates both mouse and human DCs. In both cases the DC stimulatory capacity was higher when the peptide was delivered via NPs as compared to free peptide. One possible explanation is that the

delivery is more efficient, since the NPs are readily taken up by DCs and each NP will deliver many peptides, whereas free peptide will diffuse around the cells and the uptake is much less effective. In addition packaging of Hp91 inside of PLGA-NPs or conjugation to the surface most likely protects the peptide from degradation. The increase in Hp91 potency when delivered via NPs could be due to enhanced delivery into intracellular compartments that contain the receptor or other interacting molecules. The NPs with the Hp91conjugated to the surface were the most potent formulation for activating DCs. This is likely because with the Hp91 on the surface, the peptides are more readily available to interact with receptors. This confirms the theory that bioactive surfaces on nanoparticle drug delivery vehicles are an efficient method for interacting with immune cells.

The peptide release characteristics show that at pH 5 the peptide is released slower than at pH 7.4. One possible reason for this is due to the protonation of carboxyl groups on the peptide at lower pH values, which would make the peptide less polar and therefore more likely to remain encapsulated in the hydrophobic polymer core. The slow release at pH 5, which is present in endosomes could also contribute to the increase effect of the peptide, as a DC might carry a reservoir that is slowly

released and can exert the effect on DCs over a prolonged period of time within the cell. The peptide conjugated to the surface of the PLGA spheres is released slower than the peptide only encapsulated by the PLGA. This is expected as the peptide is covalently linked to the PLGA and must either be cleaved off the PLGA or the PLGA must be sufficiently degraded to be released from the particle.

Furthermore, Hp91 conjugated to the surface of NPs can potentially crosslink the receptor leading to stronger DC activation. The receptor for Hp91 on DCs remains to be identified. However, the fact that Hp91 packaged inside of NPs not only activates the DCs but shows increased potency as compared to free peptide suggests that the receptor is not on the cell surface, but most likely in an intracellular compartment, possibly endosomes, like other adjuvant binding receptors including TLR 3, 7/8 and 9.(104) In conclusion, we show that the ISP Hp91 when delivered via PLGA-NPs not only maintains its ability to activate DCs, but PLGA-NPs carrying Hp91 are stronger in activating DCs than is free peptide. This warrants further exploration in vaccine settings. It remains that the surface conjugated molecules are the most potent and active when interacting with DCs.

The use of PLGA nanoparticles as vaccine delivery vehicles has broad implications for a large number of diseases. Not only can

nanoparticle formulations improve the prophylactic properties of vaccines, they also show promise for the treatment of many diseases such as cancer. However, there is still a great need for systemic delivery of therapeutic molecules. For this application, nanoparticle drug delivery vehicles need different properties from vaccine delivery vehicles. The next chapters will discuss drug delivery vehicles based on similar PLGA core particles, but with surface coatings that make them more suitable for systemic delivery.

Chapter 2, in part, is a reprint of the material as it appears in Nanomedicine, 2010, Corbin Clawson, Chien-Tze Huang, Diahnn Futalan, Daniel Martin Seible, Rebecca Saenz, Marie Larsson, Wenxue Ma, Boris Minev, Fiona Zhang, Mihri Ozkan, Cengiz Ozkan, Sadik Esener, and Davorka Messmer. The dissertation author was the primary investigator and co-author of this paper.

3. A Drug Delivery Vehicle with pH Triggered PEG Shedding

3.1 Introduction

As was previously discussed, nanoparticle drug delivery vehicles with peptides conjugated on the outside present a bioactive surface that is efficient at interacting with immune cells. The surface of the drug delivery vehicle is important in interactions with cells other than immune cells. Most drug delivery vehicles have the ultimate goal of delivering their cargo to the interior of a cell. A nanoengineered

surface coating becomes invaluable if it can facilitate the delivery of the cargo into the desired intracellular compartment.(105)

The ability to deliver drugs more effectively and efficiently to the site of interest translates into less harmful systemic side effects and more beneficial therapeutic action.(8) This ability is particularly useful in the fight against cancer, where harmful side effects limit the tolerable dose of chemotherapeutics.(106) Using polyethylene glycol (PEG) has become a popular strategy to create long-circulating drug delivery nanoparticles and other vehicles by reducing protein adsorption, macrophage uptake, and particle aggregation, thus increasing systemic circulation lifetime.(8, 71, 72) Although useful in increasing circulation half-life, the PEG layer may become a detriment upon reaching the target tissue, hindering the entry of the nanoparticle into the cell or preventing its escape from the endosome after being endocytosed.(30)

A drug delivery vehicle with pH-sensitive PEG shedding would be especially useful in cancer drug delivery by exploiting the slightly acidic extracellular space of tumors (around pH ~ 6.5).(5, 107) Upon arrival at the tumor site, a correctly tuned pH-sensitive particle would be able to shed its PEG coating, thus enabling it to fuse with the cell membrane and be internalized.(108) Additionally, nanoparticles taken up via the

endosomal pathway can be tuned to lose the protective PEG coating upon acidification of the late endosome or early lysosome.(109) Fusing with the endosomal membrane then becomes possible and escape from the endosome can be achieved.(110, 111) The importance of endosomal escape cannot be underestimated, especially for the delivery of degradable payloads like siRNA and other biologics that are typically degraded inside the highly acidic lysosome.(112) Previous research has shown PEG shedding to improve intracellular drug delivery using polymersomes(74) and polyplex micelles.(75) Other PEG shedding molecules that rely on the reduction of disulfide bonds have been used in liposomes and lipoplexes to some success.(113) More recently, Gao *et al.* have demonstrated a technique to directly observe PEG shedding using a pair of dye and quencher, confirming the benefits of PEG shedding to intracellular delivery.(76)

Herein we report a novel approach to enable pH-triggered PEG shedding from lipid-polymer hybrid nanoparticles by using a lipid-(succinate)-mPEG conjugate that is highly sensitive to acidic hydrolysis via a di-ester succinate linker between the lipid and PEG moieties. The relatively slow hydrolysis rate of the di-ester bonds allows the PEG shedding to be more finely tuned, offering controllable shedding over a wide range of pH values unavailable with other strategies. The

shedability of the lipid-(succinate)-mPEG layer was tested using a previously developed drug delivery platform, lipid-polymer hybrid nanoparticles. The hybrid nanoparticles have been demonstrated to be an effective drug delivery vehicle with controllable drug loading and release characteristics,(114) their superior *in vitro* and *in vivo* stability,(115, 116) and excellent scalability for large scale production.(69)

3.2 Experimental Methods

3.2.1 Materials

Poly(lactic-co-glycolic acid) (PLGA, 50:50, 0.82 dL/g) was purchased from Lactel Absorbable Polymers (Pelham, AL). All lipids including 1,2-dioleoyl-sn-glycero-3-phosphoethanolamine (DOPE) and 1,2-dipalmitoyl-sn-glycero-3-phospho(ethylene glycol) (PtdEG), and 1,2-distearoyl-sn-glycero-3-phosphoethanolamine-N-[carboxy(polyethylene glycol)-2000] (DSPE-PEG carboxylic acid) were purchased from Avanti Polar Lipids (Alabaster, AL). Oleic acid was purchased from Alfa Aesar (Ward Hill, MA). Methoxy poly(ethylene glycol) (M_W = 2000 Da, mPEG-2000) was purchased from Sigma-Aldrich (St. Louis, MO) and modified in our lab to have a carboxyl end group, making mPEG-COOH. *N,N'*-diisopropyl carbodiimide (DIPC), *p*-

toluenesulfonic acid monohydrate, tetrahydrofuran (THF), and *N,N*-dimethylaminopyridine (DMAP) were purchased from Sigma-Aldrich (St. Louis, MO).

3.2.2 Synthesis of lipid-(succinate)-mPEG conjugate

The pH sensitive lipid-(succinate)-mPEG was synthesized by conjugating mPEG-COOH (Mw = 2000 Da) to a PtdEG phospholipid molecule using a dual-ester bond linkage. The synthesis reaction was carried out as follows. First, 4-(*N,N*-dimethylamino) pyridinium-4-toluenesulfonate (DPTS) was prepared by mixing equal parts of saturated tetrahydrofuran (THF) solutions of *N,N*-dimethylaminopyridine (DMAP) and *p*-toluenesulfonic acid monohydrate at room temperature. The precipitate was filtered, washed three times with THF and dried under vacuum. Next, 5 mg of PtdEG was dissolved in chloroform at 10 mg/mL. mPEG-COOH was also dissolved in chloroform at 10 mg/mL and mixed with the PtdEG at a molar ratio of 2 mPEG-COOH:1 PtdEG. Then DPTS at a molar ratio of 6 DPTS:1 PtdEG was added to the chloroform mixture and vortexed vigorously for 5 minutes. An equalvalent amount of DIPC as that of DPTS was then slowly added into the solution while stirring. The reaction was allowed to proceed overnight at room temperature while stirring. After the

reaction was complete, the volume of chloroform was reduced using a dry argon stream and the lipid-(succinate)-mPEG product was precipitated with cold ether. The precipitate was then resuspended in chloroform and washed three times with saturated brine. The chloroform layer was collected and used as a stock solution for subsequent studies. NMR spectroscopy was carried out to characterize the produced lipid-(succinate)-mPEG conjugate. ^{1}H NMR ($CDCl_3$): δ = 0.87 (-CH_3, a), 1.25-1.13 (-CH_2, Lipid, b), 1.65 (-CH_2, Lipid, c), 2.3 (-CH_2-COOR, d), 2.65 (-CH_2-CH_2-, succinate, f), 3.1 (-COH, i), 3.3 (-OCH_3, h), 3.64 (-CH_2-CH_2-, PEG, g), 4.13 (-CH_2-COH-CH_2-, e) ppm.

3.2.3 Synthesis of lipid-polymer hybrid nanoparticles

To prepare lipid-polymer hybrid nanoparticles, DOPE/oleic acid (molar ratio = 4:1, 91.4 µg of DOPE and 8.7 µg of oleic acid to make 1 mg of PLGA particles), or DOPE/oleic acid/lipid-(succinate)-mPEG were dissolved in THF and added to water at desirable molar ratios. The amount of lipid-(succinate)-mPEG was varied and DOPE was reduced by a corresponding molar amount. The lipid solution in H_2O/THF was heated to 68°C while stirring. The PLGA polymer was dissolved in THF at 1 mg/mL and 1mL was added dropwise to the heated lipid solution while stirring. The mixture solution was then

vortexed for 3 minutes at high speed and then 1 mL of additional water was added dropwise to the solution. The solution was allowed to stir for 2 hours in a chemical hood to allow the organic solvent to evaporate and the nanoparticles to solidify. The nanoparticles were then washed three times using an Amicon Ultra centrifugal filter (Millipore, Billerica, MA) with a molecular weight cutoff of 10 kDa. The nanoparticles were then collected and suspended to 1 mL of water. The nanoparticle size and surface zeta potential were obtained from three repeat measurements using a dynamic light scattering (Malvern Zetasizer, ZEN 3600) with backscattering angle of 173°.

3.2.4 pH sensitivity of nanoparticles

In order to test the pH sensitivity of the nanoparticles, particles with lipid-(succinate)-mPEG replacing 15% of DOPE were suspended in either a pH = 7.4 buffer (PBS) or a pH = 5 buffer (potassium hydrogen phthalate/NaOH). As a control, nanoparticles with DSPE-PEG replacing 15% of DOPE were suspended in the same pH = 7.4 and 5 buffers. The DSPE-PEG was chosen as a negative control because the PEG is linked to the lipid via an amide bond, which is more stable than the synthesized ester bond of the lipid-(succinate)-mPEG. The size of the nanoparticles was measured by dynamic light scattering after 1, 3,

6, and 24 hours of incubation to determine the stability of the particles. In addition, nanoparticles with different amounts of lipid-(succinate)-mPEG replacing the DOPE were tested in different pH buffers ranging from pH = 7.4 to pH = 3. The size of the particles in the different buffers was measured after 20 hours of incubation using dynamic light scattering. The morphology and size of the particles were further characterized using scanning electron microscopy (SEM). Samples for SEM were prepared by dropping 5 µL of a dilute nanoparticle solution onto a polished silicon wafer. After drying the droplet at room temperature overnight, the sample was coated with chromium and then imaged by SEM. In order to adjust the pH value of the dilute nanoparticle solution without adding excess salts, 1 mM HCl was titrated in until the solution reached pH = 5.

3.3 Results and Discussion

3.3.1 Nanoparticle and surface coating design

Figure 3.1 shows a schematic representation of the lipid-polymer hybrid nanoparticle system as designed. The nanoparticle core is made of a hydrophobic polymer and is used to encapsulate poorly

water soluble and difficult to deliver therapeutic agents. In this study, poly(lactic-*co*-glycolic acid) (PLGA) was used to form the particle core for its biocompatibility and biodegradability. A lipid monolayer consisting of 1,2-dioleoyl-sn-glycero-3-phosphoethanolamine (DOPE) and oleic acid is self-assembled onto the surface of the polymeric core to solubilize it in aqueous environments and also to serve as a diffusion barrier against encapsulated drugs leaching out.(117) In addition, the DOPE/oleic acid formulation was chosen for its fusogenic properties(118-120), which are revealed upon the shedding of the PEG layer. The lipid-(succinate)-mPEG molecules form a "stealth" corona on the surface of the hybrid nanoparticle with the phospholipid portion of the lipid-(succinate)-mPEG inserting into the DOPE/oleic acid monolayer. It is expected that the resulting nanoparticle is sterically stabilized prior to PEG shedding, while it becomes fusogenic and unstable when the PEG layer comes off at acidic pH values.

Figure 3.2 A shows the scheme for synthesizing the lipid-(succinate)-mPEG molecule by conjugating mPEG-COOH (Mw = 2000 Da) to a 1,2-dipalmitoyl-sn-glycero-3-phospho(ethylene glycol) (PtdEG) phospholipid molecule via a dual-ester bond linkage. Sequential ester bonds in the resulting lipid-(succinate)-mPEG conjugate increase the

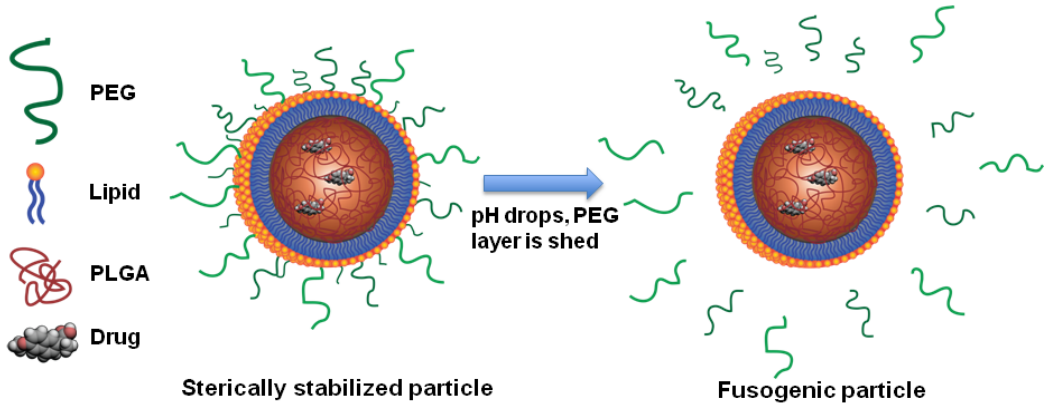

Figure 3.1. Schematic of a lipid-polymer hybrid nanoparticle with pH-triggered PEG shedding. The hybrid nanoparticle consists of a drug-loaded PLGA polymeric core, a fusogenic DOPE/oleic acid monolayer shell, and a sterically stabilizing PEG corona. The PEG layer comes off in response to environmental acidity, making the particle fusogenic toward lipid membranes.

sensitivity of the conjugate to hydrolosis by offering two hydrolysable ester bonds capable of releasing the PEG from the phospholipid. When one of the ester bonds is activated through protonation, it becomes more electrophilic, which will then catalyze the hydrolysis of the neighboring ester bond. Upon the hydrolysis of either ester bond, the PEG molecule is shed. The production of lipid-(succinate)-mPEG conjugate was first confirmed by ^{1}H NMR spectroscopy with all the characteristic peaks of PtdEG, mPEG and the di-ester bonds, respectively, as indicated in Figure 3.2 B.

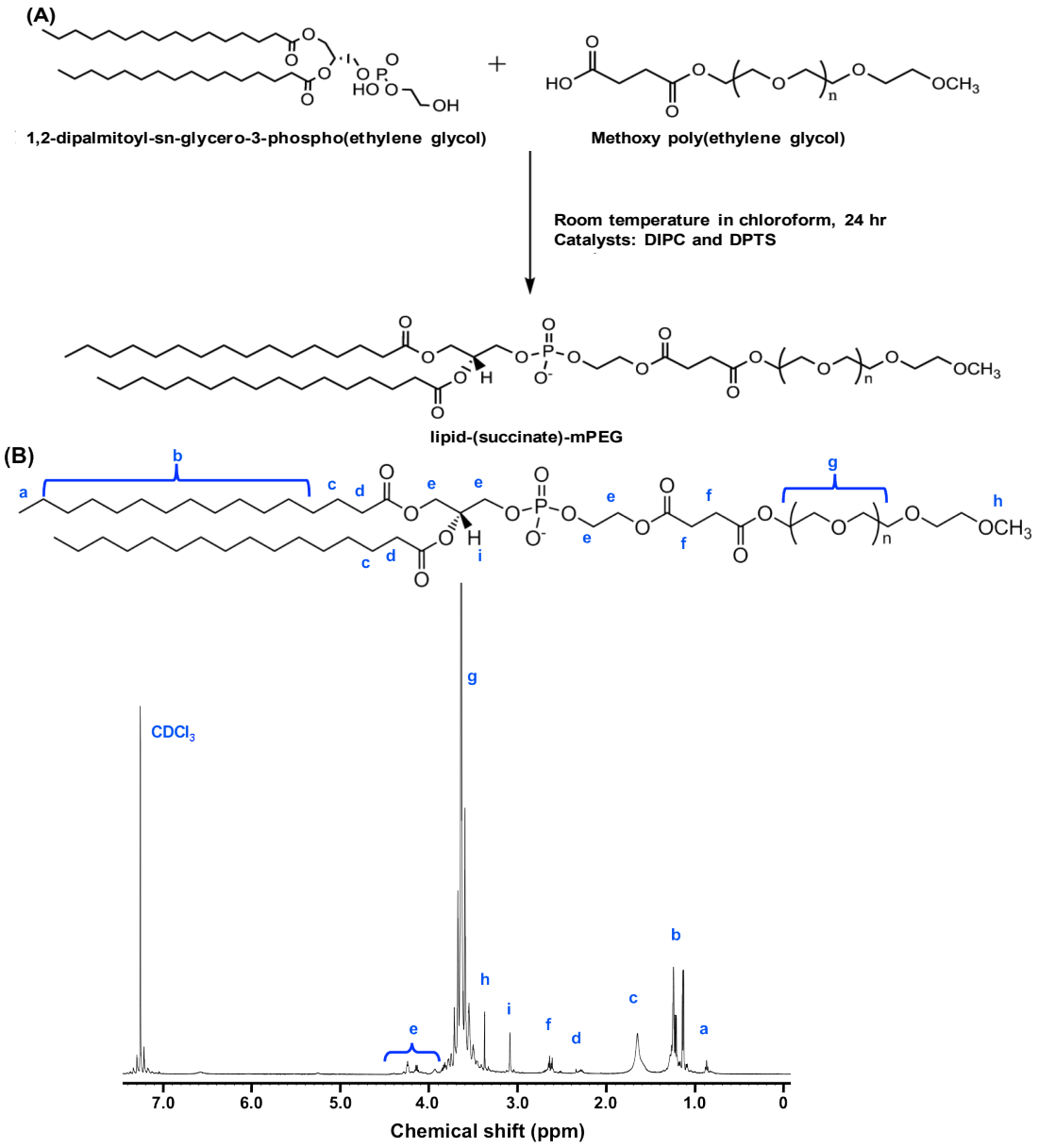

Figure 3.2. Synthesis and characterization of lipid-(succinate)-mPEG conjugate. (A) Schematic description of the synthesis of lipid-(succinate)-mPEG conjugate that is sensitive to acidic pH. (B) ^{1}H NMR spectrum of the synthesized lipid-(succinate)-mPEG conjugate.

The resulting lipid-(succinate)-mPEG was then used to replace a molar percentage of DOPE in the DOPE/oleic aicd monolayer to prepare lipid-polymer hybrid nanoparticles following a previously described method that takes advantage of nanoprecipitation and lipid self-assembly in order to create a simple and scalable manufacturing process.(69, 121, 122)

3.3.2 Nanoparticle characterization

Figure 3.3 shows the DLS intensity curve for lipid-polymer hybrid nanoparticles with 50% lipid-(succinate)-mPEG incorporated into the surface. The average size for the 50% formulation is 64nm with a PDI of 0.1. Figure 3.4 summarizes the measured hydrodynamic size the hybrid nanoparticles with various amounts of lipid-(succinate)-mPEG incorporated into the lipid shell.

By simply varying the amount of lipid-(succinate)-mPEG, we are able to synthesize particles within the desired size range of 50~150 nm. Particle size predictably decreases with increasing amounts of the stabilizing lipid-(succinate)-mPEG, reaching a minimum size of 64 nm when 50 mol% lipid-(succinate)-mPEG is used. When only 15 mol% lipid-(succinate)-mPEG is used the size is 123 nm. Note that extensive studies have been reported that particles with a hydrodynamic size

around 100 nm or less are desirable for systemic drug delivery because of their favorable *in vivo* pharmacokinetics and tumor accumulation. (20, 77, 123)

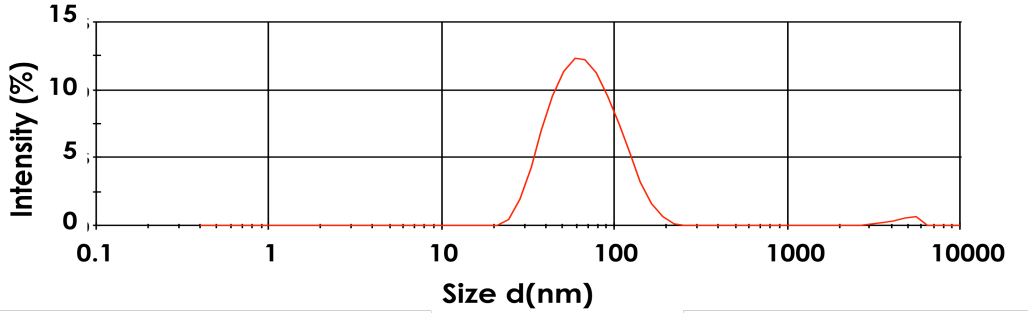

Figure 3.3. Dynamic light scattering intensity of lipid-polymer hybrids with 50% lipid-(succinate)-mPEG incorporated onto the surface. Average size is 64nm with a PDI of 0.2.

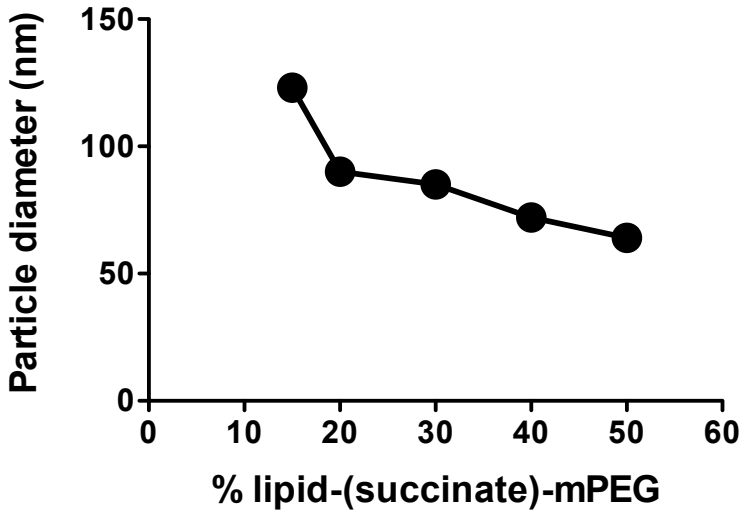

Figure 3.4. Hydrodynamic size (diameter, nm) of the lipid-polymer hybrid nanoparticles synthesized with various amounts of lipid-(succinate)-mPEG replacing a molar percentage of DOPE lipid in the lipid monolayer shell. All samples are at pH = 7.4.

3.3.3 Bioresponsive PLGA surface coating imparts pH sensitivity

The pH-sensitive stability of the synthesized hybrid nanoparticles was first examined by scanning electron microscopy (SEM) to image the size and morphology of the particles at different pH values. As shown in figure 3.5 A, the particles with 15 mol% lipid-(succinate)-mPEG at pH = 7.4 show individually dispersed particles that are spherical in shape with little to no aggregation. The morphology of the particles appears smooth. In contrast, when the particles were titrated with HCl to pH = 5, they appear clumped and aggregated indicative of a destabilized lipid shell. As shown in figure 3.5 B, the majority of the particles have aggregated into clumps at least several hundred nanometers in size with only a few individually dispersed particles visible. Individual spherical particles can be seen to make up the aggregates; however, the overall shape and morphology is flat and lumpy.

Once the linking ester bond is hydrolyzed and the stabilizing PEG coating attached to the lipid shell is released, the particles are free to contact other particles and the lipid layers can fuse, causing aggregation. The resulting structure consists of multiple PLGA particles clumped and surrounded by a most likely multi-lamellar lipid layer. This result suggests the fusogenic properties of the hybrid nanoparticles after the PEG layer is shed.

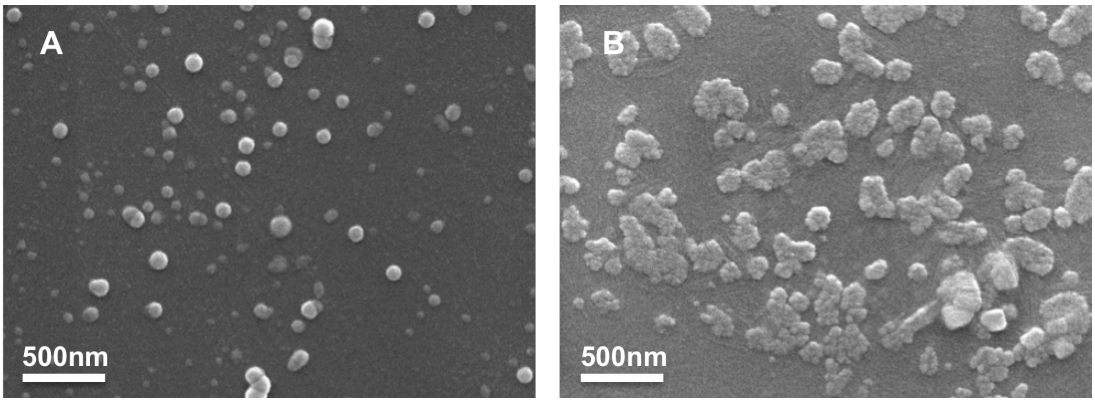

Figure 3.5. Scanning electron microscopy (SEM) images of lipid-polymer hybrid nanoparticles, in which lipid-(succinate)-mPEG makes up 15 mol% of the lipid monolayer shell. (A) At pH = 7.4, isolated particles show spherical morphology and little aggregation. (B) At pH = 5, particles have aggregated and show irregular morphology.

Next, we examined the time-dependent particle aggregation of the 15 mol% lipid-(succinate)-mPEG nanoparticles at pH=7.4 and 5 over 24 hours. As shown in Figure 3.6, the hydrolysis of the ester bonds is shown to proceed over the course of several hours. The particles with 15 mol% lipid-(succinate)-mPEG show only a slight size increase from 107 nm to 135 nm at pH = 7.4 over the 24 hour period. This confirms the slow rate of hydrolysis expected at neutral pH. At pH = 5, the 15% lipid-(succinate)-mPEG particles show a dramatic and rapid increase in size due to aggregation. After 1 hour the size had already increased to 905 nm and the size continues to increase over 6 hours. For the control

samples, instead of using lipid-(succinate)-mPEG, 15 mol% DSPE-PEG was used to replace the corresponding amount of DOPE in the DOPE/oleic acid lipid shell. It was found that the size of these control particles remained constant at 65 nm for both pH =7.4 and 5 conditions for the duration of the 24-hour test. The lack of size increase in the control particles which have PEG linked to the lipid shell via an amide bond rather than the more easily hydrolysable ester bond indicates that the mechanism triggering the aggregation is the depletion of the PEG layer due to ester hydrolysis.

3.3.4 Tuning of nanoparticle pH sensitivity

Finally, the stability of the hybrid nanoparticles at different pH values was correlated to the amount of lipid-(succinate)-mPEG incorporated into the lipid shell of the particles. Hydrolysis of the di-ester bond that links the mPEG to the PtdEG lipid occurs under either acidic or basic conditions but very slowly at neutral pH. Figure 3.7 shows the size of particle aggregates with varying amounts of pH-sensitive lipid-(succinate)-mPEG incorporated into the lipid shell incubated for 20 hours over a range of pH values.

The greater the amount of lipid-(succinate)-mPEG incorporated into the particle's lipid shell, the more stable the particle becomes, even at low pH, thus, tuning the pH sensitivity of the particle. With only

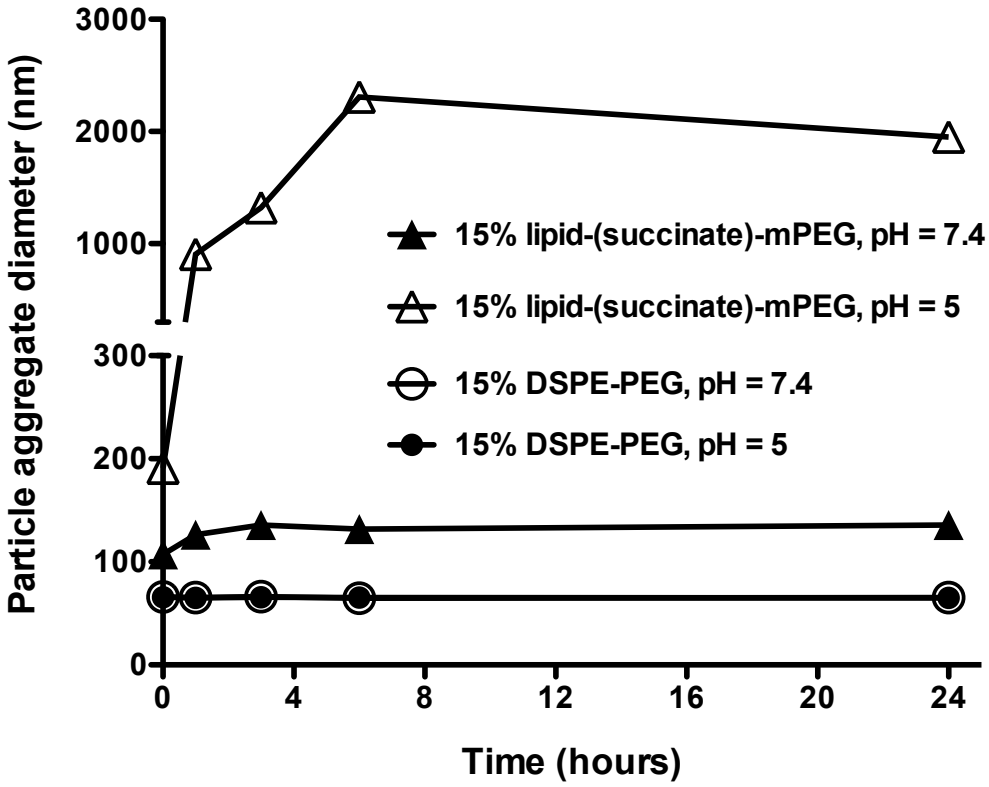

Figure 3.6. Time dependent particle aggregation at pH = 7.4 and pH = 5 over 24 hours. Lipid-(succinate)-mPEG was incorporated into the lipid monolayer shell at a molar ratio of 15%. Non-hydrolyzable DSPE-PEG was used in the same ratio as a negative control. At pH = 7.4, both formulations are stable over the 24 hours, with the lipid-(succinate)-mPEG particles increasing in size by only 28 nm (from 107 nm to 135 nm). At pH = 5, the DSPE-PEG particles remain stable while the lipid-(succinate)-mPEG particles begin to aggregate immediately and continue for 6 hours before plateauing at around 2000 nm.

15 mol% lipid-(succinate)-mPEG, the particles completely destabilize when the pH is lowered to 6, resulting in large micron sized aggregates (average size 1370 nm). The 20 mol% lipid-(succinate)-mPEG particles begin to destabilize at pH 6 forming dimers and trimers (average size 263 nm) but do not fully aggregate until the pH is lowered to 5. The 20 mol% lipid-(succinate)-mPEG particles are said to be fully sensitive to acidic environments at or below pH = 5. The 30 mol% lipid-(succinate)-mPEG particles show full destabilization at pH = 4. Particles with 40 mol% lipid-(succinate)-mPEG begin to destabilize at pH = 3 increasing in size from 97 nm to 175 nm but do not show full destabilization. The 50 mol% lipid-(succinate)-mPEG particles do not show any measurable destabilization over the pH range tested.

These results demonstrate that the more lipid-(succinate)-mPEG on the surface of the particles, the more ester bonds must be hydrolyzed before the PEG layer becomes sufficiently depleted to allow the aggregation of particles.

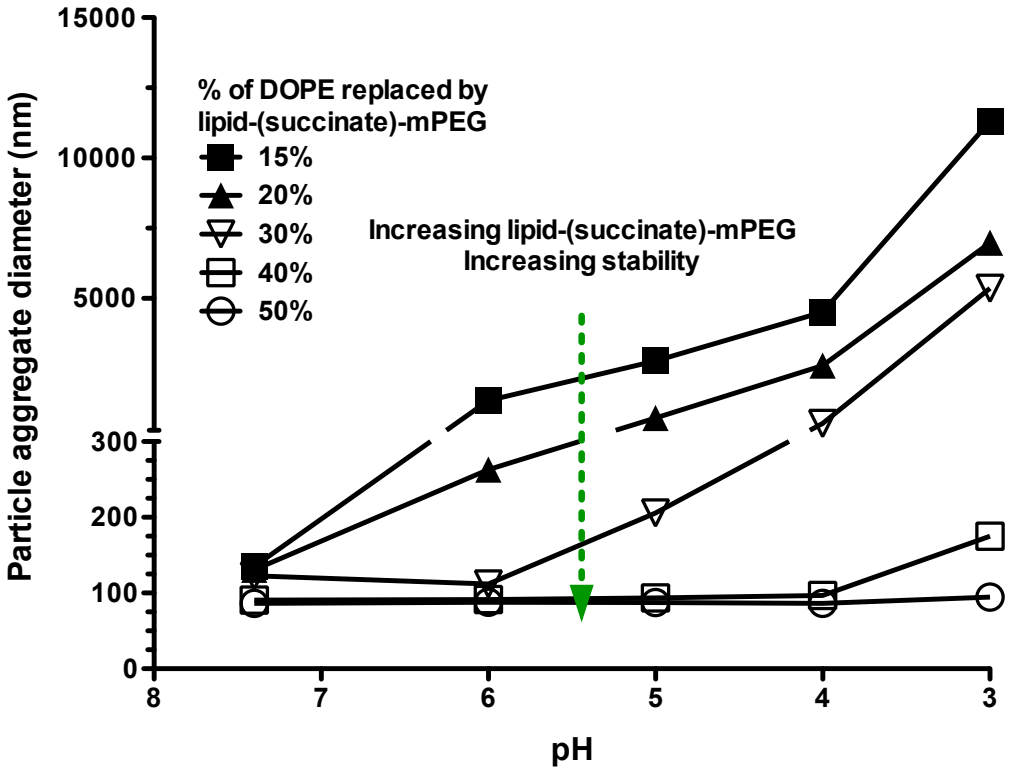

Figure 3.7. Particle aggregate size (diameter, nm) at varying pH values after 20 hours incubation. Lipid-polymer hybrid nanoparticles show increasing stability with increasing amounts of lipid-(succinate)-mPEG incorporated to the lipid monolayer shell. With 15 mol%, complete aggregation occurs at pH = 6. With 20 mol%, 30 mol% and 40 mol% lipid-(succinate)-mPEG, aggregating begins at pH = 6, 5, and 3, respectively. With 50 mol% lipid-(succinate)-mPEG, aggregation is not observed over the range of pH values tested.

3.4 Conclusion

We synthesized a novel lipid-(succniate)-mPEG conjugate, of which the PEG moiety can be shed readily at acidic conditions. By incorporating lipid-(succinate)-mPEG onto the surface of lipid-polymer hybrid nanoparticles, the particles are made fusogenic, triggered by a reduction in pH values.

The amount of lipid-(succinate)-mPEG incorporated into the lipid shell of the hybrid nanoparticles determines the pH value at which the particles destabilize and begin to aggregate. We found that the higher the amount of lipid-(succinate)-mPEG incorporated into the particle's lipid shell, the more stable the particles become, even at low pH. The wide range of pH values for which the particles can be tuned to shed the PEG coating adds potential functionality to the nanoparticle drug delivery toolkit. The aggregation of the lipid-coated polymeric nanoparticles indicates a promising method of fusing nanoparticles with cellular or endosomal membranes, making drug delivery more efficient and effective. Moreover, the novel lipid-(succinate)-mPEG conjugate may be used to make a range of other

drug delivery vehicles, including polymeric micelles, liposomes, lipoplexes, and nanoemulsions, environmentally sensitive.

This technology represents a significant and useful improvement over a non-sheddable PEG coating. However, as different tasks require different tools, this system may not be the best choice for all drug delivery vehicle systems. The next chapter will focus on an alternative to PEG that can be used for systemic delivery and long circulating drug delivery vehicles.

Chapter 3, in part, has been submitted for publication as it may appear in Small, 2011, Corbin Clawson, Linh Ton, Santosh Aryal, Sadik Esener, Liangfang Zhang. The dissertation author was the primary investigator and author of this paper.

4. A Drug Delivery Vehicle with a Biomimetic Stabilizer to Replace PEG

4.1 Introduction

As previously discussed, PEG is the current state of the art in long circulating nanoparticle technologies. In the previous chapter we discussed an improvement upon the PEG coating by making the PEG sheddable in response to an environmental trigger. This is particularly useful for the delivery of sensitive biomolecules. However, there is a need for an alternative to PEG in order to increase the number of tools available to drug delivery vehicle designers.

For systemic delivery of therapeutic or diagnostic agents, clearance from the bloodstream is one of the most challenging hurdles to overcome.(124-126) Drug delivery vehicles need to lie within a sweet

spot of physical characteristics including size, surface charge or zeta-potential, solubility, and steric stability in order to navigate the bodies numerous defenses against foreign material and pathogens.(73, 127-132) Apart from size, most, if not all, of the optimal characteristics are governed by the nanoparticle surface properties. Charged surface molecules dominate the zeta potential. Solubility can be altered through the use of surfactant or amphiphilic molecules that alter the polarity or hydrophobicity at the nanoparticle surface. Steric stability is likewise a property conferred by surface molecules which prevent aggregation and adsorption of proteins. PEG performs well in conferring desirable surface properties to nanoparticles in all these categories.

As useful as PEG has been proven to be in creating long-circulating nanoparticles, alternatives should be explored. Just as the overuse of a single antibiotic can lead to resistant pathogens, relying on a single technology to solve a problem within a complex and adaptive system such as the human body can lead to problems down the road. Recent studies have shown that over 25% of the population already produces anti-PEG antibodies(79, 80), which is no surprise given the ubiquitous nature of PEG in everyday products such as toothpaste and shampoo. The presence of anti-PEG antibodies is also

strongly correlated with the rapid clearance of certain PEGylated biomolecules. (133)

Lipid-polymer hybrid nanoparticles have been shown to be a suitable long-circulating drug delivery vehicle platform.(46) But the typical lipid-polymer hybrid nanoparticle formulation relies on PEG to impart long circulation properties. In the search for an alternative to PEG that could be used with the lipid-polymer hybrid platform, we turned to nature for a solution. The body naturally produces hybrid nanoparticles called high-density lipoproteins (HDL) and low-density lipoproteins (LDL) that circulate in the blood stream and transport fats and cholesterol through the body. These natural particles are composed of a hydrophobic core made up of cholesterol, triglycerides, fats, and fatty acids. Surrounding the core is a monolayer of amphiphilic phospholipids that stabilize the hydrophobic core in the aqueous blood. Incorporated into the phospholipid monolayer are apolipoproteins. The apolipoproteins stabilize the particles and aid in increasing the circulation half-life of the lipoprotein particles, as well as serve as signaling and receptor molecules.(134-136)

Based on the lipid-polymer hybrid nanoparticle, we developed a biomimetic system that simulates the characteristics of natural lipoprotein particles consisting of a hydrophobic PLGA core, a

phospholipid monolayer surrounding the PLGA core, and apolipoproteins integrated into the lipid monolayer shell. Previous studies have used peptide sequences derived from apolipoproteins to solubilize lipids and form nanoparticles capable of delivering cargo.(137, 138) Our work is differentiated from these studies primarily by the use of polymeric nanoparticle cores instead of lipids. The polymeric core allows for controllable release characteristics based on the polymer composition as well as a wider range of diameters, which can lead to greater drug loading. We present here the fabrication and characterization of this biomimetic nanoparticle and open the way for its use in the future as a drug delivery platform. We call the new nanoparticle based theranostic platform Nano Polymer Hybrid Apolipoprotein Theranostic System, or NanoPHATS. A diagram of a NanoPHATS particle is presented in Figure 4.1.

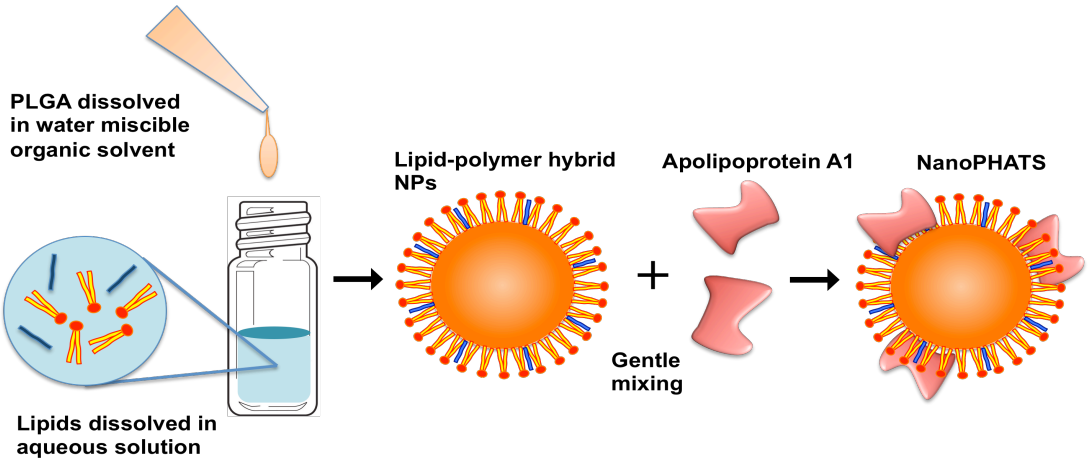

Figure 4.1. Schematic showing fabrication of NanoPHATS and the incorporation of Apolipoprotein A1 onto the surface of a polymer nanoparticle covered with a lipid monolayer. The lipid-polymer nanoparticle resembles the structure of natural lipoprotein particles onto which Apolipoproteins preferentially adhere. B) Scanning electron microscope images of the NanoPHATS showing relatively uniform size and spherical shape. Average size 84nm by DLS and confirmed by SEM.

4.2 Experimental Methods

4.2.1 Materials

Apolipoprotein A1 was purchased from Ray Biotech (Norcross, GA). PLGA (50:50, 0.82 dL/g) was purchased from Lactel Absorbably Polymers (Pelham, AL). 1,2-distearoyl-sn-glycero-3-phosphoethanolamine-N-[carboxy(polyethylene glycol)-2000] (DSPE-PEG carboxylic acid) was purchased from Avanti Polar Lipids (Alabaster, AL). Lecithin (avg. MW – 330) was purchased from Alfa Aesar (Ward Hill, MA). The bicinchoninic acid (BCA) assay was purchased from Pierce (Rockford, IL). Phosphate buffered saline (PBS) was purchased from Invitrogen (Carlsbad, CA). 4 mL capacity Amicon filters (10,000 MWCO) were purchased from Millipore (Billerica, MA). The Zetasizer Nano dynamic light scattering instrument used was manufactured by Malvern (Worcestershire UK).

4.2.2 NanoPHATS fabrication methods

The NanoPHATS were synthesized using the nanoprecipitation method. Aqueous lipid solutions were prepared by dissolving either lecithin or lecithin and DSPE-PEG in a 4% ethanol solution. The concentration of lecithin for NanoPHATS was 150μg in 4mL of 4% EtOH,

or 37.5μg/mL. For 20% molar DSPE-PEG lipid-hybrid NPs, the amount of lecithin was reduced to 120μg/mL and a corresponding molar amount of DSPE-PEG (259μg) was added to replace the lecithin. The aqueous solutions were heated to 68°C for 3 minutes to ensure the lipids were in a fluid state. PLGA was dissolved at 1mg/mL in acetonitrile and 1mL was added dropwise to 4mL of either plain water, the lecithin solution, or the lecithin and DSPE-PEG lipid solution while the solutions were stirred on a heated magnetic stir plate. The solution was vortexed vigorously for three minutes and 1mL of water was added. The solution was then allowed to stir in a chemical hood at room temperature for two hours to allow the acetonitrile to evaporate. In order to remove residual acetonitrile and any unincorporated lipids, the particle solution was then washed twice using an Amicon centrifuge filter with a 10,000 MWCO at 2500xg for 12 minutes and concentrated to 1mg PLGA/mL. Apolipoprotein A1 was then added to the particle solution at a ratio of 1:25 protein to PLGA. The solution was gently mixed overnight to allow the protein to incorporate into the lipid shell of the hybrid NPs.

Control particles used in experiments had either no lipid coating at all on the PLGA (Bare PLGA NPs), only a lecithin coating (lecithin coated NPs), or lecithin and 20 mol% DSPE-PEG coating (PEG coated NPs).

4.2.3 NanoPHATS characterization methods

NanoPHATS particle size and zeta-potential were measured using a dynamic light scattering instrument. To test particle stability in high ionic strength solutions, 10x phosphate buffered saline (PBS) was added to particle solutions to achieve a final 1x PBS concentration and DLS measurements were taken immediately. In addition, absorbance was measured on a Tecan spectrophotometer at 560nm immediately after adding PBS and repeatedly over the next hour. Gentle shaking for 5 seconds was done between each measurement to prevent settling of aggregated particles.

A bicinchoninic acid (BCA) assay was used to determine the amount of Apolipoprotein A1 successfully incorporated into the surface of the lipid-polymer hybrid nanoparticle surface. The absorbance was compared to samples with known protein concentrations in order to quantify an unknown protein concentration.

To test particle stability in PBS, the 10X PBS was added to the particle solutions in a 1:9 ratio to make 1X PBS and particle solutions. The size was then measured using a Malvern Zetasizer Nano. Absorbance measurements were also taken using a Tecan spectrophotometer in a 96 well plate. The particles were added to the plate and 10X PBS was added to make the solution a final 1X PBS

concentration. Absorbance was immediately measured and at approximately 4 minute intervals over 1 hour. In between measurements, gentle shaking of the plate was automatically performed by the spectrophotometer in order to prevent the settling of larger aggregates out of solution. To test particle stability in serum, the absorbance method was again used. The particle solutions were added to a 96 well plate and an equal amount of serum was added to produce a 50% serum and particle solution. The absorbance was measured over the course of one hour with gentle shaking of the plate for five seconds between each measurement to ensure any aggregates did not settle to the bottom of the well and distort the measurement.

4.2.4 Method to determine *in vivo* circulation half-life

The NanoPHATS were then tested *in vivo* to determine the circulation half-life. PEG coated NPs were used as a positive control. 1,1'-dioctadecyl-3,3,3',3'-tetramethylindodicarbocyanine perchlorate ('DiD' oil) is a hydrophobic fluorescent dye and was loaded into the hydrophobic PLGA core of the NPs. 100 μL of the NP solution at a concentration of 1mg NPs/mL was administered to mice via tail vein injection. Approximately 30 μL of blood was collected through retro-

orbital bleeding at various time points over the course of 24 hours. The whole blood was plated in a 96 well plate and PBS was added to bring the volume up to 100 μL. The fluorescence signal of the whole blood was measured using a Tecan spectrophotometer using an excitation wavelength of 630nm and an emission wavelength of 675nm. The background signal from blood collected before NP injection was subtracted from each sample. The measurements were normalized to the signal measured from the sample taken immediately after injection.

4.3 Results and Discussion

4.3.1 Characterization and stability results

The size of the nanoparticles had an average size of 86nm and a zeta-potential of -24mV as shown in Figure 4.2 B. Micrographs were taken of the particles using a scanning electron microscope as presented in Figure 4.2 A. Physical size was shown to correlate with the size measured by DLS. The particles appear spherical and individual, isolated particles were observed. By varying the PLGA concentration

during the nanoprecipitation process, smaller or larger particle sizes can be easily achieved ranging from 50nm to 200nm.

The Apo A1 incorporation efficiency of the NanoPHATS was measured using a BCA assay (Figures 4.3, 4.4). The amount of protein incorporated into the surface was found to be 38 μg per mg of PLGA when the particles were left to stir gently overnight. As a total of 40 μg of Apo A1 was used in the fabrication of the NanoPHATS, this corresponds to a 94% incorporation efficiency. When the Apo A1 was added to the aqueous solution prior to the nanoprecipitation of PLGA, the amount of protein incorporated into the lipid monolayer was significantly lower. This may be due to the higher levels of solvent present that increase the solubility of the protein in the aqueous phase and preventing incorporation into the lipid layer. This method resulted in only 30 μg incorporation, or a 74% incorporation efficiency.

The BCA assay is a colorimetric assay to measure total protein concentration in a solution. According to the manufacturer, peptide bonds in proteins reduce Cu^{2+} ions in a cupric sulfate solution to Cu^{1+} ions. The Cu^{1+} ions chelate with two molecules of bicinchoninic acid, which changes color and absorbs strongly at 562nm. The amount of Cu^{1+} ions produced is proportional to the amount of protein in solution. The BCA assay is not an endpoint reaction and should therefore not be

left to react indefinitely. However, by increasing the overall reaction volume and allowing the reaction to take place at 37°C, the sensitivity of the assay can be improved to >0.5 μg/mL.

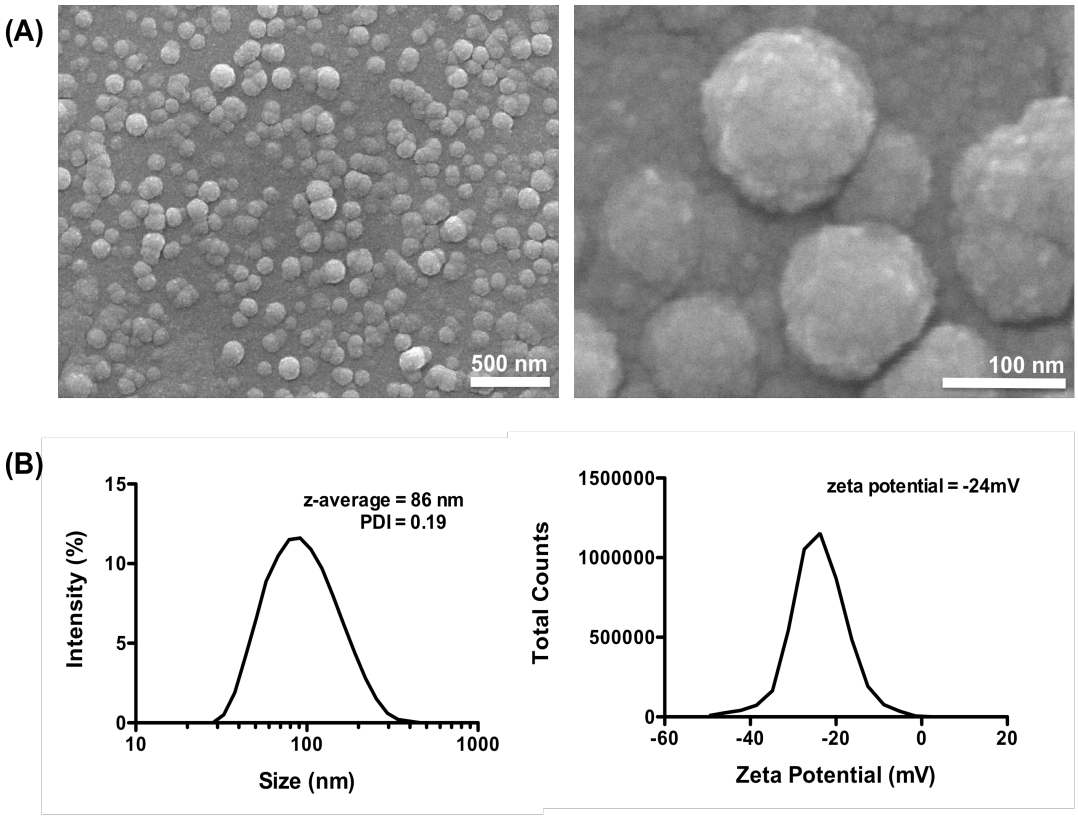

Figure 4.2. A) Scanning electron microscope images of the NanoPHATS showing relatively uniform size and spherical shape. Size consistent with DLS measurements. B) Average size 86nm by DLS with PDI = 0.19. Zeta potential = -24mV as measured by DLS.

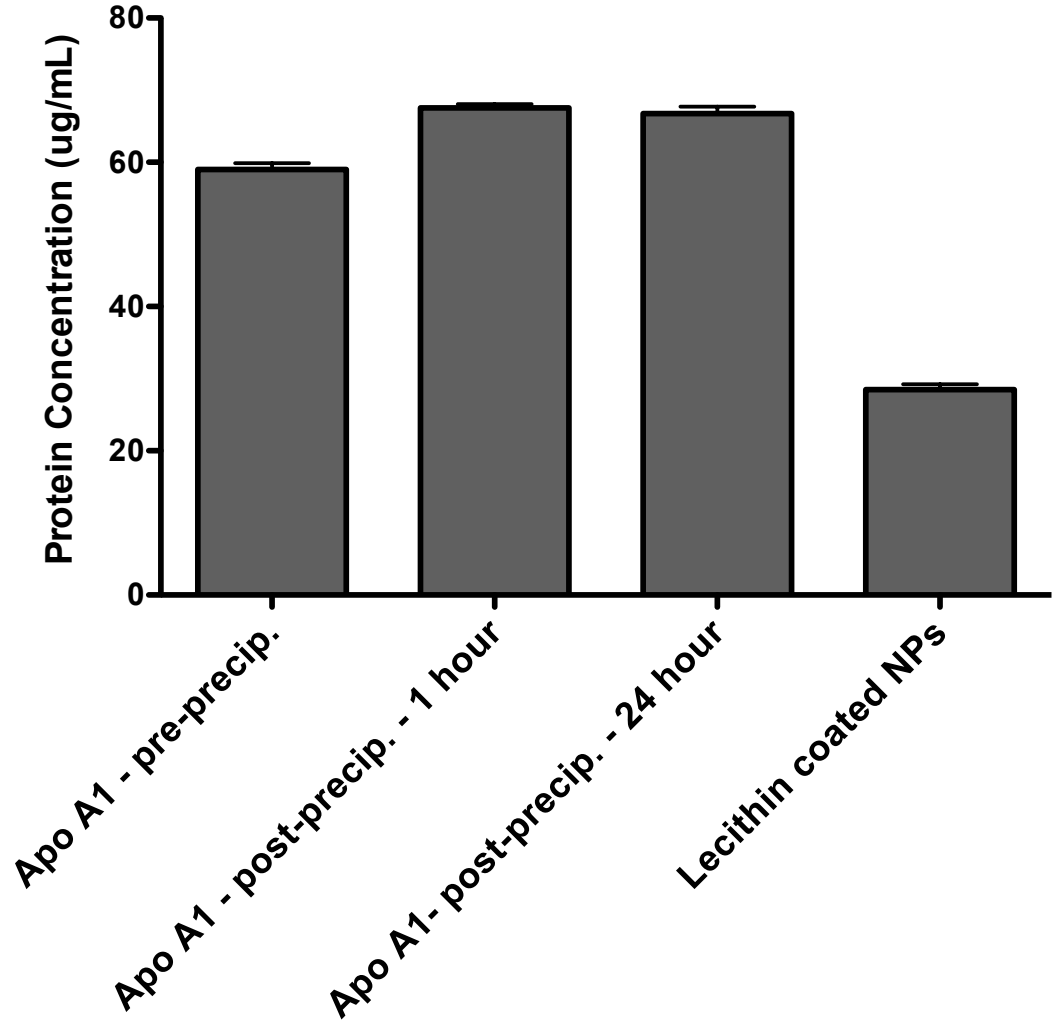

Figure 4.3. Protein concentration of NanoPHATS comparing three different fabrication techniques: 1. Apo A1 is added to the aqueous solution before PLGA nanoprecipitation, 2. Apo A1 is added after the PLGA nanoprecipitation into the aqueous solution and is allowed to stir at 4°C for 1 hour, and 3. Apo A1 is added after the PLGA nanoprecipitation and allowed to stir at 4°C for 24 hours. Lecithin coated NPs were used to determine the background of the assay.

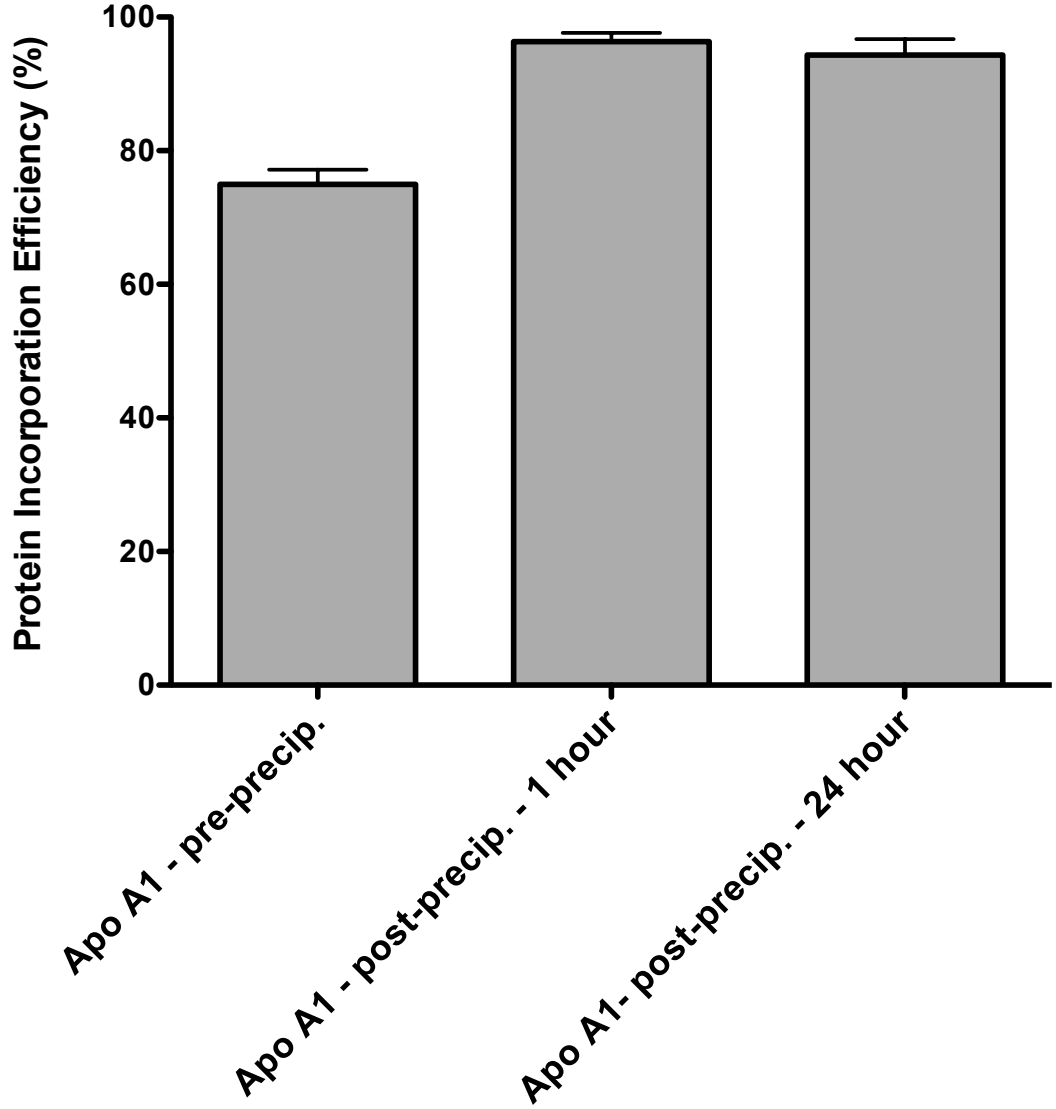

Figure 4.4. Quantified Apo A1 incorporation efficiency. All measurements made using the BCA protein quantitation assay.

Ions in high ionic strength solutions shield the surface charge of particles, reducing the electrostatic repulsion and destabilizing the particles. DLS measurements as shown in Figure 4.5 A indicate the size of bare PLGA nanoparticles as well as lecithin-coated nanoparticles increases significantly. The sizes of DSPE-PEG stabilized nanoparticles and the Apolipoprotein A1 stabilized NanoPHATS do not increase significantly over the initial size. In addition, absorbance was measured on a Tecan spectrophotometer at 560nm immediately after adding PBS and repeatedly over the next hour. As particles form larger aggregates, more light is scattered. The increased scattering can be measured as an increase in absorbance.

This is based on the principle of Mie scattering, in which particles whose size is close to the wavelength of the incident light scatter light dependent on their size. The larger the particle, the more light is scattered. Mie scattering is relatively independent of wavelength. As particles aggregate, more light is scattered, thus increasing the absorbance measurement. This measurement method is only qualitative for the purposes of this experiment. The actual determination of particle size from Mie scattering measurements involves complex mathematics and precise knowledge of particle characteristics such as refractive index, dielectric constant, and

absorption coefficient. The characterization of these NPs to this degree is beyond the scope of this work. However, the absorbance measurement can still give a reliable and repeatable qualitative look at the particle stability.

The bare PLGA NPs and the lecithin coated NPs both show a marked increase in size as measured by DLS as well as an increase in absorbance. Figure 4.5 shows the increase in size of Bare NPs and Lecithin NPs in PBS, and the stability of PEG NPs and NanoPHATS in the same PBS solution, as measured by both DLS and absorbance.

To test particle stability in serum, the absorbance method was again used. The particle solutions were added to a 96 well plate and an equal amount of serum was added to produce a 50% serum and particle solution. The absorbance was measured over the course of one hour with gentle shaking of the plate for five seconds between each measurement to ensure any aggregates did not settle to the bottom of the well and distort the measurement. The increase in relative absorbance was calculated, subtracting the absorbance values from the initial time point, and then normalized to the highest measurement. Figure 4.6 shows the normalized absorbance for bare PLGA NPs, lecithin coated NPs, 20% PEG coated NPs, and NanoPHATS.

Figure 4.5. Stability of different nanoparticles in a high ionic strength solution (phosphate buffered saline). A) Dynamic light scattering measurement of hydrodynamic diameter in 1X PBS for bare PLGA NPs, lecithin coated PLGA NPs, lecithin + 20 mol% lipid-PEG coated PLGA NPs, and NanoPHATS. B) Absorbance measurements in PBS of coated and uncoated PLGA NPs over time indicating the increased scattering by aggregated particles. NanoPHATS and 20% PEG coated NPs do not aggregate in PBS as evidenced by no increase in absorbance.

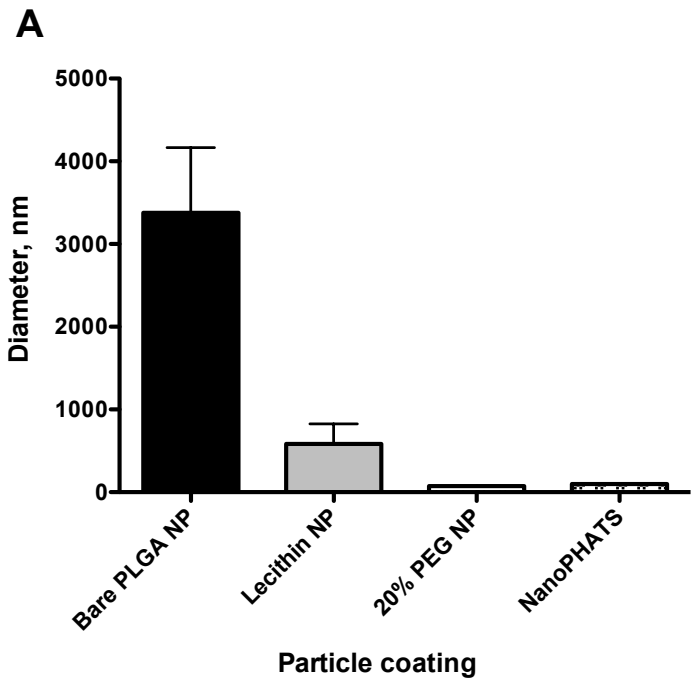
A
5000
4000
3000
2000
1000
0
Diameter, nm
Bare PLGA NP
Lecithin NP
20% PEG NP
NanoPHATS
Particle coating

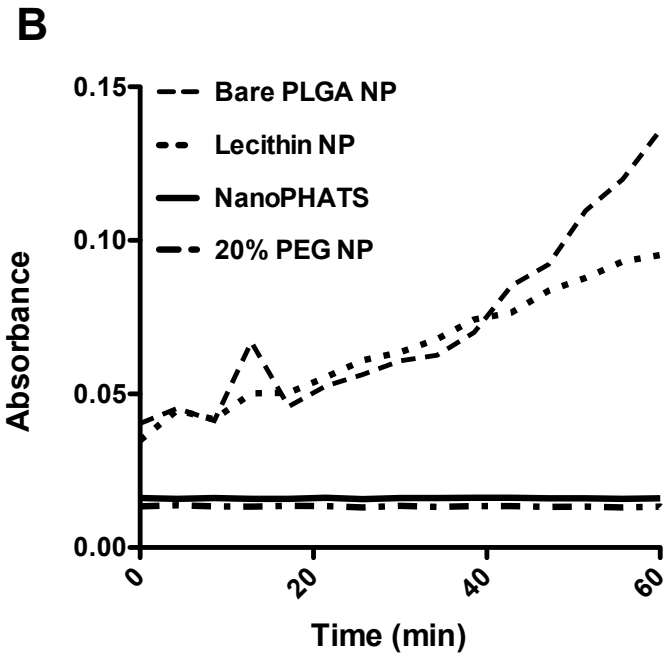
B
0.15
0.10
0.05
0.00
Absorbance
Bare PLGA NP
Lecithin NP
NanoPHATS
20% PEG NP
0
20
40
60
Time (min)

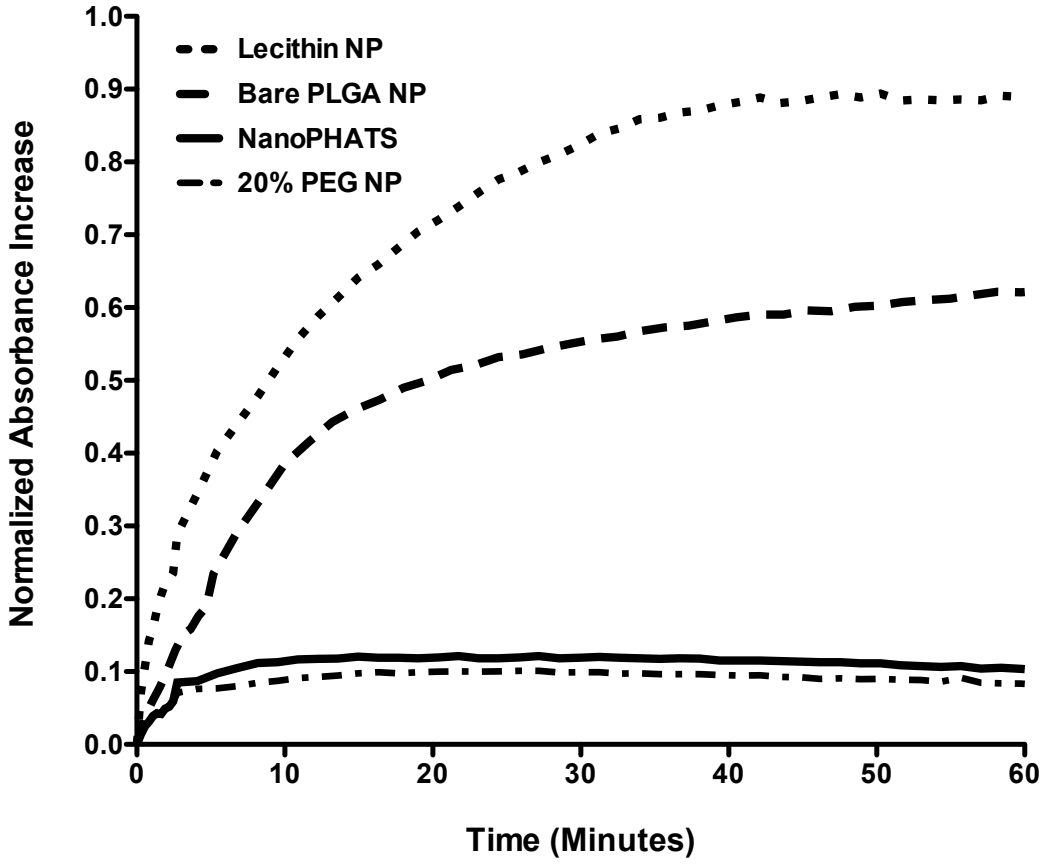

Figure 4.6. Serum stability of various coated and uncoated nanoparticles, as measured by absorbance. Various nanoparticle solutions were added to fetal bovine serum in a 1:1 ratio making the final serum concentration 50%. Absorbance values were normalized to the highest absorbance level after subtracting the average background from plain 50% serum. Uncoated PLGA NPs and lecithin coated NPs increase the absorbance significantly, indicating aggregation. Both 20 mol% PEG coated and NanoPHATS show only slight increases in absorbance, indicating minimal aggregation and protein binding.

The lecithin coated nanoparticles increased in absorbance the most, followed by bare PLGA NPs. NanoPHATS and PEG coated NPs only had a modest increase in absorbance. The NanoPHATS showed an increase of only 12% of that of the lecithin NPs and the PEG coated NPs 10% of the lecithin NPs.

4.3.2 *In vivo* circulation half-life results

The NanoPHATS were then tested *in vivo* to determine the circulation half-life. PEG coated NPs were used as a positive control. 1,1'-dioctadecyl-3,3,3',3'-tetramethylindodicarbocyanine perchlorate ('DiD' oil) is a hydrophobic fluorescent dye and was loaded into the hydrophobic PLGA core of the NPs. DiD oil is only weakly fluorescent in aqueous environments but is very photostable in lipophilic environments. Thus, any dye that diffuses out of the NPs into the blood stream contributes minimally to the overall signal. 100 μL of the NP solution at a concentration of 1mg NPs/mL was administered to mice via tail vein injection. Approximately 30 μL of blood was collected through retro-orbital bleeding at various time points over the course of 24 hours. The whole blood was plated in a 96 well plate and PBS was added to bring the volume up to 100 μL. The fluorescence signal of the whole blood was measured using a Tecan spectrophotometer using

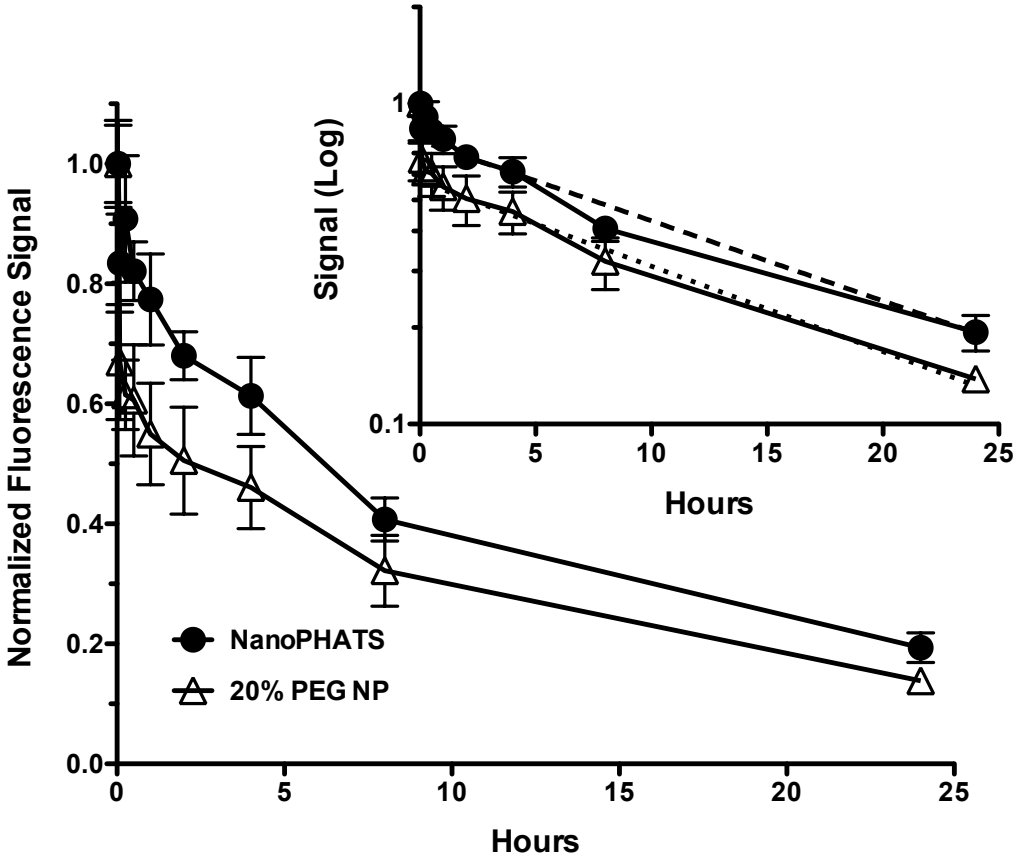

Figure 4.7. *In vivo* circulation data for fluorescent NanoPHATS and 20 mol% lipid-PEG coated NPs. NPs administered to 3 mice each via tail vein injection. The signal was normalized to the first time point sample. The inset shows the fluorescence signal plotted on a log scale. The data show a two-phase curve, the second phase representing the elimination of the particles from the blood stream. The circulation half-life was calculated from the slope of the second phase decrease.

an excitation wavelength of 630nm and an emission wavelength of 675nm. The background signal from blood collected before NP injection was subtracted from each sample. The measurements were normalized to the signal measured from the sample taken immediately after injection. The measured fluorescence for both 20% PEG coated NPs and NanoPHATS are presented in Figure 4.7.

The fluorescent signal shows a bimodal decay. It was assumed the particles followed a standard two-compartment model with the alpha phase indicating the biodistribution half-life and the beta phase indicating the elimination half-life. The elimination half-life was calculated using the formula given in Equation 4.1,

$$t_{1/2} = \frac{\ln(2)}{\lambda} \tag{4.1}$$

where λ is the absolute value of the slope of the β-phase of the curve when plotted on a semi-log scale. The first hour was taken to be the α-phase and those data points were excluded when determining the β-phase slope. The circulation half-life was found to be 27.7 hours for the NanoPHATS and 26.0 hours for the PEG coated NPs.

4.4 Conclusion

A biomimetic, nanoparticle based theranostic system we call Nano Polymer Hybrid Apolipoprotein Theranostic System (NanoPHATS) was developed to provide an alternative to PEGylated nanoparticles. NanoPHATS, consisting of a hydrophobic PLGA polymer core, a lipid monolayer shell, and Apolipoprotein A1 molecules integrated onto the surface, can be synthesized with a size range of 50-200nm. The NanoPHATS show excellent stability in high ionic solutions, such as PBS, as well as in high serum protein solutions. NanoPHATS also show an *in vivo* circulation half-life equivalent to PEGylated lipid-polymer hybrid nanoparticles. Drawbacks of PEG coatings, such as possible immunogenicity, are avoided by using endogenous lipoproteins as the stabilizing agent. NanoPHATS represent an important addition to the engineer's toolbox for designing drug and theranostic delivery vehicles for the treatment of diseases.

Chapter 4, in part, is currently being prepared for submission for publication of the material. Corbin Clawson, Li Zhang, Linh Ton, Sadik Esener, Liangfang Zhang.

5. Conclusions and Future Directions

Drug delivery vehicles represent an important field of research that has already been shown to improve the efficacy of numerous therapeutic formulations. There remains a great many opportunities for further advancements in this field. The work of this dissertation aims to present important improvements in three specific areas of drug delivery technology:

1. The co-delivery of antigen and adjuvant molecules for improved immunostimulation, especially through the used of surface presentation of bioactive molecules.

2. The development of a stabilizing coating for drug delivery vehicles that can be shed in response to an environmental stimulus in order to promote intracellular delivery of cargo.

3. The development of a biomimetic stabilizing coating that can replace PEG to avoid immunogenicity.

The results presented here show significant advancements in these areas. Adding to the drug delivery vehicle toolkit available to researchers and clinicians, these technologies can aid in overcoming the difficulties in treating cancer as well as have a broad impact on the field of drug delivery as a whole. The following sections will reiterate the important conclusions presented by this work.

5.1 PLGA Vaccine Delivery Vehicles

Vaccination remains the most effective prophylaxis available for a wide variety of infectious diseases and is even being explored for the treatment of cancer.(27, 28) PLGA nanoparticles were chosen as a vaccine drug delivery vehicle for the purpose of co-delivery of both antigen and adjuvant biomolecules. Hp91, a novel immunostimulatory peptide, was chosen as the adjuvant and bovine serum albumin the antigen. Encapsulation efficiency and release kinetics of Hp91 were determined for two different formulations: 1. Hp91 encapsulated inside

the PLGA nanoparticles, and 2. Hp91 conjugated to the surface of the PLGA nanoparticles.

In order to determine if the activity of the Hp91 peptide was affected by encapsulation or conjugation, the nanoparticles were tested for their stimulatory activity on mouse and human dendritic cells, the professional antigen presenting cells of the immune system. Both formulations not only preserved the activity of Hp91, but were anywhere from 6 fold to 44 fold more potent in stimulating mouse and human dendritic cells than free Hp91 peptide. The surface presentation of the Hp91 peptide greatly enhanced the immunostimulatory properties. The accessibility of the adjuvant by the cell when conjugated to the surface of the nanoparticles is likely the reason for increased activity. Bioactive surface are therefore an important area for further research.

The PLGA nanoparticle system presented here shows promise as a vaccination platform, especially in that both antigen and adjuvant can be protected from protease degradation and simultaneously delivered to immune cells. The protective properties of polymer encapsulation open the possibility of gastrointestinal vaccine systems, which would undoubtedly increase patient convenience and compliance when compared to subcutaneous injection vaccines.

The beneficial controlled release characteristics of the polymer nanoparticles may for a vaccine depot to form at the site of injection. This may increase the efficacy and lead to a reduction in antigen material necessary to confer immunity, thus improving efficacy and safety. The effects of the polymer composition of the nanoparticle on release kinetics should be explored in order to optimize the system for vaccine use.

The co-delivery of both antigen and adjuvant remains a key benefit, especially in the development of cancer vaccines, where tolerance to self-antigens is difficult to overcome. In order to avoid the generation of tolerance in the immune system, the immune cells must encounter both antigen and adjuvant simultaneously. The work presented here effectively shows this critical co-delivery ability of PLGA nanoparticles, making them a promising cancer vaccine platform.

Future work using PLGA nanoparticles as cancer vaccine drug delivery vehicles should be pursued ambitiously, as the potential benefits are enormous. Areas of interest are the development of gastrointestinal vaccine formulations, the optimization of release kinetics by altering polymer composition, and the development of a cancer vaccine using PLGA nanoparticles.

5.2 PEG Shedding Drug Delivery Vehicle

For systemic delivery, nanoparticles need to have long circulation half-lives in order to increase their probability of finding the target tissue. Poly(ethylene glycol) coatings have become the standard for imparting long circulation characteristics on drug delivery vehicles. Once the long circulating particle reaches its destination, whether it is a solid tumor or some other tissue, the cargo must find its way to its cellular target. Cutting edge technologies are using biomolecules as the therapeutic cargo. Such proteins, peptides, and nucleic acids risk being degraded if they are endocytosed. The endosome and lysosome become highly acidic (pH ~ 4) and any biomolecules are degraded completely in this environment. The PEG coating which previously imparted the beneficial long circulation half-life now becomes detrimental to the delivery of sensitive cargo. The steric stabilization of the PEG prevents the nanoparticle from disrupting the endosomal membrane and escaping into the cytosol. In order to overcome this barrier to the delivery of sensitive cargo to the cytosol, a novel PEG coating was developed capable of being shed in response to a drop in local pH.

The molecule designed consists of a phospholipid conjugated to a PEG polymer chain via a succinate linker. The succinate linker incorporates a double ester bond that is sensitive to hydrolysis. In acidic environments, the ester bond is broken, releasing the PEG chain and exposing the phospholipid. Lipid-polymer hybrid nanoparticles were fabricated with the novel lipid-(succinate)-mPEG molecule incorporated into a fusogenic lipid monolayer on the surface of a PLGA nanoparticle core. Upon the release of the PEG coating, the fusogenic lipid monolayer is free to interact and fuse with other lipid layers, including cellular and endosomal membranes.

The nanoparticles were shown to be stable over 24 hours at neutral pH, but destabilized quickly at pH 5. This was confirmed by DLS and SEM, showing the destabilized structures. Finally, formulations were developed to allow the destabilization of the nanoparticles at any pH over a wide range of acidic values from neutral to pH = 3. This ability is critical so that the PEG shedding system can be used in various applications. For example, a nanoparticle that destabilizes at pH = 4 would be appropriate for lysosomal escape while a nanoparticle that sheds its PEG coating at pH = 6.5 would be optimal for intratumoral delivery where the extracellular space is only slightly acidic.

Future work in this area should include the *in vivo* and *in vitro* testing to confirm cytosolic delivery. Endosomal and lysosomal tracking dyes can be used to monitor the uptake and escape of the nanoparticle cores into the cytosol. Application of lipid-(succinate)-mPEG to other drug delivery vehicles such as liposomes and lipid micelles would greatly expand the utility of the system. Significant work needs to be done in the scale up synthesis and purification of the lipid-(succinate)-mPEG molecule as it is now only produced at the 10-100 mg scale.

5.3 Biomimetic Stabilizer to Replace PEG

While PEG coatings are the current state of the art for stabilizing nanoparticle drug delivery vehicles and imparting long circulation half-lives, there exist some reasons to explore alternatives. There is a demonstrated risk of immunogenicity, which can lead to accelerated blood clearance after repeated dosing. This becomes an important issue as drug delivery vehicle usage in the clinic increases every year.

In order to offer an alternative that would not cause an immunogenic response, we looked to nature for inspiration.

A biomimetic stabilizing coating was developed based on the body's own long circulation nanoparticles, high-density lipoproteins (HDL) and used to create a novel drug delivery vehicle platform we call NanoPHATS. Apolipoprotein A1 is the major component of HDL and serves as an amphiphilic surface-active molecule to solubilize hydrophobic glycerides and cholesterols in the aqueous blood. Apo A1 incorporates itself into a phospholipid monolayer that surrounds the hydrophobic core. Apolipoprotein A1 was used to stabilize a drug delivery vehicle consisting of a hydrophobic PLGA polymer core and a phospholipid monolayer coating.

Using the one step nanoprecipitation fabrication process, sub 100 nm particles with spherical morphology achieved. The Apo A1 incorporation efficiency was measured to be 94% and the particles were stable in high ionic strength solutions as well as 50% serum. Stability is serum is an important characteristic as serum proteins are often the cause of opsonization and destabilization, leading to rapid blood clearance.

Finally, the *in vivo* circulation half-life of NanoPHATS was compared to PEGylated nanoparticles using a mouse model. The

circulation half-life of NanoPHATS exceeded that of the PEGylated particles, confirming the stabilizing properties of Apo A1. In addition, the ability of the Apo A1 to hid the particles from the immune system by mimicking natural HDL and LDL particles is proven by the long circulation half-life, something that would not be possible if the particles were recognized by the immune system.

Future work on the NanoPHATS system can involve the delivery of model therapeutics in a mouse model. NanoPHATS would be an excellent candidate for chemotherapeutic delivery to solid tumors or for the treatment of blood cancers owing to its long circulation half-life. In addition, the ability of NanoPHATS to target atherosclerotic plaques should be explored as the apolipoprotein surface coating may aid in the infiltration of the nanoparticles into existing arterial plaques.

References

1. Merriam-Webster's Collegiate Dictionary. 11th ed. Springfield, Mass.: Merriam-Webster, Inc.; 2003.

2. Kaufmann M, von Minckwitz G, Bear HD, Buzdar A, McGale P, Bonnefoi H, et al. Recommendations from an international expert panel on the use of neoadjuvant (primary) systemic treatment of operable breast cancer: new perspectives 2006. Ann Oncol. 2007;18(12):1927-34.

3. Dawood S, Merajver SD, Viens P, Vermeulen PB, Swain SM, Buchholz TA, et al. International expert panel on inflammatory breast cancer: consensus statement for standardized diagnosis and treatment. Ann Oncol. 2011;22(3):515-23.

4. Rakha EA, Reis JS, Ellis IO. Combinatorial biomarker expression in breast cancer. Breast Cancer Res Treat. 2010;120(2):293-308.

5. De Milito A, Fais S. Tumor acidity, chemoresistance and proton pump inhibitors. Future Oncol. 2005;1(6):779-86.

6. Gottesman MM, Pastan I. BIOCHEMISTRY OF MULTIDRUG-RESISTANCE MEDIATED BY THE MULTIDRUG TRANSPORTER. Annu Rev Biochem. 1993;62:385-427.

7. Cole SPC, Bhardwaj G, Gerlach JH, Mackie JE, Grant CE, Almquist KC, et al. OVEREXPRESSION OF A TRANSPORTER GENE IN A MULTIDRUG-RESISTANT HUMAN LUNG-CANCER CELL-LINE. Science. 1992;258(5088):1650-4.

8. Langer R. Drug delivery and targeting. Nature. 1998;392(6679):5-10.

9. Ren F, Chen R, Wang Y, Sun Y, Jiang Y, Li G. Paclitaxel-Loaded Poly(n-butylcyanoacrylate) Nanoparticle Delivery System to Overcome Multidrug Resistance in Ovarian Cancer. Pharmaceutical Research (Dordrecht). 2011;28(4):897-906.

10. de Niederhausern S, Bondi M, Messi P, Iseppi R, Sabia C, Manicardi G, et al. Vancomycin-resistance Transferability from VanA Enterococci to Staphylococcus aureus. Curr Microbiol. 2011;62(5):1363-7.

11. Raghunath D. Emerging antibiotic resistance in bacteria with special reference to India. J Biosci. 2008;33(4):593-603.

12. Werner G, Strommenger B, Witte W. Acquired vancomycin resistance in clinically relevant pathogens. Future Microbiol. 2008;3(5):547-62.

13. Yoshikawa T, Okada N, Oda A, Matsuo K, Matsuo K, Mukai Y, et al. Development of amphiphilic gamma-PGA-nanoparticle based tumor vaccine: potential of the nanoparticulate cytosolic protein delivery carrier. Biochemical and Biophysical Research Communications. 2008;366(2):408-13.

14. Zaks K, Jordan M, Guth A, Sellins K, Kedl R, Izzo A, et al. Efficient immunization and cross-priming by vaccine adjuvants containing TLR3 or TLR9 agonists complexed to cationic liposomes. Journal of Immunology. 2006;176(12):7335-45.

15. Janeway CA, Travers P, Walport M, Schlomchick MJ. Immunobiology. 5 ed. New York: Garland Science; 2001.

16. Banchereau J, Steinman RM. Dendritic cells and the control of immunity. Nature. 1998;392(6673):245-52.

17. Steinman RM. The control of immunity and tolerance by dendritic cell. Pathol Biol (Paris). 2003;51(2):59-60.

18. Lemoine D, Preat V. Polymeric nanoparticles as delivery system for influenza virus glycoproteins. J Control Release. 1998;54(1):15-27.

19. Uto T, Wang X, Sato K, Haraguchi M, Akagi T, Akashi M, et al. Targeting of antigen to dendritic cells with poly(gamma-glutamic acid) nanoparticles induces antigen-specific humoral and cellular immunity. Journal of Immunology. 2007;178(5):2979-86.

20. He C, Hu Y, Yin L, Tang C, Yin C. Effects of particle size and surface charge on cellular uptake and biodistribution of polymeric nanoparticles. Biomaterials. 2010;31(13):3657-66.

21. Heit A, Schmitz F, Haas T, Busch DH, Wagner H. Antigen co-encapsulated with adjuvants efficiently drive protective T cell immunity. Eur J Immunol. 2007;37(8):2063-74.

22. Fang RH, Aryal S, Hu CMJ, Zhang LF. Quick Synthesis of Lipid-Polymer Hybrid Nanoparticles with Low Polydispersity Using a Single-Step Sonication Method. Langmuir. 2010;26(22):16958-62.

23. Audran R, Peter K, Dannull J, Men Y, Scandella E, Groettrup M, et al. Encapsulation of peptides in biodegradable microspheres prolongs their MHC class-I presentation by dendritic cells and macrophages in vitro. Vaccine. 2003;21(11-12):1250-5.

24. de Jong S, Chikh G, Sekirov L, Raney S, Semple S, Klimuk S, et al. Encapsulation in liposomal nanoparticles enhances the immunostimulatory, adjuvant and anti-tumor activity of subcutaneously administered CpG ODN. Cancer Immunology, Immunotherapy. 2007;56(8):1251-64.

25. Diwan M, Tafaghodi M, Samuel J. Enhancement of immune responses by co-delivery of a CpG oligodeoxynucleotide and tetanus toxoid in biodegradable nanospheres. J Control Release. 2002;85(1-3):247-62.

26. Jiang WL, Schwendeman SP. Stabilization of tetanus toxoid encapsulated in PLGA microspheres. Molecular Pharmaceutics. 2008;5(5):808-17.

27. Fournier P, Schirrmacher V. Randomized clinical studies of anti-tumor vaccination: state of the art in 2008. Expert Rev Vaccines. 2009;8(1):51-66.

28. Gattinoni L, Powell DJ, Jr., Rosenberg SA, Restifo NP. Adoptive immunotherapy for cancer: building on success. Nat Rev Immunol. 2006;6(5):383-93. PMCID: 1473162.

29. Di Lisi D, Bonura F, Macaione F, Peritore A, Meschisi M, Cuttitta F, et al. Chemotherapy-induced cardiotoxicity: role of the tissue Doppler in the early diagnosis of left ventricular dysfunction. Anti-Cancer Drugs. 2011;22(5):468-72.

30. Hong RL, Huang CJ, Tseng YL, Pang VF, Chen ST, Liu JJ, et al. Direct comparison of liposomal doxorubicin with or without polyethylene glycol coating in C-26 tumor-bearing mice: Is surface coating with polyethylene glycol beneficial? Clin Cancer Res. 1999;5(11):3645-52.

31. Christiansen S. Clinical management of doxorubicin-induced heart failure. Journal of Cardiovascular Surgery. 2011;52(1):133-7.

32. Hydock DS, Lien CY, Jensen BT, Schneider CM, Hayward R. Exercise Preconditioning Provides Long-Term Protection Against Early Chronic Doxorubicin Cardiotoxicity. Integrative Cancer Therapies. 2011;10(1):47-57.

33. Murata A, Matsuno K, Yabe-Nishimura C. NOX1-derived reactive oxygen species promote Doxorubicin-induced cardiotoxicity. Journal of Pharmacological Sciences. 2011;115:153P-P.

34. Tomonari M, To H, Nishida M, Mishima T, Sasaki H, Kurose H. Mechanism of the Cardioprotective Effects of Docetaxel Pre-administration Against Adriamycin-Induced Cardiotoxicity. Journal of Pharmacological Sciences. 2011;115(3):336-45.

35. Moghimi SM, Hunter AC, Murray JC. Nanomedicine: current status and future prospects. Faseb Journal. 2005;19(3):311-30.

36. Farokhzad OC, Cheng JJ, Teply BA, Sherifi I, Jon S, Kantoff PW, et al. Targeted nanoparticle-aptamer bioconjugates for cancer chemotherapy in vivo. Proceedings of the National Academy of Sciences of the United States of America. 2006;103(16):6315-20.

37. Kukowska-Latallo JF, Candido KA, Cao ZY, Nigavekar SS, Majoros IJ, Thomas TP, et al. Nanoparticle targeting of anticancer drug improves therapeutic response in animal model of human epithelial cancer. Cancer Res. 2005;65(12):5317-24.

38. Nishiyama N, Kataoka K. Current state, achievements, and future prospects of polymeric micelles as nanocarriers for drug and gene delivery. Pharmacology & Therapeutics. 2006;112(3):630-48.

39. Sengupta S, Eavarone D, Capila I, Zhao GL, Watson N, Kiziltepe T, et al. Temporal targeting of tumour cells and neovasculature with a nanoscale delivery system. Nature. 2005;436(7050):568-72.

40. Douglas SJ, Davis SS, Illum L. NANOPARTICLES IN DRUG DELIVERY. Crc Critical Reviews in Therapeutic Drug Carrier Systems. 1987;3(3):233-61.

41. Gwinn MR, Vallyathan V. Nanoparticles: Health effects - Pros and cons. Environmental Health Perspectives. 2006;114(12):1818-25.

42. ten Tije AJ, Verweij J, Loos WJ, Sparreboom A. Pharmacological effects of formulation vehicles - Implications for cancer chemotherapy. Clin Pharmacokinet. 2003;42(7):665-85.

43. Yezhelyev MV, Gao X, Xing Y, Al-Hajj A, Nie SM, O'Regan RM. Emerging use of nanoparticles in diagnosis and treatment of breast cancer. Lancet Oncology. 2006;7(8):657-67.

44. Weiss M. MODELING OF INITIAL DISTRIBUTION OF DRUGS FOLLOWING INTRAVENOUS BOLUS INJECTION. Eur J Clin Pharmacol. 1983;24(1):121-6.

45. Langer R, Folkman J. POLYMERS FOR SUSTAINED-RELEASE OF PROTEINS AND OTHER MACROMOLECULES. Nature. 1976;263(5580):797-800.

46. Chan JM, Zhang LF, Yuet KP, Liao G, Rhee JW, Langer R, et al. PLGA-lecithin-PEG core-shell nanoparticles for controlled drug delivery. Biomaterials. 2009;30(8):1627-34.

47. Gref R, Minamitake Y, Peracchia MT, Trubetskoy V, Torchilin V, Langer R. Biodegradable Long-Circulating Polymeric Nanospheres. Science. 1994;263(5153):1600-3.

48. Pridgen EM, Alexis F, Langer RS, Farohkzad OC. Biodegradable, Targeted Polymeric Nanoparticle Drug Delivery Formulation for Cancer Therapy. Methods in Bioengineering: Nanoscale Bioengineering and Nanomedicine. 2009:197-235.

49. Shi JJ, Votruba AR, Farokhzad OC, Langer R. Nanotechnology in Drug Delivery and Tissue Engineering: From Discovery to Applications. Nano Letters. 2010;10(9):3223-30.

50. Sharraya A, Yang J, Sandoval S, Alfaro J, Kummel A, Trogler WC. Folate conjugated PLGA silica coreshell nanoparticles for drug delivery. Proceedings of the American Association for Cancer Research Annual Meeting. 2010;51:645-6.

51. Yang J, Lind JU, Trogler WC. Synthesis of hollow silica and titania nanospheres. Chemistry of Materials. 2008;20(9):2875-7.

52. Dillen K, Vandervoort J, Van den Mooter G, Verheyden L, Ludwig A. Factorial design, physicochemical characterisation and activity of ciprofloxacin-PLGA nanoparticles. Int J Pharm. 2004;275(1-2):171-87.

53. Fonseca C, Simoes S, Gaspar R. Paclitaxel-loaded PLGA nanoparticles: preparation, physicochemical characterization and in vitro anti-tumoral activity. J Control Release. 2002;83(2):273-86.

54. Nakatsuka MA, Lee JH, Nakayama E, Hung AM, Hsu MJ, Mattrey RF, et al. Facile one-pot synthesis of polymer-phospholipid composite microbubbles with enhanced drug loading capacity for ultrasound-triggered therapy. Soft Matter. 2011;7(5):1656-9.

55. Folkman J. ANGIOGENESIS IN CANCER, VASCULAR, RHEUMATOID AND OTHER DISEASE. Nat Med. 1995;1(1):27-31.

56. Iyer AK, Khaled G, Fang J, Maeda H. Exploiting the enhanced permeability and retention effect for tumor targeting. Drug Discov Today. 2006;11(17-18):812-8.

57. Maeda H, Sawa T, Konno T. Mechanism of tumor-targeted delivery of macromolecular drugs, including the EPR effect in solid tumor and clinical overview of the prototype polymeric drug SMANCS. Journal of Controlled Release. 2001;74(1-3):47-61.

58. Maeda H, Wu J, Sawa T, Matsumura Y, Hori K. Tumor vascular permeability and the EPR effect in macromolecular therapeutics: a review. Journal of Controlled Release. 2000;65(1-2):271-84.

59. Hu CMJ, Kaushal S, Cao HST, Aryal S, Sartor M, Esener S, et al. Half-Antibody Functionalized Lipid-Polymer Hybrid Nanoparticles for Targeted Drug Delivery to Carcinoembryonic Antigen Presenting Pancreatic Cancer Cells. Molecular Pharmaceutics. 2010;7(3):914-20.

60. Montet X, Funovics M, Montet-Abou K, Weissleder R, Josephson L. Multivalent effects of RGD peptides obtained by nanoparticle display. Journal of Medicinal Chemistry. 2006;49(20):6087-93.

61. Montet X, Montet-Abou K, Reynolds F, Weissleder R, Josephson L. Nanoparticle imaging of integrins on tumor cells. Neoplasia. 2006;8(3):214-22.

62. Mulder WJM, Strijkers GJ, Habets JW, Bleeker EJW, van der Schaft DWJ, Storm G, et al. MR molecular imaging and fluorescence microscopy for identification of activated tumor endothelium using a bimodal lipidic nanoparticle. Faseb Journal. 2005;19(12):2008-+.

63. Park JH, Kwon SG, Nam JO, Park RW, Chung H, Seo SB, et al. Self-assembled nanoparticles based on glycol chitosan bearing 5 beta-cholanic acid for RGD peptide delivery. Journal of Controlled Release. 2004;95(3):579-88.

64. Schiffelers RM, Ansari A, Xu J, Zhou Q, Tang QQ, Storm G, et al. Cancer siRNA therapy by tumor selective delivery with ligand-targeted sterically stabilized nanoparticle. Nucleic Acids Research. 2004;32(19).

65. Zhang CF, Jugold M, Woenne EC, Lammers T, Morgenstern B, Mueller MM, et al. Specific targeting of tumor angiogenesis by RGD-conjugated ultrasmall superparamagnetic iron oxide particles using a clinical 1.5-T magnetic resonance scanner. Cancer Res. 2007;67(4):1555-62.

66. Zhang L, Gu FX, Chan JM, Wang AZ, Langer RS, Farokhzad OC. Nanoparticles in medicine: Therapeutic applications and developments. Clinical Pharmacology & Therapeutics. 2008;83(5):761-9.

67. Vicente S, Prego C, Csaba N, Alonso MJ. From single-dose vaccine delivery systems to nanovaccines. J Drug Deliv Sci Technol. 2010;20(4):267-76.

68. Fifis T, Gamvrellis A, Crimeen-Irwin B, Pietersz GA, Li J, Mottram PL, et al. Size-dependent immunogenicity: therapeutic and protective properties of nano-vaccines against tumors. Journal of Immunology. 2004;173(5):3148-54.

69. Fang RH, Aryal S, Hu C-MJ, Zhang L. Quick Synthesis of Lipid-Polymer Hybrid Nanoparticles with Low Polydispersity Using a Single-Step Sonication Method. Langmuir. 2010;26(22):16958-62.

70. Li Y-P, Pei Y-Y, Zhang X-Y, Gu Z-H, Zhou Z-H, Yuan W-F, et al. PEGylated PLGA nanoparticles as protein carriers: synthesis, preparation and biodistribution in rats. Journal of Controlled Release. 2001;71(2):203-11.

71. Owens DE, Peppas NA. Opsonization, biodistribution, and pharmacokinetics of polymeric nanoparticles. Int J Pharm. 2006;307(1):93-102.

72. Venkataraman S, Ong WL, Ong ZY, Loo SCJ, Ee PLR, Yang YY. The role of PEG architecture and molecular weight in the gene transfection performance of PEGylated poly(dimethylaminoethyl methacrylate) based cationic polymers. Biomaterials. 2011;32(9):2369-78.

73. Yoo JW, Chambers E, Mitragotri S. Factors that Control the Circulation Time of Nanoparticles in Blood: Challenges, Solutions and Future Prospects. Curr Pharm Design. 2010;16(21):2298-307.

74. Cerritelli S, Velluto D, Hubbell JA. PEG-SS-PPS: Reduction-sensitive disulfide block copolymer vesicles for intracellular drug delivery. Biomacromolecules. 2007;8(6):1966-72.

75. Takae S, Miyata K, Oba M, Ishii T, Nishiyama N, Itaka K, et al. PEG-detachable polyplex micelles based on disulfide-linked block catiomers as bioresponsive nonviral gene vectors. J Am Chem Soc. 2008;130(18):6001-9.

76. Gao WW, Langer R, Farokhzad OC. Poly(ethylene glycol) with Observable Shedding. Angew Chem-Int Edit. 2010;49(37):6567-71.

77. Alexis F, Pridgen E, Molnar LK, Farokhzad OC. Factors affecting the clearance and biodistribution of polymeric nanoparticles. Mol Pharm. 2008;5(4):505-15.

78. Morales CS, Zhang L, Langer R, Farokhzad O. Understanding the immunological properties of functionalized lipid-polymeric nanoparticles. Proceedings of the American Association for Cancer Research Annual Meeting. 2009;50:151-2.

79. Armstrong JK. The occurrence, induction, specificity and potential effect of antibodies against poly(ethylene glycol). Veronese FM, editor: Birkhauser Verlag Ag; 2009.

80. Koide H, Asai T, Hatanaka K, Shimizu K, Yokoyama M, Ishida T, et al. Elucidation of Accelerated Blood Clearance Phenomenon Caused by Repeat Injection of PEGylated Nanocarriers. Yakugaku Zasshi-J Pharm Soc Jpn. 2009;129(12):1445-51.

81. Uto T, Wang X, Sato K, Haraguchi M, Akagi T, Akashi M, et al. Targeting of antigen to dendritic cells with poly(gamma-glutamic acid) nanoparticles induces antigen-specific humoral and cellular immunity. J Immunol. 2007;178(5):2979-86.

82. Diwan M, Elamanchili P, Lane H, Gainer A, Samuel J. Biodegradable nanoparticle mediated antigen delivery to human cord blood derived dendritic cells for induction of primary T cell responses. J Drug Target. 2003;11(8-10):495-507.

83. Elamanchili P, Diwan M, Cao M, Samuel J. Characterization of poly(D,L-lactic-co-glycolic acid) based nanoparticulate system for enhanced delivery of antigens to dendritic cells. Vaccine. 2004;22(19):2406-12.

84. Messmer D, Yang H, Telusma G, Knoll F, Li J, Messmer B, et al. High mobility group box protein 1: an endogenous signal for dendritic cell maturation and Th1 polarization. J Immunol. 2004;173(1):307-13.

85. Telusma G, Datta S, Mihajlov I, Ma W, Li J, Yang H, et al. Dendritic cell activating peptides induce distinct cytokine profiles. International Immunology. 2006;18(11):1563-73.

86. Govender T, Stolnik S, Garnett MC, Illum L, Davis SS. PLGA nanoparticles prepared by nanoprecipitation: drug loading and release studies of a water soluble drug. J Control Release. 1999;57(2):171-85.

87. Ayalasomayajula SP, Kompella UB. Subconjunctivally administered celecoxib-PLGA microparticles sustain retinal drug levels and alleviate diabetes-induced oxidative stress in a rat model. Eur J Pharmacol. 2005;511(2-3):191-8.

88. Lee SY, Oh JH, Kim JC, Kim YH, Kim SH, Choi JW. In vivo conjunctival reconstruction using modified PLGA grafts for decreased scar formation and contraction. Biomaterials. 2003;24(27):5049-59.

89. Zhou T, Lewis H, Foster RE, Schwendeman SP. Development of a multiple-drug delivery implant for intraocular management of proliferative vitreoretinopathy. J Control Release. 1998;55(2-3):281-95.

90. des Rieux A, Fievez V, Garinot M, Schneider YJ, Preat V. Nanoparticles as potential oral delivery systems of proteins and vaccines: a mechanistic approach. J Control Release. 2006;116(1):1-27.

91. Ulery BD, Phanse Y, Sinha A, Wannemuehler MJ, Narasimhan B, Bellaire BH. Polymer Chemistry Influences Monocytic Uptake of Polyanhydride Nanospheres. Pharm Res. 2009;26(3):683-90.

92. Inaba K, Inaba M, Romani N, Aya H, Deguchi M, Ikehara S, et al. Generation of large numbers of dendritic cells from mouse bone marrow cultures supplemented with granulocyte/macrophage colony-stimulating factor. The Journal of Experimental Medicine. 1992;176(6):1693-702.

93. Morelli AE, Zahorchak AF, Larregina AT, Colvin BL, Logar AJ, Takayama T, et al. Cytokine production by mouse myeloid dendritic cells in relation to differentiation and terminal maturation induced by lipopolysaccharide or CD40 ligation. Blood. 2001;98(5):1512-23.

94. Jonuleit H, Kuhn U, Muller G, Steinbrink K, Paragnik L, Schmitt E, et al. Pro-inflammatory cytokines and prostaglandins induce maturation of potent immunostimulatory dendritic cells under fetal calf serum-free conditions. Eur J Immunol. 1997;27(12):3135-42.

95. Blander JM, Medzhitov R. Toll-dependent selection of microbial antigens for presentation by dendritic cells. Nature. 2006;440(7085):808-12.

96. Heit A, Schmitz F, Haas T, Busch DH, Wagner H. Antigen co-encapsulated with adjuvants efficiently drive protective T cell immunity. Eur J Immunol. 2007;37(8):2063-74.

97. Reddy ST, van der Vlies AJ, Simeoni E, Angeli V, Randolph GJ, O'Neil CP, et al. Exploiting lymphatic transport and complement activation in nanoparticle vaccines. Nat Biotechnol. 2007;25(10):1159-64.

98. Yoshikawa T, Okada N, Oda A, Matsuo K, Matsuo K, Mukai Y, et al. Development of amphiphilic gamma-PGA-nanoparticle based tumor vaccine: potential of the nanoparticulate cytosolic protein delivery carrier. Biochem Biophys Res Commun. 2008;366(2):408-13.

99. de Jong S, Chikh G, Sekirov L, Raney S, Semple S, Klimuk S, et al. Encapsulation in liposomal nanoparticles enhances the immunostimulatory, adjuvant and anti-tumor activity of subcutaneously administered CpG ODN. Cancer Immunol Immunother. 2007;56(8):1251-64.

100. Fujimura T, Nakagawa S, Ohtani T, Ito Y, Aiba S. Inhibitory effect of the polyinosinic-polycytidylic acid/cationic liposome on the progression of murine B16F10 melanoma. Eur J Immunol. 2006;36(12):3371-80.

101. Zaks K, Jordan M, Guth A, Sellins K, Kedl R, Izzo A, et al. Efficient immunization and cross-priming by vaccine adjuvants containing TLR3 or TLR9 agonists complexed to cationic liposomes. J Immunol. 2006;176(12):7335-45.

102. Fifis T, Gamvrellis A, Crimeen-Irwin B, Pietersz GA, Li J, Mottram PL, et al. Size-dependent immunogenicity: therapeutic and protective properties of nano-vaccines against tumors. J Immunol. 2004;173(5):3148-54.

103. Vogt A, Combadiere B, Hadam S, Stieler KM, Lademann J, Schaefer H, et al. 40 nm, but not 750 or 1,500 nm, nanoparticles enter epidermal CD1a+ cells after transcutaneous application on human skin. J Invest Dermatol. 2006;126(6):1316-22.

104. Kaisho T, Akira S. Toll-like receptor function and signaling. J Allergy Clin Immunol. 2006;117(5):979-87; quiz 88.

105. Zhang L, Gu FX, Chan JM, Wang AZ, Langer RS, Farokhzad OC. Nanoparticles in Medicine: Therapeutic Applications and Developments. Clin Pharmacol Ther. 2007;83(5):761-9.

106. Ferrari M. Cancer nanotechnology: opportunities and challenges. Nature Nanotechnology. 2007;2(8):37-47.

107. Frerart F, Sonveaux P, Rath G, Smoos A, Meqor A, Charlier N, et al. The acidic tumor microenvironment promotes the reconversion

of nitrite into nitric oxide: towards a new and safe radiosensitizing strategy. Clin Cancer Res. 2008;14(9):2768-74.

108. Tannock IF, Rotin D. ACID PH IN TUMORS AND ITS POTENTIAL FOR THERAPEUTIC EXPLOITATION. Cancer Res. 1989;49(16):4373-84.

109. Modi S, Swetha MG, Goswami D, Gupta GD, Mayor S, Krishnan Y. A DNA nanomachine that maps spatial and temporal pH changes inside living cells. Nat Nanotechnol. 2009;4(5):325-30.

110. Yuba E, Kojima C, Harada A, Tana, Watarai S, Kono K. pH-Sensitive fusogenic polymer-modified liposomes as a carrier of antigenic proteins for activation of cellular immunity. Biomaterials. 2009;31(5):943-51.

111. Asokan A, Cho MJ. Exploitation of intracellular pH gradients in the cellular delivery of macromolecules. Journal of Pharmaceutical Sciences. 2002;91(4):903-13.

112. Liu C, Zhao G, Liu J, Ma N, Chivukula P, Perelman L, et al. Novel biodegradable lipid nano complex for siRNA delivery significantly improving the chemosensitivity of human colon cancer stem cells to paclitaxel. J Control Release. 2009;140(3):277-83.

113. Romberg B, Hennink WE, Storm G. Sheddable coatings for long-circulating nanoparticles. Pharm Res. 2008;25(1):55-71.

114. Aryal S, Hu C-M, Zhang L. Combinatorial drug conjugation enabled nanoparticle dual drug delivery. Small. 2010;6:1442-8.

115. Chan JM, Zhang L, Tong R, Ghosh D, Gao W, Liao G, et al. Spatiotemporal controlled delivery of nanoparticles to injured vasculature. Proc Natl Acad Sci USA. 2010;107(5):2213-8.

116. Zhang L, Zhang L. Lipid-polymer hybrid nanoparticles: synthesis, characterization and applications. Nano LIFE. 2010;1:163-73.

117. Liu XL, Testa B, Fahr A. Lipophilicity and Its Relationship with Passive Drug Permeation. Pharm Res. 2011;28(5):962-77.

118. Simıes S, Moreira JoN, Fonseca C, D¸zg¸nes N, Pedroso de Lima MC. On the formulation of pH-sensitive liposomes with long circulation times. Advanced Drug Delivery Reviews. 2004;56(7):947-65.

119. Torchilin VP, Zhou F, Huang L. pH-Sensitive Liposomes. Journal of Liposome Research. 1993;3(2):201-55.

120. Drummond DC, Zignani M, Leroux J-C. Current status of pH-sensitive liposomes in drug delivery. Progress in Lipid Research. 2000;39(5):409-60.

121. Valencia PM, Basto PA, Zhang L, Rhee M, Langer R, Farokhzad OC, et al. Single-step assembly of homogenous lipid-polymeric and lipid-quantum dot nanoparticles enabled by microfluidic rapid mixing. ACS Nano. 2010;4(3):1671-9.

122. Zhang L, Chan JM, Gu FX, Rhee J-W, Wang AZ, Radovic-Moreno AF, et al. Self-Assembled Lipid,àíPolymer Hybrid Nanoparticles: A Robust Drug Delivery Platform. ACS Nano. 2008;2(8):1696-702.

123. Perrault SD, Walkey C, Jennings T, Fischer HC, Chan WC. Mediating tumor targeting efficiency of nanoparticles through design. Nano Lett. 2009;9(5):1909-15.

124. Huynh NT, Roger E, Lautram N, Benoit JP, Passirani C. The rise and rise of stealth nanocarriers for cancer therapy: passive versus active targeting. Nanomedicine. 2010;5(9):1415-33.

125. Nikitin M, Yuriev M, Brusentsov N, Vetoshko P, Nikitin P. Non-Invasive in vivo Mapping and Long-Term Monitoring of Magnetic Nanoparticles in Different Organs of Animals. AIP Conference Proceedings. 2010:452-7.

126. Shinohara N, Nakazato T, Tamura M, Endoh S, Fukui H, Morimoto Y, et al. Clearance Kinetics of Fullerene C-60 Nanoparticles from Rat Lungs after Intratracheal C-60 Instillation and Inhalation C-60 Exposure. Toxicological Sciences. 2010;118(2):564-73.

127. Lammers T, Kiessling F, Hennink WE, Storm G. Nanotheranostics and Image-Guided Drug Delivery: Current Concepts and Future Directions. Molecular Pharmaceutics. 2010;7(6):1899-912.

128. Lee SM, Song Y, Hong BJ, MacRenaris KW, Mastarone DJ, O'Halloran TV, et al. Modular Polymer-Caged Nanobins as a Theranostic Platform with Enhanced Magnetic Resonance Relaxivity and pH-Responsive Drug Release. Angewandte Chemie-International Edition. 2010;49(51):9960-4.

129. Maiseyeu A, Badgeley MA, Mihai G, Modi S, Deiuliis JA, Kampfrath T, et al. Rosiglitazone-Loaded Theranostic Nanolatexes for Simultaneous Inflammation Imaging and Therapy. Arteriosclerosis Thrombosis and Vascular Biology. 2010;30(11):E228-E9.

130. Melancon MP, Elliott A, Ji X, Shetty A, Yang Z, Tian M, et al. Theranostics With Multifunctional Magnetic Gold Nanoshells Photothermal Therapy and T2* Magnetic Resonance Imaging. Investigative Radiology. 2011;46(2):132-40.

131. Menciassi A, Sinibaldi E, Pensabene V, Dario P. From miniature to nano robots for diagnostic and therapeutic applications. 2010 32nd Annual International Conference of the IEEE Engineering in Medicine and Biology Society (EMBC 2010). 2010:1954-7.

132. Janib SM, Moses AS, MacKay JA. Imaging and drug delivery using theranostic nanoparticles. Adv Drug Deliv Rev. 2010;62(11):1052-63.

133. Hawkins DS, Park JR, Thomson BG, Felgenhauer JL, Holcenberg JS, Panosyan EH, et al. Asparaginase pharmacokinetics after intensive polyethylene glycol-conjugated L-asparaginase therapy for children with relapsed acute lymphoblastic leukemia. Clin Cancer Res. 2004;10(16):5335-41.

134. Mahley RW. APOLIPOPROTEIN-E - CHOLESTEROL TRANSPORT PROTEIN WITH EXPANDING ROLE IN CELL BIOLOGY. Science. 1988;240(4852):622-30.

135. Tsompanidi EM, Brinkmeier MS, Fotiadou EH, Giakoumi SM, Kypreos KE. HDL biogenesis and functions: Role of HDL quality and quantity in atherosclerosis. Atherosclerosis. 2010;208(1):3-9.

136. Wong NCW. Novel therapies to increase apolipoprotein AI and HDL for the treatment of atherosclerosis. Current Opinion in Investigational Drugs. 2007;8(9):718-28.

137. Yang M, Jin HL, Chen JA, Ding LL, Ng KK, Lin QY, et al. Efficient Cytosolic Delivery of siRNA Using HDL-Mimicking Nanoparticles. Small. 2011;7(5):568-73.

138. Zhang ZH, Chen J, Ding LL, Jin HL, Lovell JF, Corbin IR, et al. HDL-Mimicking Peptide-Lipid Nanoparticles with Improved Tumor Targeting. Small. 2010;6(3):430-7.